UNIVERSITÄTSKLINIKUM HAMBURG-EPPENDORF

Zentrum für Molekulare Neurobiologie Hamburg (ZMNH),
Institut für Entwicklungsneurophysiologie Entwicklung

Direktor der Einrichtung
Prof. Dr. Ileana L. Hanganu-Opatz

Titel der Dissertation

"Thousand and one amino acid kinase 2 (*TAOK2*) is a repressor of translation and ameliorates exaggerated protein synthesis in *16p11.2* microdeletion"

Dissertation

zur Erlangung des Doktorgrades PhD
an der Medizinischen Fakultät der Universität Hamburg.

vorgelegt von:

Melad Henis
Asiut, Egypt

Hamburg 2021

(wird von der Medizinischen Fakultät ausgefüllt)

Angenommen von der
Medizinischen Fakultät der Universität Hamburg am: 21.12.2021

Veröffentlicht mit Genehmigung der
Medizinischen Fakultät der Universität Hamburg.

Prüfungsausschuss, der/die Vorsitzende: Prof. Dr. Matthias Kneussel

Prüfungsausschuss, zweite/r Gutachter/in: Prof. Dr. Thomas Oertner

Contents

1. Introduction:

1.1 Autism spectrum disorders (ASDs)

ASDs is a neurodevelopmental disorder (NDD) that has no single known cause, with a variety of symptoms and severity between the individuals. ASDs affect a high proportion of the human population, with an incidence of 1 in 54 children (Maenner et al., 2020). ASD individuals, however, have common symptoms, typically including impaired social interaction, cognitive, and repetitive behaviors (Belmonte et al., 2004). Genetics and environmental factors contribute significantly to the onset of this disorder. There is recent evidence showing that ASDs are highly inheritable developmental disorders affecting neuronal dendritic tree development, synaptogenesis, and excitatory/inhibitory balance (Kulkarni & Firestein, 2012; Südhof, 2008). The pathology of the NDDs, including autism, is greatly influenced by the aberrant brain connectivity, where defects in axonal projections and synapses contribute to the development of ASD in autistic patients and mouse models (Bourgeron, 2015; Cline, 2005). It is noteworthy that translational control at the level of growth cones and synapses plays an essential role in axonal connectivity and synaptic plasticity (Glock et al., 2017). Thus, one of the known hypothesis for the development of the ASDs is the altered translation control machinery resulting in upregulated protein synthesis at the synaptic level (Kelleher et al., 2008).

Genetic studies have revealed a great association of the copy number variations (CNVs) with the neurodevelopmental and neuropsychiatric conditions including ASDs (Cook & Scherer, 2008), which are encountered frequently in the human 16p11.2 locus, which contains 31 genes, (Steinberg et al., 2014). The *16p11.2* microdeletion is linked to ASDs and contributes to approximately 1% of all diagnosed cases of ASD (Weiss et al., 2008). In contrast, reciprocal microduplications of the *16p11.2* lead to schizophrenia (McCarthy et al., 2009). However, it remains unclear which of the ~30 genes localized in the *16p11.2* region is causally related to behavioral, functional, and anatomical changes observed in ASDs.

1.2 Thousand and one amino acid kinase 2 (TAOK2)

The human *TAOK2* gene is localized in the *16p11.2* chromosomal region and implicated in neurodevelopmental disorders (Weiss et al., 2008). TAOK2 is a member of the mammalian sterile 20 (STE20)-like kinases family and of the MAP3K family and encodes a serine/threonine kinase (Moore et al., 2000). The *TAOK2* gene is highly

expressed in the human brain during the early stages of development and its regulation is under control of FMRP, making it a high-risk gene associated with CNVs. (Darnell et al., 2011). Additionally, changes in the expression of the *TAOK2* gene in ASD patients with 16p11.2 CNVs have the greatest association with head diameter in comparison to other *16p11.2* genes (Luo et al., 2012). Recently, *TAOK2* gene-dosage-dependent abnormalities in multiple brain regions size were described. The *TAOK2* deficient mouse model reveals similar anatomical, physiological, and behavioral abnormalities identified in *16p11.2* deletion mice models and patients (M. Richter et al., 2019). Importantly, *Taok2* $^{d/d}$ mice show abnormalities in brain morphology with increased volume in subcortical structures and reduced cortex volume (M. Richter et al., 2019), resembling the phenotype of the*16p11.2* deletion mouse model (Portmann et al., 2014). Semi deficiency or complete removal of *TAOK2* in heterozygous and knockout (KO) mice models respectively show abnormalities in cognition and social behaviors in a gene dosage-dependent manner. In addition to the morphological abnormalities observed in the brain size of *TAOK2* knockout mice, *TAOK2* deficient mice have synaptic and dendritic deficits and abnormalities in hippocampal-prefrontal brain connectivity (M. Richter et al., 2019). Interestingly, no other gene from the *16p11.2* chromosomal region has yet been related to morphological abnormalities in the brain (Escamilla et al., 2017), which suggests that TAOK2 might be a crucial contributor to the phenotypes described for *16p11.2* CNV carriers.

1.2.1 TAOK2 isoforms and function

There are two isoforms of murine TAOK2, the long TAOK2α isoform with 1235 amino acids and the shorter TAOK2β with 1049 amino acids. Both TAOK2-α/β isoforms share the exon 1-16 (same residues 1 to 745); however, they have an alternative C-terminal composition (Mitsopoulos et al., 2003; Yasuda et al., 2007) but it is less understood, how each isoform plays a different role in the brain. Whole-genome and exome sequencing of ASD families different from the *16p11.2* microdeletion cohort identified novel *de novo* and inherited mutations in both isoforms of TAOK2 (M. Richter et al., 2019).

TAOK2 participates in the regulation of microtubule dynamics and organization in cell lines (Moore et al., 2000), where residues 1064-1235 of TAOK2 isoform α were identified as microtubule-binding domain (Mitsopoulos et al., 2003). Moreover, the autophosphorylation of the kinase domain of TAO2 (1-320) is important to initiate kinase

activity (Zhou et al., 2004). In mouse cortex, the interplay of TAOK2, receptor protein Sema3A (Semaphorin 3A) and Nrp1 (Neuropilin 1) leads to reduction in axonal growth and dendrites in the excitatory neurons via stimulation of the c-Jun N-Terminal Kinase (JNK) pathway (De Anda et al., 2012). TAOK2, specifically the isoform β, is necessary during activity-dependent synapse growth as it facilitates N-Cadherin internalization (Yasuda et al., 2007). Furthermore, phosphorylation of TAOK2 by MST3 regulates synapse development in cultured neurons from the hippocampus through binding and relocation of Myosin Va (Ultanir et al., 2014). Additionally, TAOK2 phosphorylates Septin7 kinase which stabilizes PSD95 in dendritic spines and enhances spine maturation (Yadav et al., 2017). Finally, a recent study performed by us has clearly demonstrated that *TAOK2* is a high-risk gene for NDDs through regulation of RhoA-mediated signaling, where TAOK2β but not TAOK2α, binds RhoA and controls spine formation and synapse development (M. Richter et al., 2019).

In non-neuronal cells, TAOK2 has been involved in apoptosis induction by modulating the cellular morphology via TAOK2/ JNK/ caspase activation pathway after stimulation by apoptosis-inducing agents (Zihni et al., 2006). TAOK2 has been identified to be a target substrate for caspases (Zihni et al., 2006, 2007) and is involved in the Hippo signaling cascade, which suggests that TAOK2 is a tumor suppressor gene (Fang et al., 2020). In this regard, transcriptome analysis of lung adenocarcinoma revealed TAOK2 downregulation compared to its level in the normal lung (Ya Li et al., 2020). These studies showed the role of dysregulated TAOK2 in development of the tumor however, the role of TAOK2, as a tumor suppressor is not well understood.

1.3 Translation Regulation in ASDs

Disturbances in the functional components that control translation are implicated in several human diseases including cancers, neuropsychiatric disorders, and metabolic disorders. Additionally, genetic mutations associated with abnormal translation have been recognized in many NDDs (Scheper et al., 2007), e.g., ASDs and epilepsy.

Firstly, I would like to give a brief overview of the eukaryotic translation before writing about translation dysregulation in ASD.

1.3.1 Eukaryotic translation:

Translation of cellular mRNAs into proteins is a highly regulated process in gene expression. Controlling translation of the existing mRNAs permits adaptive protein

changes faster than the transcriptional regulation in response to different endogenous or exogenous stimuli (Gingras et al., 2001). Thus, translation regulation is important in modulating gene expression and subsequent maintenance of protein levels in response to different physiological or pathological processes. Of note, neurons are highly specialized cells that depend on gene regulation for the maintenance of their normal morphology and synaptic function (Kapur et al., 2017). Generally, the translation process includes four main cyclic stages of initiation, elongation, termination, and recycling of ribosomes (Schuller & Green, 2018) (Figure 1).

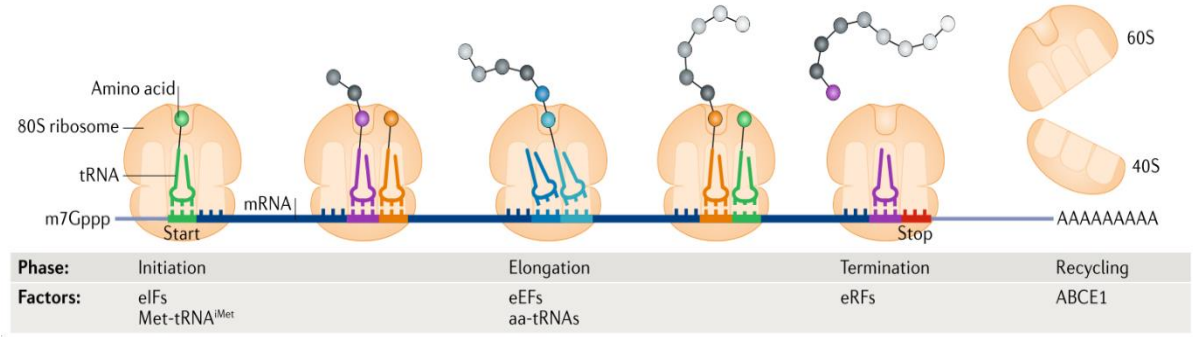

Figure 1: Overview of the eukaryotic translation process. Translation is a cyclic series of initiation, elongation, termination, and recycling where untranslated mRNA and the ribosomal subunits, eukaryotic translation factors, and tRNAs orchestrate to be translated. Figure modified from (Schuller & Green, 2018)

1.3.1.1 Translation initiation

It is the first step of the translation process, where the mRNAs engage in cap-dependent translation initiation and recognition of the AUG start codon (Kapur et al., 2017). Many eukaryotic translation initiation factors (eIFs) are involved in the assembly of an 80S ribosome at the AUG start codon. Translation initiation starts by binding of eukaryotic initiation factor eIF2 to the GTP and the initiator methionyl-tRNA (Met-tRNAi) to form the ternary complex (eIF2-GTP-tRNAiMet). The small 40s ribosomal subunit binds to the ternary complex together with other initiation factors eIF1, eIF1A, eIF5, and eIF3, and forms the 43S preinitiation complex (PIC) (Aitken & Lorsch, 2012). The 43S PIC binds to the mRNA through its recruitment to the 5´ methylguanine mRNA Cap. This recruitment process is facilitated by eIF4F complex (eIF4E, eIF4G proteins and the helicase eIF4A) (Hinnebusch & Lorsch, 2012). The scaffolding eIF4G interacts with eIF3 and stabilizes the PIC and interacts with poly (A) binding protein (PABP) leading to mRNA circularization. This resulting complex migrates and scans along the

5’UTR of the transcript with the start codon at the suitable context of the initiator tRNA anticodon in a process of ribosome scanning (Hinnebusch, 2017).

1.3.1.2 Translation elongation

It is the second step of mRNA translation where the functional 80S ribosomes move progressively along the mRNA to synthesize the encoded amino acids. This process is accomplished by coordinated events of aminoacyl- tRNAs and eukaryotic elongation factors (eEFs) (Schuller & Green, 2018).

1.3.3.3 Translation termination and ribosome recycling.

Translation termination in eukaryotes starts when the elongating ribosomes face a stop codon (UAA, UGA, or UAG) in the ribosomal A site (Dever & Green, 2012). eRF1 and eRF3 are release factors involved in the termination process in the eukaryotes. eRF1 is the main catalytic factor in translation termination and is delivered to the ribosomes by the GTPase, eRF3 (Frolova et al., 1996).

Following translation termination, the ATP binding cassette protein 1 (ABCE1) interacts with eRF1. This interaction dissociates the 80S complex and its uncharged tRNA in the ribosomal P site into 40S and 60S ribosomal subunits. After the release of the mRNA and the deacylated tRNA, the dissociated ribosomal subunits rebind to the initiation factors for another round of translation initiation in a process called ribosome recycling (Pisarev et al., 2007).

1.3.2 Dysregulated protein synthesis associated with ASDs:

Several human disorders due to mutations in one single gene are often associated with cognitive abnormalities and are linked to autism. Moreover, the products encoded by the mutated gene in several monogenic disorders are associated with ASDs symptoms and act as a repressor of protein synthesis (Kelleher et al., 2008).

1.3.2.1 Fragile X syndrome (FXS)

Translational control has been identified as a player in learning and memory functions, and its abnormal regulation is implicated in many neuropsychiatric disorders. Fragile X syndrome (FXS) is one of these disorders firstly identified as a genetic disorder that connects translation regulation to cognition (Verkerk et al., 1991). FSX is considered a major reason for hereditary mental retardation due to functional loss of the Fragile X mental retardation gene *(FMR1)* at the X chromosome (Bagni & Greenough, 2005). FMRP, a protein encoded by the *FMR1* gene, is an RNA-binding protein involved in

mRNA translation regulation (Bagni & Greenough, 2005) and associated with certain neuronal mRNAs and inhibit their translation (Zalfa et al., 2007). At the synaptic level, FMRP inhibits translation through its binding partner CYFIP1 that directly interacts with the initiation factor eIF4E and leads to blockage of cap-dependent initiation (Napoli et al., 2008).

1.3.2.2 ASD linked disorders associated with Ras/ERK and PI3K/mTOR signaling pathways

Activation Ras/ERK signaling cascade and PI3K/mTOR pathways, especially the mammalian target of rapamycin complex1 (mTORC1) is observed in several disorders linked to ASD and cognitive abnormalities such as neurofibromatosis type 1 (NF1) (Bailey et al., 1998), Phosphatase and tensin homolog (PTEN) (Butler et al., 2005) and Tuberous sclerosis complex (TSC) (Ehninger & Silva, 2011). mTORC1 activation plays a role in neuronal translation through its activator effect of cap-dependent translation (Figure 2) (Kelleher et al., 2008).

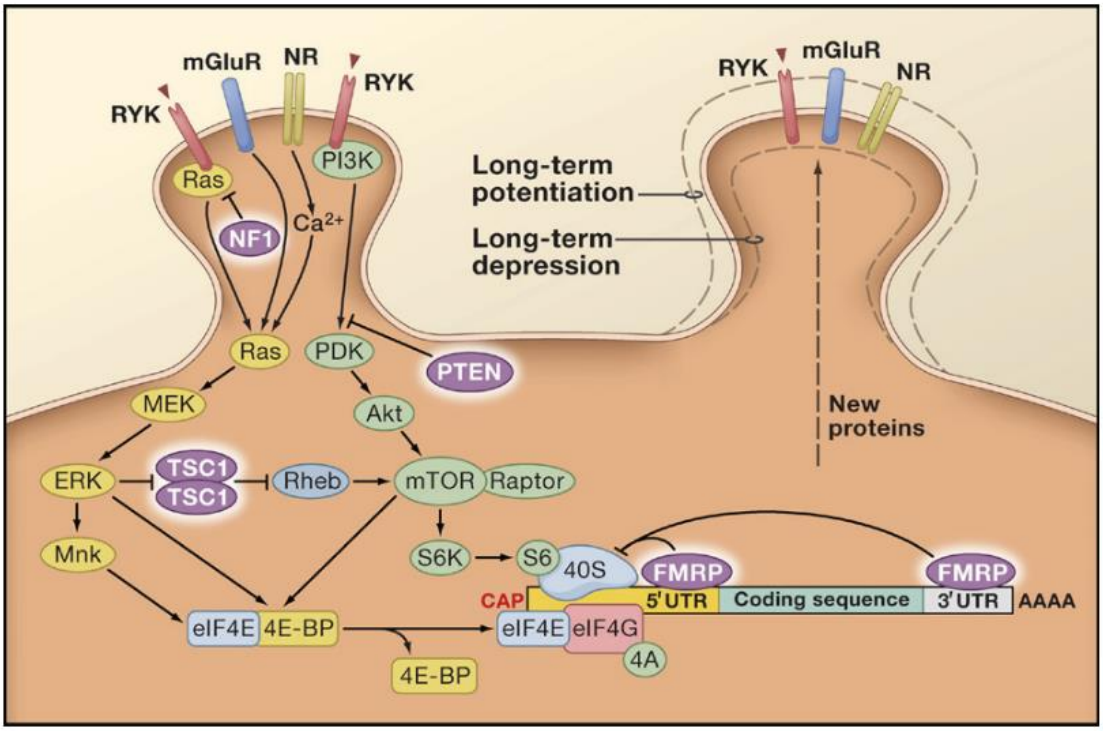

Figure 2: Neuronal Signaling Pathways in Translational Regulation in neuron: Figure modified from (Kelleher et al., 2008).

Inactivating mutations in the neurofibromin 1 (NF1) gene cause Neurofibromatosis type I disease. Normally, NF1's GTPase-activating protein inhibits the activity of

the Ras/ERK pathway, while its inactivation leads to upregulation of Ras signaling and its downstream effectors and PI3K/mTOR pathways (Dasgupta & Gutmann, 2003).

Mutations in TSC1 that encodes hamartin or TSC2 that encodes tuberin causes a Tuberous sclerosis complex (TSC), a neurodevelopmental autosomal disorder characterized by neuropathies associated with ASDs (Kwiatkowski & Manning, 2005). TSC1/2 inhibits the mTORC1 signaling pathway through formation of a complex between its GTPase activating domain and the small GTP-binding protein Ras homologue enhanced in brain (RHEB) (Hoeffer & Klann, 2010). Thus, TSC1/2 loss enhances activity of mTORC1 (Sarbassov et al., 2005), and subsequent activation of translation.

PTEN lipid phosphatase is considered as another inhibitor for the phosphatidylinositol 3-kinase (PI3K)-mTOR signaling pathway and is involved in ASD parthenogenesis. Mechanistically, PTEN counteracts the PI3K-dependent pathway through dephosphorylation of PI3P to PIP2 and subsequent down-regulation of the pathway. PTEN dysfunction leads to increased mTORC1 activity in neurons (Kwon et al., 2006), and has been noticed in about 5% of ASD patients with marked macrocephaly (Butler et al., 2005). Interestingly, there is a link between PTEN mutations and macrocephaly, because the PI3K-mTOR signaling pathway is involved in cell size regulation via translation control mediated action (Fingar et al., 2002).

The genes mentioned above regulate mTOR-signaling pathways, and mTORC1 activation directly stimulates translation. There are different well-known mTORC1 substrates regulate translation such as the p70 ribosomal S6 protein kinases (P70S6K) and the initiation factor 4E-BPs. The p70 ribosomal kinases, are 2 kinases S6K1 and S6K2 encoded by different genes and both kinases phosphorylate the ribosomal protein S6 (S6) (Fenton & Gout, 2011). Additionally, S6K1 regulates translation initiation through phosphorylation of the initiation factor eIF4B and polypeptide elongation rate by phosphorylation of the eukaryotic elongation factor 2 kinase (eEF2K) (Ma & Blenis, 2009). Once eEF2 is phosphorylated at Thr56, it becomes inactivated and cannot bind to the ribosomes leading to translation inhibition (CARLBERG et al., 1990). Furthermore, mTORC1 regulates cap-dependent translation, which is a major step in translation initiation. While the action of eIF4E is blocked by binding of 4E-BPs and inhibiting its association with the mRNA; thus, deactivating translation initiation (J. D. Richter &

Sonenberg, 2005), activation of mTORC1 leads to phosphorylation of 4E-BPs and release of the sequestrated eIF4E to associate and activate the mRNA cap structure (Sonenberg & Hinnebusch, 2007).

1.4 Hypothesis and Aims of the project

TAOK2 regulates multiple cellular processes depending on its kinase-dependent or - independent activity, which affects the activity of the target molecules or its ability to bind and regulate other molecules. Previous studies showed that TAOK2 plays a role in dendritic arborization (De Anda et al., 2012), synapse development (Yadav et al., 2017; Yasuda et al., 2007), and maintenance of normal synaptic connectivity in different brain regions (M. Richter et al., 2019). Furthermore, TAOK2 has been associated with different cellular processes in non-neuronal cells, such as development, differentiation, and cell growth (Fang et al., 2020). Thus, deficiency of TAOK2 might contribute to the pathogenesis of several neurodevelopmental disorders like ASDs and cancers. How TAOK2 is contributing to these processes, however, is still not well understood. Interestingly, proteins controlling translational machinery were identified as potential interaction partners of TAOK2 (Ultanir et al., 2014). Furthermore, we showed that TAOK2α is localized with the microtubule's network in developing neurons, whileTAOK2β is present in the spines and maintains normal synapse development (M. Richter et al., 2019). Therefore, I envision that TAOK2 might regulate these different physiological and pathophysiological pathways implicated in neuronal development through the regulation of translation control.

Disturbances in the translational control are associated with many NDDs including ASDs (Scheper et al., 2007) and different genes associated with ASD such as *FMRP, PTEN, and TSC* are involved in translation regulation either directly or indirectly (Kelleher et al., 2008). Despite the importance of TAOK2 in brain development and its association with ASD, the role of the TAOK2 in translation control at the molecular and cellular levels is not well understood. Thus, it is noteworthy to investigate the role of the novel ASD risk gene TAOK2 (SFARI Category 2; strong ASD risk gene; *https://gene.sfari.org/database/human-gene/TAOK2*) in translational control. Accordingly, the specific aims of my project were: 1) To identify the association of TAOK2 with translational control machinery complex and its effect the global translation. 2) To determine the isoform-specific effect of TAOK2 on translation control 3) To determine the

mechanism by which TAOK2 regulates translation control. 4) To test whether reintroduction of TAOK2 in cortices of *16p11.2* microdeletion mice rescues potential translational control defects. To achieve these aims, I took advantage using different translational and protein analytic assays on brain tissues and cortical neurons from different mice models lacking *Taok2* or *16p11.2* microdeletion, N2a cells and lymphoblastoid cells derived from autistic patients with *TAOK2* de novo mutations.

2. Material and Methods:

Animals

C57BL6/J *TAOK2* Knock out (*TAOK2* $^{d/d}$) mice were generated as previously described (Kapfhamer et al., 2013; M. Richter et al., 2019) and *16p11.2del* $^{+/d}$ (Horev et al., 2011). Animals were raised, genotyped, and housed with the standard regulations at the Central Animal Facility at University Medical Center Hamburg-Eppendorf, Hamburg (UKE). All mice experiments were performed according to the German and European Animal Welfare Act. The used experimental procedures have the approval of the Animal Research Ethics Board (AREB), the local authorities of the State of Hamburg (TVA N007/2018), and the animal care committee of UKE. The animals used in this study were four weeks old mice from both genders.

2.1 Materials

2.1.1 Medium and reagents for cell culture:

Primary neuron culture reagents

Reagent	Source	Final concentration
Primary Neuro Basal Medium	Invitrogen (21103049)	1x (500mL)
L- Glutamine 200mM	Invitrogen (25030024)	2 mM
B 27 Supplement	Invitrogen	1X
HBSS (without CA^{2+}/Mg^{2+})	Invitrogen (14170088)	0.25% (vol/vol)
DMEM with GlutaMAX	Invitrogen (6196526)	1x (500mL)
FBS	Gibco (105000649	10 %
Pen/Strep	Invitrogen (15140122)	1X
Poly-L-Lysine (PLL)	Sigma (P2636-500mg)	5µg /ml
Laminin	Sigma (L2020)	3-5µg/ml
Hibernate E buffer	Invitrogen	1X

Papain	Sigma (P5306-25mg)	31.25µg/ml
DNase I	Sigma (D4263-5VL)	10µg/ml
Cytosine β-D- arabinofuranoside (Ara-C)	Sigma (C1768-100g)	0.5 µM

Neuro-2a (N2a) cell culture reagents

Reagent	Source	Final concentration
DMEM with GlutaMAX	Invitrogen (6196526)	1x (500mL)
FBS	Gibco (10500064)	10 %
Pen/Strep	Invitrogen (15140122)	1X
L- Glutamine 200mM	Invitrogen (25030024)	2 mM
0.25% Trypsin – EDTA	Gibco (25200056)	1X

Lymphoblastoid cell line cells (LCLs) reagents

Reagent	Source	Final concentration
RPMI 1640	PAN Biotech (P04-18500)	1x (500mL)
FBS	Gibco (10500064)	15 %

2.1.2 Plasmids:

Plasmids used for transient transfection of N2a cells

Plasmid name	Plasmid information
pCMVhuTAOK2β-myc (short variant)	Plasmid encodes humanTAOK2-short variant with Myc tag sequence and pCMV6-entry as a vector backbone
pCMVhuTAOK2α-myc (long variant)	Plasmid encodes humanTAOK2-long variant with Myc tag sequence and pCMV6-entry as a vector backbone
pCMVhuTAOK2β_A135P	Site directed de novo mutated plasmid at the kinase domain of TAOK2β with Myc tag sequence and pCMV6-entry as a vector backbone
pCMVhuTAOK2α _A135P	Site directed de novo mutated plasmid at the kinase domain of TAOK2α with Myc tag sequence and pCMV6-entry as a vector backbone

pCMVhuTAOK2β_P1022*	Site directed de novo mutated plasmid at the regulatory domain of TAOKβ and pCMV6-entry as a vector backbone
pSuperRNAi-TAOK2	Plasmid containing short RNA interfering gene for TAOK2 on a pSuperRNAi as a vector backbone
pCDNA3.1-myc	Plasmid expressing Myc at the c terminal region used as a positive control for transfection
pEGFP-F	Plasmid encoding the enhanced GFP sequence with a farnesylated signal

Plasmids used for in utero electroporation for the neurons

Plasmid name	Plasmid information
pAAV-CAG hu-TAOK2β wt	Plasmid encodes humanTAOK2-short variant with pAAV-CAG as a vector backbone
pAAV-CAG-tDimer	Plasmid encoding the tDimer tagged to the RFP with the pAAV as a vector backbone

2.1.3 Polysomes profiling reagents of the brain regions:

Polysomes lysis buffer for the cortex

Reagent	Source	Final concentration
HEPES KOH (pH7.4)		20 mM
KCl	Roth (6781.1)	150 mM
$MgCl_2$	Thermo Fisher Scientific (AM9530G)	5 mM
Dithiothreitol (DTT)	Sigma (D9779)	0,5 mM
Roche Mini Complete EDTA Free	Roche (11836170001)	1X according to the manufacturer's
Cycloheximide (CHX)	Sigma (C7698)	100 µg/mL
RNAsin	Promega (N2515)	40 U/mL
Superasin	Invitrogen (AM2694)	20 U/mL
Triton X-100	Roth (3051.2)	1% (vol/vol)
NP- 40	Thermo Fisher Scientific (85124)	1% (vol/vol)

Polysomes lysis buffer for the cerebellum

Reagent	Source	Final concentration
HEPES KOH (pH7.4)		20 mM
KCl	Roth (6781.1)	150 mM
$MgCl_2$	Thermo Fisher Scientific (AM9530G)	12 mM
Dithiothreitol (DTT)	Sigma (D9779)	0,5 mM
Roche Mini Complete EDTA Free	Roche (11836170001)	1X according to the manufacturer's
Cycloheximide (CHX)	Sigma (C7698)	100 µg/mL
RNAsin	Promega (N2515)	40 U/mL
Superasin	Invitrogen (AM2694)	20 U/mL
1,2-diheptanoyl-sn-glycero-3-phosphocholine (DHPC)	Merck (850306P-500MG)	300 mM
NP-40	Thermo Fisher Scientific (85124)	1% (vol/vol)

Polysomes gradient buffer for cortex and cerebellum

Reagent	Source	Final concentration
Tris-HCl (pH7.4)		20 mM
NaCL	Roth (HN00.2)	150 mM
$MgCl_2$	Thermo Fisher Scientific (AM9530G)	10 mM
Dithiothreitol (DTT)	Sigma (D9779)	1 mM
Cycloheximide (CHX)	Sigma (C7698)	100 µg/ml

2.1.4 Polysomes profiling reagents N2a cells:

Polysomes lysis buffer of N2a cells

Reagent	Source	Final concentration
Tris-HCl (pH7.4)		20 mM
KCl	Roth (6781.1)	100 mM
$MgCl_2$	Thermo Fisher Scientific AM9530G	5 mM
Dithiothreitol (DTT)	Sigma (D9779)	0,5 mM

Roche Mini Complete EDTA Free	Roche (11836170001)	1X according to the manufacturer's
Phospho STOP	Roche (4906845001)	1X according to the manufacturer's
Cycloheximide (CHX)	Sigma (C7698)	100 µg/mL
RNAsin	Promega (N2515)	40 U/mL
Superasin	Invitrogen (AM2694)	20 U/mL
Turbo DNase I	Invitrogen (AM2694)	25 U/ ml
Triton X-100	Roth (3051.2)	1% (vol/vol)
NP-40	Thermo Fisher Scientific (85124)	1% (vol/vol)

Polysomes gradient buffer for N2a cells

Reagent	Source	Final concentration
Tris-HCl (pH7.4)		20 mM
KCL	Roth (6781.1)	100 mM
$MgCl_2$	Thermo Fisher Scientific (AM9530G)	5 mM
Dithiothreitol (DTT)	Sigma (D9779)	1 mM
Cycloheximide (CHX)	Sigma (C7698)	100 µg/mL

2.1.5 Polysomes profiling reagents for LCLs:

Polysomes lysis buffer for LCLs

Reagent	Source	Final concentration
Tris-HCl (pH7.4)		20 mM
KCl	Roth (6781.1)	100 mM
MgCl2	Thermo Fisher Scientific (AM9530G)	10 mM
Dithiothreitol (DTT)	Sigma (D9779)	0,5 mM
Roche Mini Complete EDTA Free	Roche (11836170001)	1X according to the manufacturer's
PhosSTOP	Roche (4906845001)	1X according to the manufacturer's
Cycloheximide (CHX)	Sigma (C7698)	100 µg/mL
RNAsin	Promega (N2515)	40 U/mL

Superasin	Invitrogen (AM2694)	20 U/mL
Turbo DNase I	Invitrogen (AM2694)	25 U/ ml
Triton X-100	Roth (3051.2)	1% (vol/vol)
NP-40	Thermo Fisher Scientific (85124)	1% (vol/vol)

Polysomes gradient buffer for LCLs

Reagent	Source	Final concentration
Tris-HCl (pH7.4)		20 mM
KCL	Roth (6781.1)	100 mM
$MgCl_2$	Thermo Fisher Scientific (AM9530G)	5 mM
Dithiothreitol (DTT)	Sigma (D9779)	1 mM
Cycloheximide (CHX)	Sigma (C7698)	100 µg/mL

2.1.6 Buffers for the acute brain slices:

Cutting buffer

Reagent	Final concentration
NaCl	85 mM
Sucrose	75 mM
KCL	2.5 mM
Glucose	25 mM
NaH_2PO_4	1.25 mM
$MgCl_2$	4 mM
$CaCl_2$	0.5 mM
$NaHCO_3$	24 mM

Oxygenated artificial cerebrospinal fluid (ACSF)

Reagent	Final concentration
NaCl	127 mM
$NaHCO_3$	25 mM
D-Glucose	25 mM
NaH_2PO_4	1.25 mM
KCl	2.5 mM
$MgCl_2$	1 mM

30 minutes bubbling by Carbogen	
$CaCl_2$ (after bubbling)	2 mM
Adjust pH to 7.4 by using NaOH	

2.1.7 Western blot buffers:

Lysis buffer (RIPA buffer)

Reagent	Source	Final concentration
Tris-HCl (pH7.4)		50 mM
NaCl	Roth (HN00.2)	150 mM
EGTA	Roth (3054.2)	1 mM
NP-40	Sigma (I3021-100ml)	1% (vol/vol)
Sodium deoxycholate	Sigma	0.25% (vol/vol)
Na_3VO_4	Sigma (S6508-10g)	10 mM
NaF	Sigma (S7920-100g)	10 mM
Complete mini EDTA-free protease inhibitor cocktail	Roche (11836170001)	1X

Running buffer

Reagent	Source	Final concentration
SDS-Running buffer 10x (Tris, Glycine, SDS)	Bio-Rad	1X

Transfer buffer

Reagent	Source	Final concentration
SDS-Running buffer 10x (Tris, Glycine, SDS)	Bio-Rad	10%
Methanol	Roth	20%
ddH_2O		

Tris- buffered saline with Tween-20 (TBST)

Reagent	Final concentration
Tris (pH 7.5)	20 mM
NaCl	150 mM
Tween 20	0.1%

Stripping buffer

Reagent	Source	Final concentration
Tris-HCl (pH 6.8)		
SDS 20% Roti-Stock	Roth	2%
2-β Mercaptoethanol	Invitrogen	0.1 M

2.1.8 Antibodies:

Primary Antibodies

Antibody name	Host	Source	Application and dilution
Taok 2β, Polyclonal	Rabbit	SY SY (395003)	WB 1:1000 ICC 1:250 IP 10µg
IgG, Polyclonal	Rabbit	Sigma	IP 10µg
Puromycin, clone 12D10, monoclonal	Mouse	Millipore (MABE343)	WB 1:10000 IHC, ICC 1: 5000
MAP 2, Polyclonal	Chicken	SY SY (188006)	IHC 1:500
Beta3-tubulin (Tuj1)	Guinea pig	SY SY (302304)	ICC 1:500
β - Actin, monoclonal	Mouse	Sigma (A5316)	WB 1:2000
β - Actin (13E5), monoclonal	Rabbit	CST (4970)	1:5000
Myc-Tag (71D10) mAb	Rabbit	CST (2278)	WB 1:1000 ICC 1: 300
eIF2α (L57A5), monoclonal	Mouse	CST (2103)	WB 1:1000
Phospho- eIF2α, monoclonal	Rabbit	CST (3398S)	WB 1:1000
Phospho-eEF2 (Thr56), Polyclonal	Rabbit	CST (2331)	WB 1:1000
eEF2, clone 4B3-G7-H5, monoclonal	Mouse	Abcam (ab131202)	WB 1:2000

Secondary Antibodies

Antibody name	Host	Conjugate	Source	Application and dilution
Rabbit IgG	Goat	HRP	Dianova (111-035-003)	WB 1:5000

Mouse IgG	Goat	HRP	Dianova (115-035-003)	WB 1:5000
Rabbit IgG	Donkey	AF 647	Invitrogen (A315739)	ICC 1:400
Mouse IgG	Donkey	AF 488	Invitrogen (A21202)	ICC 1:400
Mouse IgG	Donkey	AF 568	Invitrogen (A10037)	IHC 1:300
Guinea Pig IgG	Goat	AF 647	Invitrogen (A21450)	ICC 1:300

2.1.9 Phosphate buffer saline (PBS) 1x

Reagent	Final concentration
NaCl	137 mM
KCl	2.7 mM
Na_2HPO_4	10 mM
KH_2PO_4	1.8 mM

2.1.10 Other Materials

Reagent	Source
Acrylamide 30% = Rotiphorese Gel 30	Roth
Tetramethylethylendiamin (TEMED)	Roth
Isopropanol = 2-Propanol	Roth
Ammoniumperoxidisulfat	Roth
Luminol	Roth
β-Mercaptoethanol 50mM	Invitrogen
p-Cumaric acid	Roth
Protein ladder Page Ruler prestained	Bio-Rad
SDS 20% Roti-Stock	Roth
Hydrogen peroxide 30%	Roth
Fluoromount-G	Southern Biotech 0100-01
Hydrochloric acid 37%	Roth
Trichloroacetic acid (TCA) 20%	Roth
Acetone	Sigma
Ethylenediaminetetraacetic acid (EDTA)	Sigma
Polyvinylidene fluoride (PVDF) membranes	Roth
Skim Milk blotting grade	Roth

Bovine Serum Albumin BSA fraction V	Roth
Puromycin	Sigma (P8833)
Cycloheximide	Sigma (01810)
Pierce™ BCA Protein Assay Kit	Thermo Fisher Scientific (23225)
Revert™ 700 Total Protein Stain for Western Blot Normalization	Licor (926-11010)
Amicon Ultra -15 centrifugation filter	Millipore (UFC910024)
(Roti®-Blue) staining solution (Roth)	Roth (A152.1)
Nitric Acid	Roth
Triton X-100	Roth (3051.2)
Mowiol	Roth (0713.2)
Donkey Serum	Sigma (D9663)
Hoechst (4′,6- diamidino-2-phenylindole) (DAPI)	Invitrogen (33258)
Dynabeads Protein A	Invitrogen (10002D)
Open-Top Polyclear centrifuge tubes (14 × 95 mm)	Seton, Petaluma, CA
Gradient Master 108 programmable gradient pourer	Biocomp
SW40Ti rotor and Beckman L7 ultracentrifuge	Beckman Coulter
Piston Gradient Fractionator	Biocomp
UV monitor	BioRad, Hercules, CA

2.2. Methods:

2.2.1 In utero electroporation (IUE)

E14.5-E15 pregnant *16p11.2del* $^{+/d}$ mice were injected subcutaneously with buprenorphine (0.1 mg/kg body weight) as a pre-operative analgesic. 30 minutes post-injection, mice were then anesthetized with isoflurane/O_2 inhalation (4% and 2–3% for induction and maintenance, respectively). Oxygen flow rate 0.65L/minute and the isoflurane were delivered by a vaporizer (Föhr Medical Instruments, Seeheim- Oberbeerbach, Germany). Later, the uterine horns were exposed and a combination of TAOK2β (2.5 µg/µl) and tDimer plasmids (0.3 µg/µl) was injected into the lateral ventricles of each embryo. Five current pulses (50ms pulse, 950ms interval; 35mV) were administrated across the heads of the embryos. Following surgery, 2-3 drops meloxicam (0.2-1 mg/kg

body weight) were provided to the mice orally with soft food to relief post-operative pain, until they were euthanized for embryo collection.

2.2.2. Cell Culture:

2.2.2.1 Primary cortical neuron culture

Culturing of primary cortical neurons was performed as described previously by (Kwan et al., 2016). Pregnant heterozygous *TAOK2* $^{+/d}$ or *16p11.2del* $^{+/d}$ mice were anesthetized with CO_2/O_2 mixture before head decapitation. Later, the abdomen was opened, and the uterine horns were exposed and the E17.5 embryos were taken out from the uteri. The head of each embryo was decapitated followed by opening of the skull and the brains were collected in 24 well plate containing HibernateTM-E medium on ice until the embryos were genotyped. Following genotyping, separation of brain hemispheres, careful removal of meninges, cerebellum, hippocampi, and the brain stem, and dissection of the cortices were performed on ice under a dissecting microscope. The dissected cortex per single embryo was first digested with papain plus DNase I for 10 minutes at 37°C. Stopping of Papain digestion was done by adding DMEM + 10%FBS, then with HBSS for washing two or 3 times. Gentle mechanical trituration for the tissue was conducted with a fire-polished Pasteur pipette. Afterwards, cells were then spun down and washed with fresh HBSS and counted. The cells were plated directly either at poly-L-lysine (PLL) or PLL plus laminin pre-coated glass coverslips ($4x10^4$ per coverslip) in Neurobasal/B27 medium. The cells were kept in culture for 7 days in vitro (7DIV) or 21 days in vitro (21DIV) at 37°C with 5% CO2 before treatment with puromycin for measurement of protein synthesis by SUnSET assay and immunofluorescence analysis. 0.5 µM Ara-C was added to the cultured cells on the 7^{th} day in vitro (7DIV) to the cells maintained up to 21DIV to inhibit the growth of the glia cells.

Cortices of *16p11.2del* $^{+/+}$ and *16p11.2del* $^{+/d}$ embryos transfected by the combination of TAOK2β and tDimer plasmids via IUE at E14.5-E15, were isolated two days later (as described above). The transfected cortical regions were identified by the red fluorescent signal and dissected on a cold surface under a stereomicroscope (Olympus SZX16) connected to a UV light source. The cells were prepared and cultured for 7DIV (as described above) before use.

Preparation of coverslips and coating

Coverslips were washed in 65% Nitric acid by vigorous shaking in a tightly sealed container under a fume hood for 2 days. Later, the nitric acid was disposed of into a special

container and the coverslips were rinsed 3 times in ddH_2O to remove the residual acid. The coverslips were rinsed with thorough shaking in ddH_2O at least 5 times each 10 minutes. Following washing, coverslips were washed again with absolute ethanol, placed on 3MM Whatman paper in a petri dish, and dried under the hood. Once the coverslips were dried, they were sterilized under UV for at least 30 minutes. The coverslips were coated overnight with PLL or PLL plus laminin at 37°C in the incubator. On the next day, coverslips were washed three times in a 24 well plate with PBS and ready for use.

2.2.2.2 Neuro 2a (N2a) cell culture:

Maintenance of N2a cell

N2a cells are rapidly dividing cells grow in DMEM + 10%FCS. The cells were passaged 2- 3 times a week in 10 cm when they reached around 90% confluency. Cells passage was done by removal of the old medium from the plate, washing the cells briefly with 1X PBS solution at room temperature (RT). Then, cells were trypsinized using 1ml of 0.25% Trypsin-EDTA, incubating the plate for 2-3 minutes in the 37˚C incubator. The activity of trypsin was stopped by the addition of a pre-warmed medium DMEM containing 10% FBS. The cells were re-suspended in a fresh medium and distributed in additional plates with the required number of cells. The plates were swirled to distribute cells evenly and returned to the incubator at 37°C, 5% CO2.

Transfection of N2a cells

Transient transfection of N2a cells was done using jetOPTIMUS transfection reagent (Cat No. 117-15) according to the manufacturer's guidelines. In brief, the cells were seeded on 10 cm plate 24 hours prior to transfection so that they are 60-80% confluent on the day of transfection. The suggested amount of plasmid DNA 9-10µg (7-8 µg from different TAOK2 variants or empty vector control (pcDNA 3.1) + 2 µg pEGFP-F plasmid) was diluted in 1 ml jetOPTIMUS buffer, followed by vortex 5 second and spin down. This was followed by addition of 12.5 µl jetOPTIMUS reagent, vortexed a few seconds, spun down and the mix was incubated for 10 minutes at RT. Afterward, the transfection mixture was added to the cells in a serum-containing medium. The dish was gently swirled to mix the transfection reagent with the growth media and returned to the incubator. The cells were incubated with the transfection complex for 4 hours at 37°C, 5% CO2 after that the medium containing the transfection complex was replaced by a pre-warmed fresh medium. After 2 hours, the cells were passaged one time into

10 cm dishes or PPL pre-coated glass coverslips depending on the experimental conditions. The cells were co-transfected with different TAOK2 variants and farnesylated-GFP plasmids. Thus, the transfection efficiency was determined directly before harvesting by taking images for GFP expressed signal in control and transfected cells or by immunohistochemical staining using antibodies against the Myc-tag protein or TAOK2β. During imaging the dishes, cells were maintained at 37°C in the microscopic chamber supplemented with 5% CO_2. The images were then captured by CoolSNAP HQ2 camera connected to NIS-Elements AR software, Nikon. The transfection efficiency for each condition were estimated by calculating the percentage of cells expressing the GFP or Myc-tag immune-staining to all cells in the imaged field using the cell counter tool in ImageJ. Only cells with 70-80% transfection efficiency and expressing the DNA constructs were harvested at 40 – 48 hours post-transfection and used for experiments. Importantly, we avoided cell overcrowding as it inhibits the overall translation in the cells.

2.2.2.3 Maintenance of Lymphoblastoid cell line cells (LCLs)

LCLs were generated by using peripheral blood, mainly mononuclear cells confined from the blood of probands and their families, which were immortalized utilizing the Epstein- Barr virus (Hui-Yuen et al., 2011) . LCLs were grown in a standard suspension condition in RPMI 1640 media supplemented with 15% FBS. 200.000 cells/ml were used for starting a culture in 5ml and every 2-3 days the medium was increased to 20 ml and the cells were split to avoid cell over confluency as they are growing in clumps. During the experiments, the cells were sedimented by centrifugation at 1000 r.p.m. for 5 minutes at RT.

2.2.3 Polysome Profiling:

There are different techniques specifically used to study translational regulation such as polysome profiling, ribosome profiling (Ingolia et al., 2009) and translating ribosome affinity purification (TRAP) (Heiman et al., 2008). However, polysome profiling is widely used. The idea of this technique depends on the separation of the translated mRNAs on a sucrose gradient based on the number of ribosomes bound to mRNAs (polysomes), from the untranslated ones. Briefly as depicted in (Figure 3), this method involves loading of cellular cytoplasmic lysate on a sucrose gradient followed by ultracentrifugation step. After centrifugation, the optical density (OD) of the mRNAs is monitored at 254nm and subjected to fractionation. The untranslated mRNAs in the upper

light fractions (less sucrose) are separated from the translationally active polysome-bounded mRNAs in the lower heavy fractions (high sucrose content). mRNA can be extracted from these polysomes fractions and specific mRNA can be subjected to northern blotting or qRT-PCR amplification analysis (Del Prete et al., 2007; Kang & Pomerening, 2012). Alternatively, high-throughput sequencing (HTS) technologies as a global analysis approach can be applied to polysomes fractions content, allowing access to the cellular actively translated mRNAs (translatome) (reviewed by Chassé et al., (2017)). Furthermore, polysome profiling enables analysis of full-length mRNAs that provides access to UTR information for isoform analysis, while ribosome profiling provides access only to the ribosome protected fragments. In addition, proteins can be purified from polysome fractions to be used for western blot and/or proteomics analysis to identify proteins associated with translational machinery ribosomal complexes.

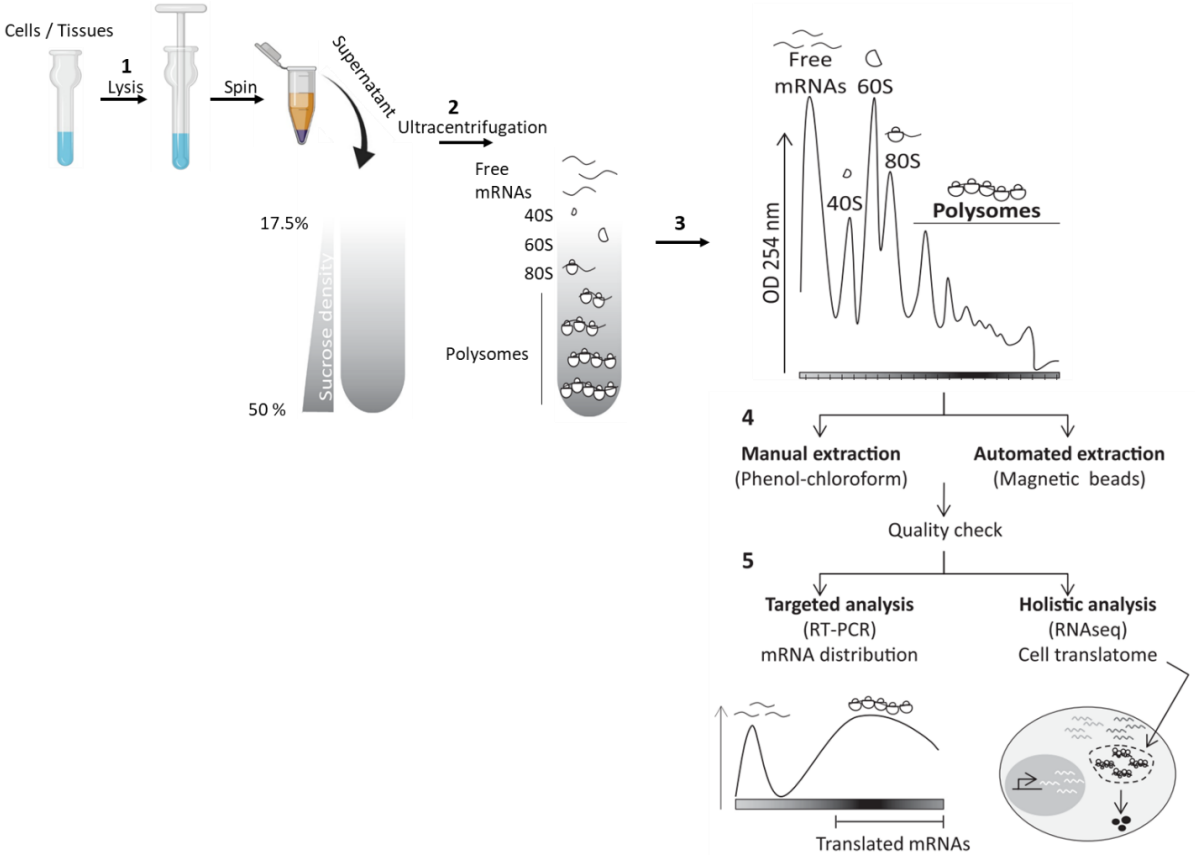

Figure 3: Overview for steps of the polysome profiling protocol to study translation. Figure modified from (Chassé et al., 2017).

Polysome profiling has been extensively used in studying alterations in general translation, such as studying effects of various cellular stress. In response to different

kinds of cellular stress affecting general translation, actively translating mRNAs shift from polysomes to non-translating lighter fractions or vice versa. Polysomes to monosomes (P/M) ratio is widely used as a readout of polysome profiling and provides acceptable evidence for the general translation status.

A critical disadvantage of this approach is the assumption that mRNAs engaged by several ribosomes are actively translated. Messenger ribonucleoprotein (mRNP) complexes (untranslated mRNAs bind to RNA-binding proteins) and stalled ribosomes have been shown to co-sediment in the same polysome fractions during sucrose purification (Graber et al., 2013). Thus, it is important to ensure that the mRNAs in the polyribosome complex in heavy fractions are engaged to actively translating ribosomes. EDTA and puromycin are widely used to disrupt polysomes. EDTA is a Mg^{2+} chelator agent that dissociates mRNPs and the ribosomal subunits from the polyribosome complex. On other hand, puromycin antibiotic dissociates ribosomes by selectively targeting actively translating polysomes during the elongation step of translation (Azzam & Algranati, 1973).

In this study, I used polysome profiling analysis for different brain tissues, LCLs and N2a cells to study general translation as following:

2.2.3.1 Polysome profiling of the brain regions

Frozen dissected cortices (prefrontal and somatosensory) from four weeks old *TAOK2* $^{+/+}$, *TAOK2* $^{+/d}$, and *TAOK2* $^{d/d}$ mice and cerebella from *TAOK2* $^{+/+}$ and *TAOK2* $^{d/d}$ mice were used for profiling. The cortex was lysed in 600ul ice-cold from polysome lysis buffer of the cortex, and the cerebellum was lysed 400ul from a similar lysis buffer containing 12 mM $MgCl_2$ using a glass homogenizer. The resulting lysates were transferred to a prechilled microcentrifuge tubes on ice and centrifuged for 10 minutes at 2,000 x g at 4°C to clear the large cellular debris. The resulting supernatants were transferred to new pre-chilled microcentrifuge tubes. Mixture of detergents from NP-40 and Triton X-100 (up to 1% final concentration) were then added to the cortical lysates, while the NP-40 and DHPC up to 1% final concentration and 300 mM, respectively, were added to the cerebellar lysates, and incubated on ice for 5 minutes. Afterward, the lysates were centrifugated for 10 minutes at 20,000 x g at 4°C and the pre-cleared lysates were transferred to a prechilled microcentrifuge tubes. After measuring the optical density at a 260 nm wavelength (OD_{260}) in each lysate by a Nanodrop spectrophotometer and adjusting the volumes to ensure equal OD unit loading, normalized

lysates were loaded into open-top polyclear centrifuge tubes containing 17.5 – 50% sucrose gradients. A programmable gradient pourer was used to prepare fresh 17.5 – 50% sucrose gradients. After loading the normalized samples into the sucrose gradients, the gradients were centrifuged at 4°C for 2.15 hours at 35,000 r.p.m. by a SW40Ti rotor in a Beckman L7 ultracentrifuge. Following centrifugation, gradients were directly fractionated, and the RNA content was continuously measured with absorbance at 254 nm by a UV monitor attached to the fractionator.

EDTA treatment for the cortex before polysome profiling to confirm the association of TAOK2 with polysomes

The same previously described standard procedures used for polysome profiling of the cortex were followed. In addition, in the EDTA treated samples, EDTA was added directly added to the pre-cleared cytoplasmic lysates (final concentration 30 mM) and maintained on ice for 10 minutes before loading into the sucrose gradient prior to centrifugation.

2.2.3.2 Polysome profiling of the N2a cells

48h post-transfected and control N2a cells with 70-80% confluency at the harvesting time were treated with 100 µg/ml cycloheximide at 37°C for 3 minutes prior to lysis. Cells were washed twice with ice-cold 1X PBS containing 100µg/ml cycloheximide (CHX). The cells were gently scraped from the plate in the residual PBS/CHX with a cell scraper. The cells from two 10 cm plates for each gradient were pooled together and spun down at 1,000 x g for 5 minutes at 4°C. 500 ul of the ice-cold N2a cells polysomes lysis buffer was added to the pelleted cells and incubated on ice for 10 minutes with a brief vortex every 2-3 minutes to avoid sedimentation of larger cellular aggregates at the bottom of the tube. Afterwards, the cells were triturated 10 times using a 27-gauge syringe and the lysates were cleared by centrifugation at 2,000 x g for 3 minutes followed by 16,900 x g for 7 minutes. The cleared cytoplasmic supernatants were transferred into ice-cold microcentrifuge tubes and the OD_{260} of each lysate was measured on the Nanodrop spectrophotometer and volumes were adjusted to ensure equal OD unit loading into each 17.5% - 50 % sucrose gradient. Sucrose gradients preparation, sample ultracentrifugation, gradient profiling, and collections of the fractions were done as previously described above.

2.2.3.3 Polysome profiling of the LCLs

1.5-2.0 × 10^9 LCLs per gradient were spun down by centrifugation at 1,000 rpm at RT then treated with a prewarmed medium supplemented with 100 µg/ml cycloheximide at 37°C for 5 minutes. After cycloheximide treatment, the cells were pelleted by centrifugation at RT, and washed 2 times with ice-cold 1x PBS supplemented with 100 µg/ml cycloheximide. The pelleted cells were resuspended in 400 ul ice-cold LCLs polysomes lysis buffer. Cells were incubated on ice for 10 minutes and vortexed briefly every 2-3 minutes to avoid sedimentation of larger cellular debris at the bottom of the tube. After triturating the cells 10 times using a 27-gauge syringe, lysates were cleared by centrifugation at 2,000 x g for 3 minutes followed by 16,900 x g for 7 minutes. The cleared cytoplasmic supernatants were transferred into ice-cold microcentrifuge tubes and the OD_{260} of each lysate was measured on a Nanodrop spectrophotometer and volumes were adjusted to ensure equal OD unit loading into each 17.5% - 50 % sucrose gradient. Sucrose gradients preparation, sample ultracentrifugation, gradient profiling, and collection of the fractions were done a previously described above.

2.2.3.4 Polysomes profiling analysis

The ratio of polysomes to monosomes (P/M) is considered as a ubiquitous readout for polysomes profiling, where the individual components (80S monosomes and polysomes) of each profile were subjected to quantitative analysis. All continuous UV readings from a certain polysome profile were subsequently exported to Microsoft Excel to adjust the scales of the x / y-axis, if required, by modifying the traces. Afterwards, the traces were exported to the Adobe Illustrator for sorting. Adobe Photoshop was used to define the area under the curve by drawing a line at the lowest point at either monosomes or polysomes within the same profile. The pixels above the line and under the monosomes or polysomes of the same profile were imputed using ImageJ (Schneider et al., 2012). The P/M ratio was calculated by dividing the area (number of these pixels) under the curve of polysome peaks by area under the curve of the monosome peak.

For the cell lines, N2a and LCLs profiles, the values of P/M ratio generated from profiles of a certain experiment were normalized to the mean of P/M ratio of the control profiles within the same experiment. In the case of cortex and cerebellum profiles, the values of P/M ratio from all experiments were normalized to the mean one control value.

2.2.4 Measurement of protein synthesis by Surface Sensing of Translation "SUnSET assay":

Puromycin is an aminonucleoside anti-microbial agent created by a gram-positive actinomycete (Streptomyces alboniger). Structurally, it is similar to aminoacyl-transfer RNA (aminoacyl-tRNA) that can be incorporated into the newly synthesized polypeptide chain and stop elongation (Nathans, 1964). Thus, puromycin binding to the growing polypeptide chain results in early termination of elongation and leads to premature release of the growing puromycylated polypeptide chain from the ribosomes (Semenkov et al., 1992). However, pre-treatment with ribosome translocation inhibitors like cycloheximide blocks puromycin incorporation (Hobden & Cundliffe, 1978). Thus, cycloheximide pre-treatment is widely used to verify that puromycin is solely labelling nascent polypeptides.

Interestingly, the development of antibodies against puromycin (Fujiwara et al., 1982) and its derivatives (Liu et al., 2012) has resulted in extensive use of puromycin in measurement of the translation level instead of common radioactive amino acids such as S35 methionine. Furthermore, it enabled to quantify the amount of global protein synthesis in individual mammalian cells and tissues by a special technique known by SUnSET (Schmidt et al., 2009).This technique was developed as an alternative to the usual radioactive labelling methods to monitor cellular mRNA translation. Its idea is based on the immunological detection of puromycin-bound peptides by an anti-puromycin antibody after application of puromycin with low concentration (below the global protein synthesis blockage level up to 18.4 µM) to living cells, tissues or living animals. SUnSET firstly was applied to the cultured cells and the changes in puromycylated newly synthesized peptides were detected by the traditional western blotting using anti-puromycin antibodies. In addition to immunoblotting, detection can be achieved in populations of live cells using fluorescence-activated cell sorting (FACS). Whereas the puromycin bound to the membrane proteins reach from the ER to the cell surface and could be detected without affecting the cells by SUnSET (Schmidt et al., 2009). Furthermore, immunodetection of the puromycin-incorporated peptides in single cells could be carried out by immunohistochemistry (IHC) (Goodman et al., 2012; Schmidt et al., 2009). Here, I measured the protein synthesis by using an adapted protocol for the SUnSET as described by (Schmidt et al., 2009) in different following biological samples:

2.2.4.1 Measurement of protein synthesis in acute brain slices

To measure the protein synthesis in the brain tissue *in vivo*, we followed an adapted protocol described by (Hoeffer et al., 2011) and (Schmidt et al., 2009). Briefly**,** 400 µm coronal brain slices were prepared from four weeks old *TAOK2* $^{+/+}$, *TAOK2* $^{+/d}$, and *TAOK2* $^{d/d}$ mice with a vibratome in the cutting solution at a low temperature. Slices were recovered at 32 °C in incubation chamber with the cutting solution for 30 minutes followed by another 30 minutes with perfused oxygenated ACSF before the treatment. Slices were then treated with puromycin (10 µg/ml) for 90 minutes to permit the newly synthesized proteins to be labelled with puromycin. The incubation media with puromycin was removed followed by 2 successive washes with oxygenated ACSF 10 minutes each before lysis for western blot processing or fixation for immunohistochemical investigations. To verify the detected signal of the newly synthesized protein by anti-puromycin antibody and it is protein synthesis-dependent, slices from wild type animals were pre-treated with 100µm/ml cycloheximide (protein translation inhibitor) for 30 minutes, and then incubation medium was supplemented with puromycin (10 µg/ml) for 90 minutes.

For immunostaining, slices were fixed with 4% paraformaldehyde in PBS (4% PFA) for 1.5 hours at RT followed by 3 washes with 1x PBS. Slices were permeabilized with 0.3% Triton X-100 in PBS, followed by incubation in blocking buffer (5% Donkey Serum in TBS, 0.5 % Triton) for 1.5 hours at RT. Slices were then incubated with mouse anti-puromycin and chicken anti-MAP2 antibodies diluted in the blocking buffer and incubated 48 hours at RT with gentle shaking. Afterward, the slices were washed three times every 5 minutes in 1x PBS and incubated with Alexa Fluor conjugated secondary antibodies in 1 x PBS with 0.3% Triton X-100 for 2 hours at RT. Slices were washed three times every 5 minutes in 1x PBS prior to incubation with DAPI in 1x PBS for 30 minutes at RT to stain the nuclei. After 3 times washes with 1x PBS, slices were then mounted on glass microscope slides. Slices were imaged by Zeiss LSM 900 confocal laser microscope equipped with Plan-Apochromat 20x/0.8 objective. Z-series images were acquired with a step size of 1µm in-between z sections. The image acquisition settings were maintained similarly during imaging the different conditions within the experiment.

For western blotting, the dissected cortical regions were lysed in sterile-filtered RIPA buffer, containing 1x proteinase inhibitors and 1x phosphatase inhibitors

(Phosph-stop) by sonication 5X every 10 seconds. The lysates were cleared by centrifugation 20.000 x g for 10 minutes at 4°C. The supernatant was transferred to another pre-chilled tube, and then the protein concentration in the samples was estimated by the Pierce™ BCA Protein Assay Kit according to the manufacturer's guidelines. Subsequently, 50 µg protein was resolved on 10% sodium dodecyl sulphate (SDS) polyacrylamide gel,western blotted and detected with antibodies against anti-puromycin and β-actin. Puromycin protein signal in the whole lane was normalized against β-actin to calculate the puromycin/ β-actin ratio of the newly synthesized protein using ImageJ.

2.2.2.2 Measurement of protein synthesis in primary cortical neurons, N2a cells and LCLs

Immunofluorescence SUnSET assay for cortical neurons and N2a cells

The culture medium was aspirated from the 7DIV or 21DIV cortical culture neurons or from N2a control cells or cells transfected TAOK2β or TAOK2βA135P plasmids at 40-48 hours post-transfection. Then, the cells were treated with puromycin (10 µg/ml) in a pre-warmed medium and incubated for 10 minutes at 37°C, 5% CO2. To verify the detected signal of newly synthesized protein by anti-puromycin antibody, cells were pre-treated with 50µg/ml of cycloheximide for 5 minutes, and then 10 µg/ml puromycin was added for 10 minutes in the culture medium at 37°C, 5% CO2. After puromycin treatment, cells were rinsed quickly with normal medium, fixed with 4% PFA in PBS containing 4% sucrose at RT for 10 minutes and washed 3 times every 10 minutes with 1x PBS. Permeabilization of the cells was conducted with 1X PBS containing 0.3% Triton X-100 and incubated in blocking buffer (5% Donkey Serum in TBS, 0.5 % Triton) for 1.5 hours at RT. Cells were immunostained with primary antibodies against the protein of interest – non-transfected neurons with (anti-puromycin, anti-beta tubulin III), transfected neurons with (anti-puromycin, anti-TAOK2β) and N2a cells with (anti-puromycin and anti-myc tag) – diluted in the same blocking buffer and incubated overnight at 4°C. The coverslips were washed three times each for 5 minutes in 1x PBS. Afterward, the cells were incubated with Alexa Fluor conjugated secondary antibodies diluted in the blocking buffer for 1.5 hours at RT. Cells were washed three times every 5 minutes in 1x PBS followed by incubation with DAPI to stain the nuclei in 1x PBS for 30 minutes at RT. After washing 3 times with 1x PBS, coverslips were submerged once in ddH_2O water and mounted on glass microscope slides using Fluoromount-G.

Microscopic imaging

The cells were imaged by Nikon microscope (Eclipse, Ti) using an inverted 60 X oil immersion objective (NA 1.4). Cells were identified by their morphology or its immunolabelling and fluorescent markers. Non-transfected neurons were identified by anti-beta tubulin III antibody, transfected neurons with tDimer (red) and TAOK2β staining and N2a transfected cells with GFP (green) and anti Myc-tag antibody against the expressing signal of its respective TAOK2 protein. Z-series images were acquired with a step size of 0.3 µm in-between z sections. The image acquisition settings were maintained similarly during imaging the different conditions within the experiment.

Fluorescent intensity measurements

All z sections for the entire cell were summed together with the maximum intensity using the z project tool in the ImageJ. Afterward, mean puromycin fluorescent intensity in cell body was measured in randomly selected labeled cells by ImageJ. Only individual cells with no adjacent cells were analyzed to avoid false-positive signals from the other cells. Transfected neurons expressing tDimer and TAOK2β plus the nearby non-transfected neurons from one coverslip of one genotype were selected and processed in parallel to control the conditions. Only N2a cells expressing Myc-tag plus GFP signals were analyzed.

Western blot - SUnSET assay for N2a cells and LCLs

N2a cells growing on a 10 cm culture dish or 5 x 10^6 LCLs were treated with a pre-warmed medium containing puromycin (10 µg/ml) for 10 minutes at 37°C, 5% CO2 to label the newly synthesized protein. To verify the detected signal of newly synthesized protein by anti-puromycin antibody, cells were pre-treated with 50 µg/ml of cycloheximide (protein translation inhibitor) for 5 minutes, then 10 µg/ml puromycin was added for 10 minutes in the culture medium at 37°C, 5% CO2. Following treatment, cells were washed twice with ice-cold 1x PBS, collected in 1.5 ml tubes, and pelleted by centrifugation at 1,200 r.p.m for 5 minutes at 4°C. The cells were lysed in RIPA buffer and immunoblotted for SUnSET analysis as previously described above (Western blot - SUnSET assay for acute slices).

2.2.4 Extraction of protein from the polysomes:

2.2.4.1 Precipitation of protein from the polysome fractions for western blot analysis

Precipitation of the protein from polysome fractions was done by using Trichloroacetic acid (TCA) protein precipitation protocol with little modification (Sanchez, 2001). Briefly, every 2-3 sucrose fractions were pooled together as in the schemes in the results section. An equal volume of 20% TCA was added to the sample in a microcentrifuge tube and incubated for 30 minutes on ice. Afterward, the tubes were centrifugated at 14, 000 rpm for 5 minutes. The supernatant was gently removed, leaving the whitish, fluffy protein pellet intact. The pellet was washed with 500µl cold acetone and spin down at 14,000 rpm for 5 minutes. The supernatants were removed and the washing step with acetone and centrifugation were again repeated. After the two-acetone washes, the supernatants were removed, and the pellets were dried by placing the tube in 50°C heat block for 5 minutes to drive off the acetone. For SDS-PAGE, 50 µl 2x Laemmli sample buffer was added to each pellet followed by a strong vortex to dissolve the pellets. The pellets of the first 3 pooled fractions were dissolved in 150 µl 2x Laemmli sample buffer. The sample was boiled for 10 minutes at 95°C in a heat block and 30 µl were loaded onto 10% SDS-polyacrylamide gel.

2.2.4.2 Protein purification from polysomes to detect TAOK2 isoforms by proteome analysis

Sucrose polysome fractions 11-22 (that represent light and heavy polysomes in the polysomes profile) from *TAOK2* $^{+/+}$ mouse cortex were collected and pooled together. The proteins were purified from the sucrose and concentrated up to 200µl final volume by several washes with ddH_2O using Amicon Ultra -15 centrifugation filter at 4°C. Protein concentration in the sample was determined by BCA method according to the manufacturer's instructions and equal amounts of protein were loaded into 10% SDS-polyacrylamide gel to separate the protein bands electrophoresis. Afterward, the gel was incubated with Coomassie stain (Roti®-Blue) for 30 minutes at RT to visualize the bands. Following staining, the gel was washed several times with 25% methanol solution until the bands were clearly visible. The approximate bands at 100-160 kDa corresponding to TAOK2 molecular weight were excised, digested, and analysed by LC-MS/MS.

2.2.5 Western blotting

30 µl sample with Laemmli buffer after TCA protein precipitation from each polysomes fractions or 30-50 µg protein determined by BCA method according to the manufacturer's guidelines from N2a cells, LCLs, and brain lysates were applied SDS gel separation and western blotting.

Proteins were separated on 10% or 7.5%-20% gradient SDS-polyacrylamide gradient gels at 30mA/gel in 1X running buffer. Proteins from the polyacrylamide gel were transferred to a PVDF membrane with wet transfer method (Gels were electrophoresed at 95 V in 1X running buffer for 1.5 hour at 4°C room with an ice block in the transfer chamber and the transfer chamber surrounded by ice or at 35 V overnight). Membranes were blocked in TBS-Tween20 0.1% with 5% BSA, or with 5% skim milk powder or 3% BSA according to the antibody's datasheet instructions for 1h at RT and followed by overnight incubation with primary antibodies on a shaker at 4 °C. After primary antibody incubation, membranes were washed for 30 minutes in 0.1% TBS-Tween20 and incubated for 2 hours at RT with horseradish peroxidase conjugated anti-IgG secondary antibodies and then washed for 30 minutes in TBS-Tween20 0.1%. Afterwards, immunoreactivity signals on the membranes were visualized by enhanced chemiluminescence NTAS, ChemoStar, ECL Imager. Western blots were analyzed using software from Fiji Software. Proteins of interest were normalized to the β actin signal as a loading control and the phospho-specific signals were normalized to its respective total protein intensity in the same lane after membrane stripping and redevelopment.

2.2.5.1 Membrane stripping

For immunoblotting against the loading control or total proteins, the PVDF membranes were stripped in the stripping buffer for 10 minutes at 50-60 °C with gentle shaking under safety hood. Afterward, the membranes were washed in TBS-Tween20 0.1% (2x 5 minutes) followed by incubation in the blocking buffer and proceeded with normal immunoblotting procedures.

2.2.6 Immunoprecipitation (IP)

The cortex of *TAOK2* $^{+/+}$ mouse or N2a cells transfected with wild type TAOK2β were lysed in ice-cold lysis RIPA buffer (pH 8.2) by a glass homogenizer or sonication 3x each 10 sec, respectively. The cellular homogenate was cleared from the cell debris by centrifugation at 13,000 rpm for 10 minutes at 4°C. 1000µg cleared homogenate

was incubated with polyclonal rabbit Taok2β (SySy) or polyclonal rabbit IgG (Millipore) antibodies prebound to Dynabeads Protein A undergoing rotation overnight at 4°C. Following incubation, the supernatant was removed using a magnetic holder and the immunoprecipitated complex (beads-antibody-antigen) was washed with a pre-cooled lysis buffer 3x 5minutes at 4°C with rotation (25rpm). This was followed by another 3x 5 washes with Tris-HCl pH 8.2 at 4°C to get rid of the remaining detergents and analyzed by LC-MS/MS. For analysis of the immunoprecipitated complex by SDS-PAGE, 50 µl Laemmli sample buffer was added to the complex and boiled for 10 minutes at 95°C in a heat block to elute the proteins. Afterwards, the eluted proteins were separated from the beads with the help of magnetic holder and loaded on 7.5-20% SDS-polyacrylamide gel and processed with the routine WB analysis and immunodetection.

2.2.7 Proteomics analysis with Liquid chromatography-mass spectrometry (LC-MS/MS):

2.2.7.1 Sample preparation for proteome analysis

Tryptic in-gel digestion was conducted following a previously described protocol (Shevchenko et al., 2007). Shrinking and swelling of gel pieces were performed with 100 % acetonitrile (ACN) and 100 mM ammonium bicarbonate (NH4HCO3). The in-gel reduction was conducted with 10 mM dithiothreitol (DTT) (dissolved in 100 mM NH4HCO3). Alkylation was performed at room temperature with 55 mM iodoacetamide (dissolved in 100 mM NH4HCO3). Digestion of proteins in the gel pieces was done by covering them with a trypsin solution containing (8 ng/µL sequencing-grade trypsin (Promega), dissolved in 50 mM NH4HCO3 with 10% ACN). The mixture was incubated overnight at 37 °C. Tryptic peptide products were further yielded by extraction with 2 % formic acid (FA), 80 % ACN. The extract was evaporated. For LC-MS/MS analysis, samples were resuspended in 20 µL of 0.1 % FA.

For the immunoprecipitated samples, protein digestion was performed on the magnetic beads. Therefore, 1% sodium deoxycholate (SDC) in 100 mM triethylammonium bicarbonate was added and the samples were boiled at 95°C for 5 minutes. Dithiothreitol was added to the sample (final concentration 10 mM) and incubated at 60°C for 30 minutes. Iodoacetamide was added to the samples (final concentration 20 mM) and incubated at 37°C for 30 minutes. Proteins were digested with trypsin (sequencing grade, Promega) at 37°C overnight. After digestion, samples were placed on a magnetic rack, left for 1 minute to settle and the supernatant was transferred to a new tube,

1% FA was added to stop digestion and precipitate SDC. Samples were then centrifuged at 16,000 x g for 5 minutes, and the supernatant was transferred to a new tube and dried in a vacuum centrifuge.

For total proteome of the Prefrontal Cortex (PFC), PFC was isolated from *TAOK2* $^{+/+}$ and *TAOK2* $^{d/d}$ mice brains (at least n=3 per genotype). Tissue was lysed in 8M Urea, protein concentration measured with BCA and 100 ug digested with Trypsin/Lys-C. After desalting, peptides were labelled with TMTpro-16plex. Flow through was fractionated to analyze the total proteome using data-dependent LC-MS/MS.

2.2.7.2 LC-MS/MS in Data Dependent mode

Samples were reconstituted in 0.1% FA and transferred into a full recovery autosampler vial (Waters). Chromatographic separation was achieved on a Dionex Ultimate 3000 UPLC system (Thermo Fisher Scientific) with a two-buffer system (buffer A: 0.1% FA in water, buffer B: 0.1% FA in ACN). Attached to the UPLC was an Acclaim PepMap 100 C18 trap (100 µm x 2 cm, 100 Å pore size, 5 µm particle size, Thermo Fisher Scientific) for desalting a purification followed by a nanoEase M/Z peptide BEH130 C18 column (75 µm x 25 cm, 130 Å pore size, 1.7 µm particle size, Waters). Peptides were separated using a 60 min gradient with increasing ACN concentration from 2% - 30% ACN. The eluted peptides were analyzed on a quadrupole orbitrap Ion trap tribrid mass spectrometer (Fusion, Thermo Fisher Scientific) in data-dependent acquisition (DDA). The fusion was operated at top speed mode analyzing the most intense ions per precursor scan ($2x10^5$ ions, 120,000 Resolution, 120 ms fill time) within 3 s and were analyzed by MS/MS in the ion trap (HCD at 30 normalized collision energy, $1x10^4$ ions, 60 ms fill time) in a range of 400 – 1300 m/z. A dynamic precursor exclusion with a speed mode of 20 s was used.

2.2.7.3 Data analysis, processing, and bioinformatics

For proteome in polysomes and the immunoprecipitated proteins, the acquired DDA LC-MS/MS data were searched against the Uniprot mouse protein database (release October 2020, 17,053 protein entries) and the TAOK2 splice variant 2 (Q6ZQ29-2) using the Sequest algorithm integrated into the Proteome Discoverer software version 2.4 in label-free quantification mode. The match between runs was enabled, performing chromatographic retention re-calibration for precursors with a 5 min retention time tolerance, no scaling, and no normalization for extracted peptide areas was done. The following parameters were applied in the searches: Mass tolerances

for precursors were set to 10 ppm and fragment mass tolerance was 0.6 DA. Carbamidomethylation was set as a fixed modification for cysteine residues and the oxidation of methionine, pyro-glutamate formation at glutamine residues at the peptide N-terminus as well as acetylation of the protein N-terminus, loss of methionine at the protein N-terminus and the Acetylation after methionine loss at the protein N-terminus were permitted as variable modifications for the search. Peptide areas were summed to protein areas and used for quantitative analysis. The only peptide with high confidence (false discovery rate < 1% using a decoy database approach) were accepted as identified. Peptide areas were summed to protein areas and used for quantitative analysis. Protein areas were imported into Perseus software version 1.5.8 for statistical analysis.

STRING v11.5 network analyses were provided by the STRING CONSORTIUM 2021 (Szklarczyk et al., 2021). The most similar abundant proteins (cv cutoff = 0.1) from the mass spec data were chosen for STRING and subsequent Over representation (ORA) analyses.

ORA analyses were performed with WebGestalt 2019 (Liao et al., 2019) for the most similar proteins in cortex and cell line, respectively. Bar plots were depicted with Benjamini-Hochberg FDR method for biological processes and molecular functions. For the cell line, the overall list contained the 197 most similar proteins, and 153 proteins for the cortex, respectively. Among them, 17 (14 for cortex) user IDs for the cell line could not unambiguously be mapped to any entrez gene ID from the selected platform illumina_mouseref_8

For total proteomics in the PFC, database search was done using the MaxQuant software (v 1.6.2.6) using the Andromeda search engine with the default search settings including an FDR set at 1% on both the peptide and protein level. The raw files of the mass-spectra data set from each condition were loaded into the MaxQuant software and a reporter ion as search type for each parameter group. TMT16pro isobaric labels were manually entered and used without correction factors. Reporter mass tolerance was set at 0.003 Da. Spectra were searched against the mouse proteins in the UniProt database (August 2020) and the common contaminant list provided by the software. The mass tolerance was set to 20 ppm and 4.5 ppm respectively. Enzyme specificity was set to Trypsin/P with digestion at C-terminal of Arg and Lys residues, even when they were followed by a Pro residue, with a maximum of two missed cleavages. Variable modifications were set to oxidation (Met) and protein

N-terminal acetylation with carbamidomethylation of Cys-residues set as a fixed modification. A minimum of one peptide (razor or unique) was required for identification with a minimum length of 7 residues. Second peptide search was allowed as well as the matching between runs option (from and to) using a 0.7-minute match time window.

Data was further processed in Perseus v.1.6.15.0. After loading the Protein Groups txt file, derived from the MaxQuant search, the potential contaminants were removed, as well as the reversed hits and proteins that were identified only by site. The reporter intensities were then log2 transformed and filtered for rows 16 valid values. Columns were normalized by subtracting the median. A multiscatter plot and principal component analysis were calculated to assess the quality of the runs. A two-sample t-test was performed comparing the WT and KO samples with a permutation-based FDR of 0.05 and an S0 value of 0.05 for truncation with 250 randomizations. Results were visualized as a volcano plot.

Functional classification of the differentially up-regulated proteins in the PFC from *TAOK2* $^{d/d}$ was performed by PANTHER (Protein Analysis Through Evolutionary Relationships, http://www.pantherdb.org).

2.2.8 Image processing

Brightness and contrast of the images were adjusted with similar setting using Photoshop CS 8.0 (Adobe systems) or ImageJ.

2.2.9 Statistical analysis

The GraphPad Prism (version 6.07) analytic software was used to perform all the statistical analysis. Number of biological replicates, experiments and statistical tests used for the comparison were mentioned within the figure legends.

3. Results:

3.1 TAOK2 associates with translational control machinery and its deficiency enhances general translation:

3.1.1 TAOK2 associates with cytoplasmic proteins linked to translational control

To identify the association of TAOK2 with the translational control machinery, I performed IP-MS analysis of immunoprecipitation complexes using a TAOK2β antibody

in cytoplasmic lysates either from *TAOK2* $^{+/+}$ mice cortices or N2a cells transfected with wild-type TAOK2β. The MS analysis of the pulled-down products by using a TAOK2β antibody identifies 153 and 197 proteins in cortex and N2a cells, respectively, with a coefficient of variation (cv) cut-off of 0.1 (Supplementary Figure 1, Supplementary Table 1 and Supplementary Figure 2, Supplementary Table 2, respectively). As expected, the network-based functional analysis using STRING for the mentioned proteins in the cortex results in a general enrichment of synaptic organization, cytoskeleton structure, neuronal development, and neurogenesis related GO terms, while 14 and 25 proteins from the identified enriched proteins in cortex and N2a cell line, respectively, out of 313 proteins accounted for GO:0006412 (translation) (Figure 4 a and 5 a). Furthermore, the overrepresentation (ORA) analysis - special form of GO analysis - for the mentioned proteins revealed the association with translational GO terms is more pronounced in the N2a cells overexpressing TAOK2β. Among ribosomal proteins, translational initiation, and elongation factors, general GO terms like ribonucleoprotein complex biogenesis and RNA binding associations account for biological and molecular functions, respectively (Figure 5 b).

a

Biological Process (Gene Ontology)				
GO-term	description	count in network	strength	false discovery rate
GO:0006412	translation	14 of 313	0.84	1.39e-06
GO:0006810	transport	63 of 3187	0.49	3.72e-15
GO:0022008	neurogenesis	36 of 1650	0.53	7.45e-09
GO:0016358	dendrite development	6 of 113	0.92	0.0015

b

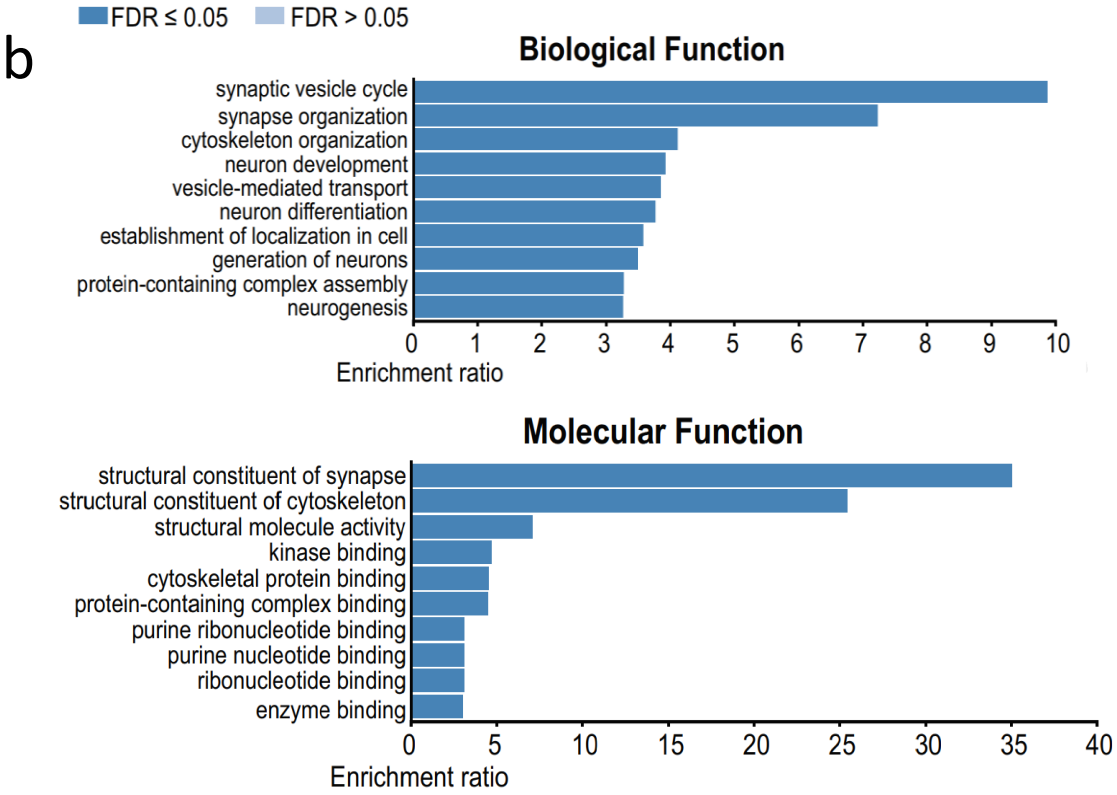

Figure 4: Functional annotation analysis of the enriched proteins of wild-type mouse cortices immunoprecipitated by TAOK2-β antibody and identified by IP-MS.

(a) Gene Ontology annotation analysis depicting the biological processes for the proteins enriched with TAOK2β in the cortex. The four following GO terms were highlighted with different colored buttons: GO:0006412 (translation; red buttons), GO:0006810 (transport; blue buttons), GO:0022008 (neurogenesis; green buttons), GO:0016358 (dendrite development; yellow buttons); (See Supplementary Table 1 for details).

(b) Over representation analysis (ORA) for the most similar proteins in cortex showing the top 10 most significantly associated GO terms in cortex. FDR: false discover rate.

a

Biological Process (Gene Ontology)				
GO-term	description	count in network	strength	false discovery rate
GO:0006412	translation	25 of 313	0.97	6.97e-14
GO:0006810	transport	49 of 3187	0.26	0.00043
GO:0022008	neurogenesis	26 of 1650	0.27	0.0153
GO:0007010	cytoskeleton organization	31 of 916	0.6	1.26e-08

b

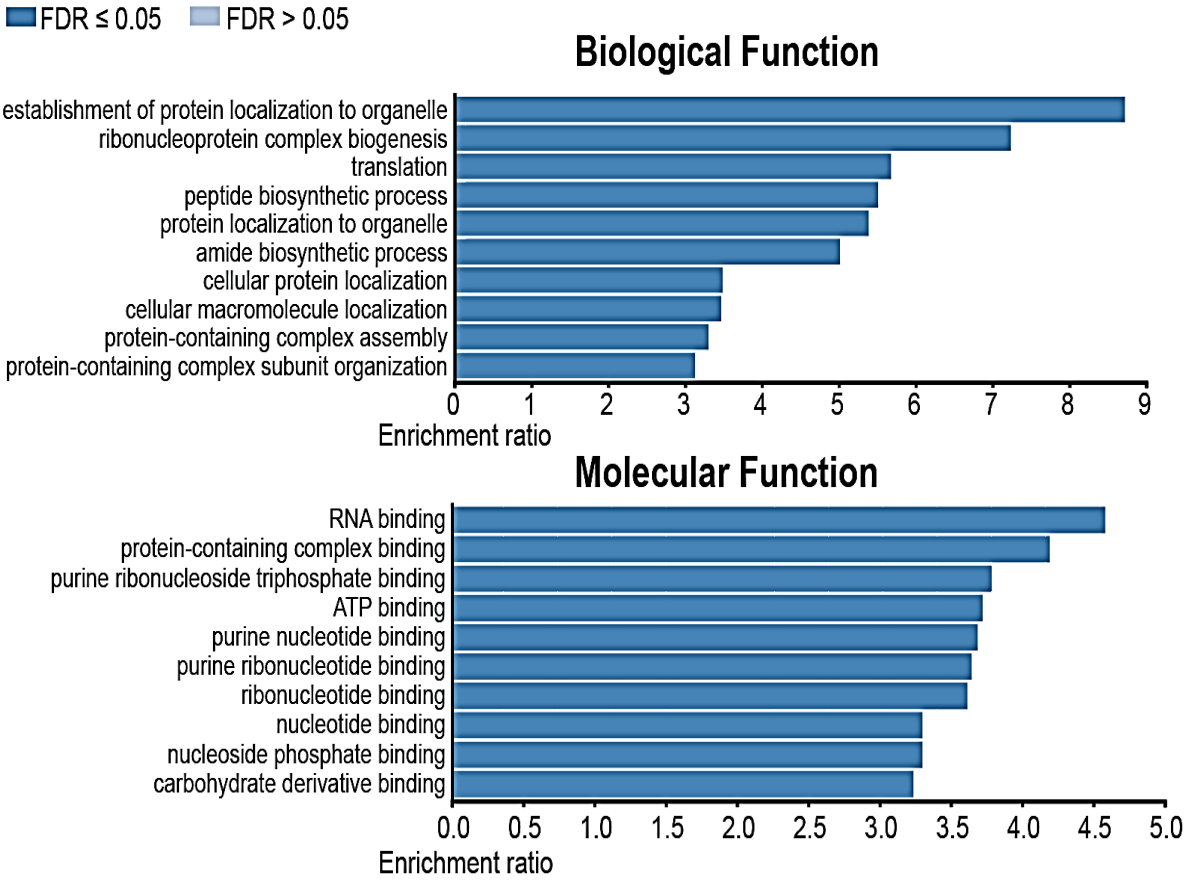

Figure 5: Functional annotation analysis of the enriched proteins in N2a cells overexpressing with wild type TAOK2-β immunoprecipitated by TAOK2-β antibody and identified by IP-MS.

(a) Gene Ontology annotation analysis depicting the biological processes for the proteins enriched with TAOK2β in N2a cells transfected with wild type TAOK2-β. The four following GO terms were highlighted with different colored buttons: GO:0006412 (translation; red buttons), GO:0006810 (transport; blue buttons), GO:0022008 (neurogenesis; yellow buttons), GO:0007010 (cytoskeleton organization; green buttons); (See Supplementary Table 2 for details).

(b) Over representation analysis (ORA) for the most similar proteins in cortex showing the top 10 most significantly associated GO terms in N2a cells overexpressing TAOK2-β**.**

3.1.2 TAOK2 is present in the polyribosome complex, and its deficiency increases global translation

3.1.2.1 Association of TAOK2 with the polyribosome complex

To further investigate the association of TAOK2 with the polyribosome complex, I performed fractionation for the polysome profiles (which is based on the separation of ribosome-associated mRNAs by density with sucrose gradient centrifugation and measuring the OD across the gradient). Afterward, the protein was extracted from the different collected gradient fractions and followed by western blot (WB) analysis. Immunoblot analysis using TAOK2β antibody on the purified proteins of polysomes extracted from different brain regions in mice (e.g., cortex Figure 6 b and cerebellum Supplementary Figure 3 d) revealed the presence of TAOK2β in polysomes (multiple ribosomes bound to an individual mRNA) of wild type mice. The detected TAOK2β signal across the translationally active polysome-associated mRNAs (heavy polysomes) is consistent with the presence of PAPB and RPL7a (house-keeping proteins in the cytoplasmic ribosomal complex). These data suggest the association of TAOK2 with the polyribosome complex.

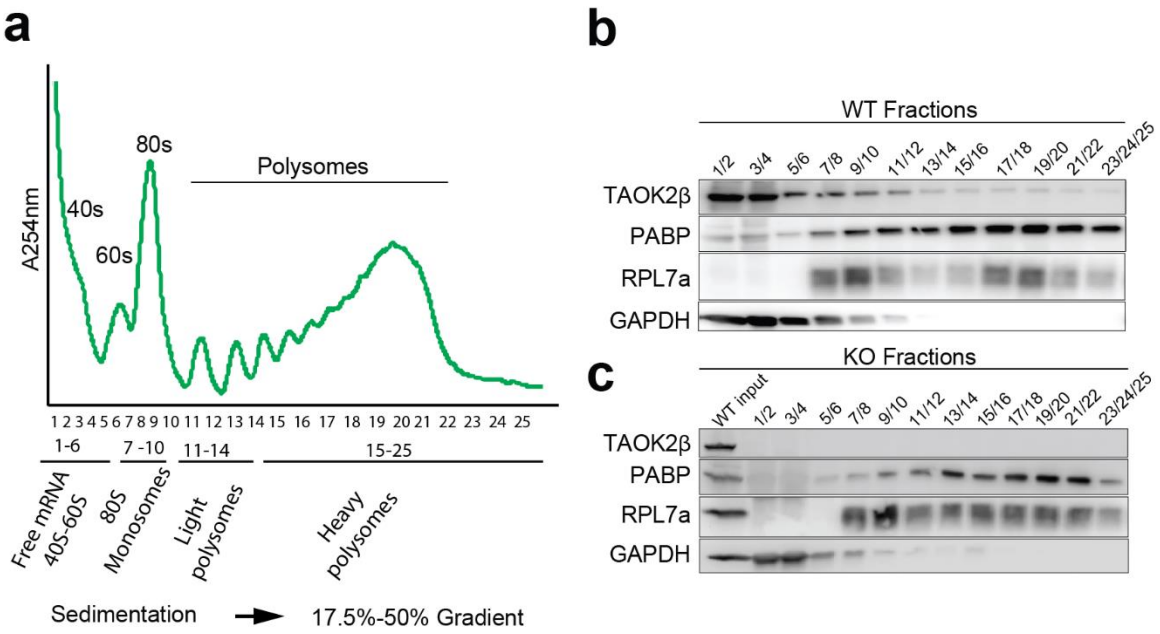

Figure 6: TAOK2 associates with cytoplasmic polyribosome complex in wild-type mouse cortex.

(a) Representative polysome profile from 4 weeks old mouse cortex fractionated on 17.5% – 50% sucrose gradient shows different parts of the polysome profile (free mRNA and free subunits, monosomes, light polysomes, and heavy polysomes) across the fractionated gradient.

(b) and **(c)** Immunoblots of the cortical polysome fractions pooled as in the scheme, showing the presence of TAOK2β across all fractions from polysomes of the *TAOK2* $^{+/+}$ (b) and its absence in the *TAOK2* $^{d/d}$ (c). PABP1 and

RPL7a were used as positive controls and GAPDH as a negative control to prove the efficiency of polysomes preparation across the gradient. Input from WT cortex was loaded before the polysomes fractions of KO to verify the specificity of the TAOK2β antibody.

To confirm the association of TAOK2β with polysomes, the cytoplasmic lysate from the cortex of *TAOK2* $^{+/+}$ mice was treated with the Mg^{2+} chelating agent EDTA that disrupts polysomes before loading on the sucrose gradient and being fractionated. The EDTA treated profile shows the disappearance of polysomes peaks due to the dissociation of ribosomes from the polyribosome complex following treatment. In contrast, the peaks of monosomes (80S) and ribosomal subunits 40S, 60S are increased. Interestingly, immunoblot analysis for the fractionated gradients from EDTA treated profiles revealed the shift of TAOK2β signal from the heavier polysome fractions to the lighter fractions (unbound ribosomal subunits and monosomes). The overall shift of TAOK2β with PABP1 and RPL7a toward the lighter fractions of the gradient confirms the presence of TAOK2β in polysomes and it is indeed associated with the cytoplasmic ribosomal complex (Supplementary Figure 4 a-c). The immunoblots data showing the presence of TAOK2β in polysomes from mouse cortex and pulling down several proteins associated with translation using TAOK2β antibody in the IP-MS experiments clearly confirm the presence of TAOK2 in the polyribosome complex.

3.1.2.2 TAOK2 isoforms and their de novo mutations are involved in translation regulation

To investigate whether the presence of TAOK2 in the polyribosome complex is isoform-specific, I transiently transfected the N2a cells with plasmids expressing the TAOK2α and β isoforms specifically. Next, polysome profiling was performed and the extracted protein from the collected polysomes fractions was analyzed by western blotting. Interestingly, WB analysis revealed the presence of both α and β isoforms in the collected polysomes fractions across the gradient (Figure 7 a, b). However, the Myc-tag signal in polysomes of N2a cells transfected with wild type TAOK2α plasmid was less pronounced than the detected signal in polysomes from cells transfected with wild type TAOK2β. This in *vitro* data indicates the more abundance of the TAOK2β isoforms than the TAOK2α isoform in polysomes of N2a cells following overexpression of each isoform individually.

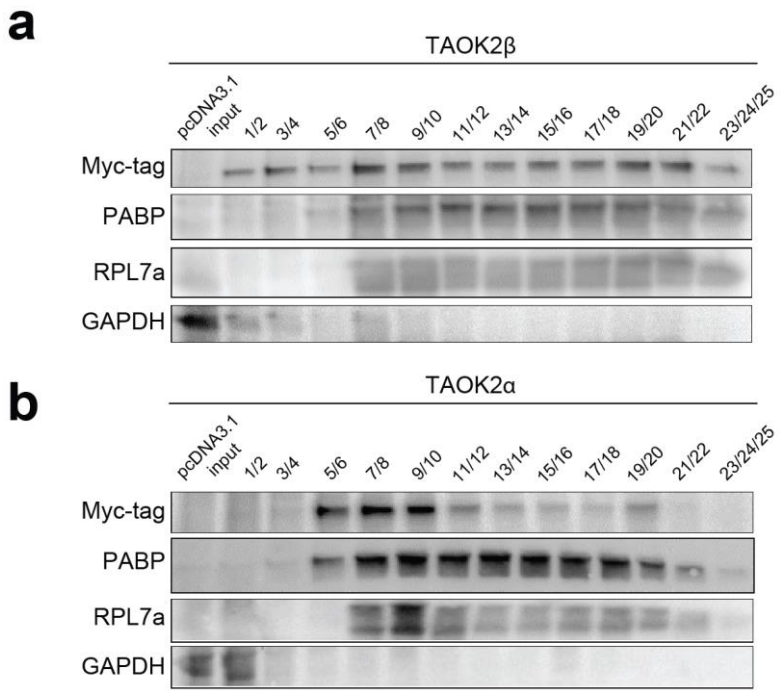

Figure 7: TAOK2β isoform is more abundant in polysomes than TAOK2α isoform in N2a cells individually overexpressing TAOK2 isoforms.

(a) and **(b)** Immunoblots against the indicated antibodies for the extracted proteins from the pooled polysomes fractions of N2a cells after overexpression (48h post-transfection) with wild-type TAOK2β (a) and TAOK2α (b) plasmids. Note the clear and abundant signal of Myc-tag antibody against the Myc-tag polypeptide protein in the pCMVhuTAOK2β-myc-tag plasmid in all polysomes across the fractionated sucrose gradient, while the Myc-tag antibody signal pCMVhuTAOK2α-myc-tag plasmid is reduced especially in the heavier polysomes fractions. PABP and RPl7a were used as house-keeping proteins in the cytoplasmic ribosomal complex and GAPDH as a negative control. Total cytoplasmic lysate from control cells transfected with empty vector control plasmid (pcDNA3.1-myc-tag) was loaded at the beginning of the blot (input) to prove the specificity of the antibody and the transfection efficiency (no signal, negative control at the input).

To determine the enrichment amount of each isoform in polysomes in *vivo*, we performed LC-MS/MS analysis for the extracted proteins from polysomes of different *Taok2* $^{+/+}$ mouse cortices. Interestingly, the β isoform has a higher abundance percentage in polysomes (65.21%) compared to the less abundance of α isoform (34.79%) (Figure 8) and (Supplementary Table 3). These data are consistent with and confirm the in *vitro* data obtained by western blotting of proteins prepared from polysomes of N2a cells transfected with TAOK2β or TAOK2α isoforms.

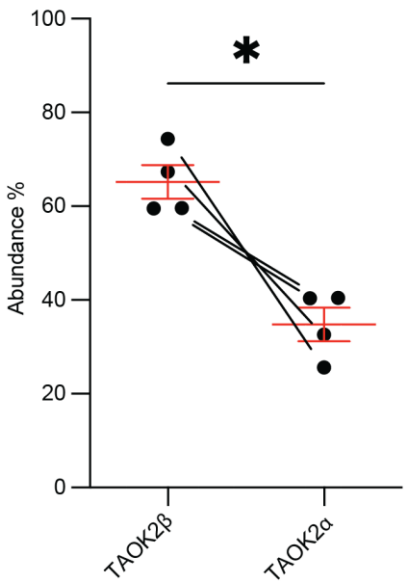

Figure 8: TAOK2β isoform is more abundant in polysomes than TAOK2α in wild type mouse cortex.

A scatter plot for the TAOK2 isoforms in polysomes of *TAOK2* $^{+/+}$ mouse cortices analyzed by (LC-MS/MS) showing the increased abundance percent of the TAOK2β (65.21%) compared to the less abundance percent of TAOK2α isoform (34.79%). n = 4 cortices from 4 weeks old *TAOK2* $^{+/+}$ mouse, n= 8, *P < 0.05, SEM. error bars, unpaired t-test.

To determine to what level the translational control is affected by each of TAOK2 isoforms and the *de novo* mutations, I quantified the global translation by the traditional polysome profiling in N2a cells transfected by TAOK2 isoforms and its mutations. I expressed TAOK2β, TAOK2α and their respective mutants (A135P missense mutation in the kinase domain present in α and β isoforms, which renders this protein a kinase-dead form of TAOK2) and the P1022* mutation present in the C-terminal region (present only in the β isoform) in N2a cells. Interestingly, the polysome/monosome (P/M) ratios of polysome profiles from cells either transfected with wild type TAOK2β or wild type TAOK2α are reduced compared to those from control cells (Supplementary Figure 5 a-f). On the other side, the polysome profiles of cells transfected with the TAOK2β mutations, either A135P (Figure 9 a, b) or P1022* (Supplementary Figure 6 a, b), which regulates the TAOK2β kinase activity, showed higher P/M ratios than the control profiles. Interestingly, while the polysome profiles of cells transfected with the TAOK2β A135P isoform showed higher P/M ratios than the control, the profiles from cells transfected with the TAOK2α A135P isoform did not show a significant change in the P/M ratios (Figure 9 d, e). Thus, these data suggest that the TAOK2β isoform plays a significant role in regulating translation through its kinase function.

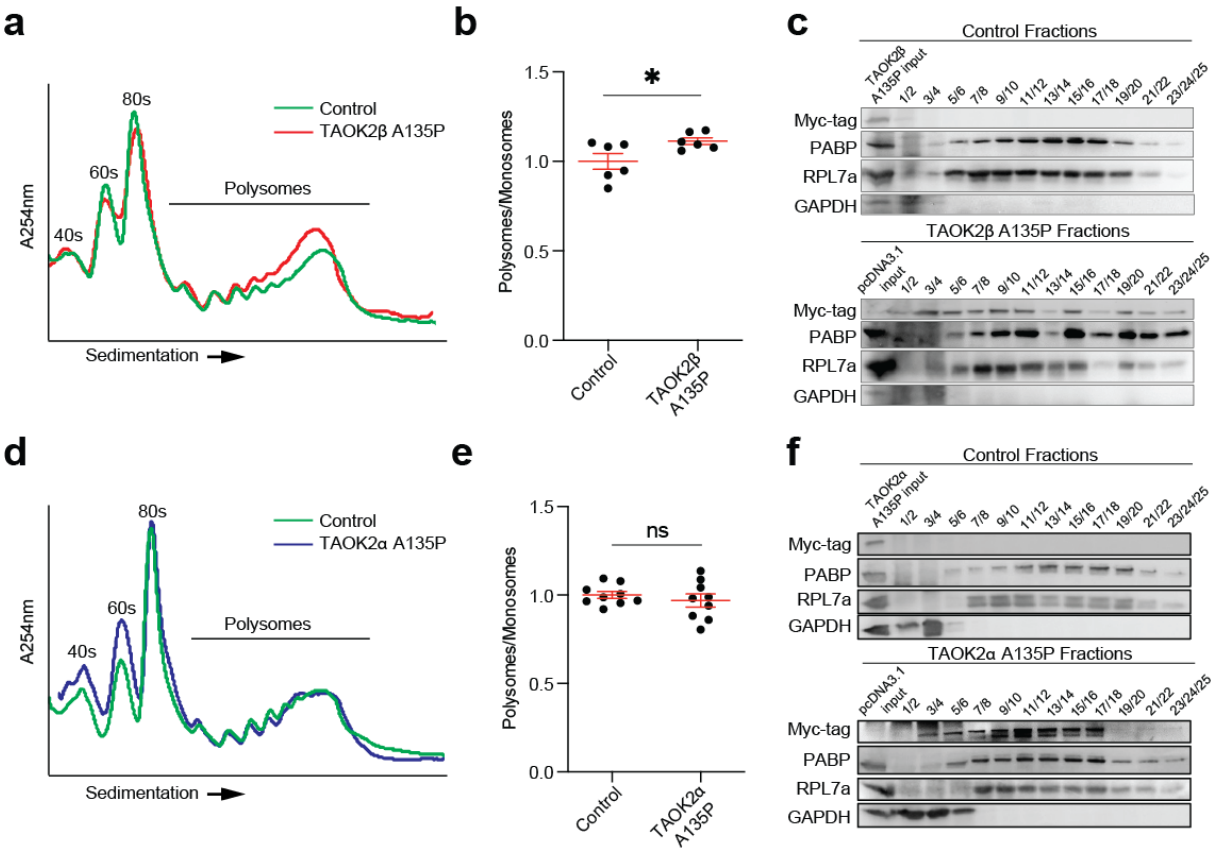

Figure 9: TAOK2β with A135P point mutation at the kinase domain enhances general translation but not TAOK2α kinase mutation (A135P).

(a) Overlay of representative polysome profiles of N2a cells transiently transfected (48h post-transfection) with TAOK2βA135P or empty vector control (pcDNA3.1-myc-tag) plasmids

(b) Quantifications of the normalized P/M ratios of polysome profiles from different independent transfection experiments reveal a statistically significant increase of P/M ratio in profiles from TAOK2βA135P transfected cells compared to the ones from the control cells. The number of biological replicates, TAOK2βA135P transfected cells n= 5, control n= 5; SEM. error bars; *P < 0.05, unpaired t-test.

(c) Immunoblots for the pooled gradient polysomes fractions representing the corresponding profile gradient against the presented antibodies for N2a cells transfected with TAOK2βA135P or control plasmids. Note the clear signal of Myc-tag antibody against the Myc-tag polypeptide protein in the TAOK2βA135P-myc tag in the all fractions of polysomes (lower), while there is no Myc-tag signal detected across the fractions of polysome profile from the control cells (upper). PABP1 and RPl7a were used as house-keeping proteins in the cytoplasmic ribosomal complex and GAPDH as a negative control across polysome profile fractions across the gradient. Input from the total cytoplasmic lysate, either from the TAOK2βA135P transfected cells or the control cells was loaded at the beginning of the blot to verify the specificity of the antibody and the transfection efficiency.

(d) Overlay of representative polysome profiles of N2a cells transiently transfected (48h post-transfection) with TAOK2αA135 or empty vector control (pcDNA3.1-myc-tag) plasmids.

(e) Quantifications of the normalized P/M ratios of polysome profiles from different independent transfection experiments reveal no significant statistical difference in the P/M ratios between the profiles from TAOK2αA135 transfected cells and the ones from the control cells. The number of biological replicates, TAOK2αA135P transfected cells n= 9, control n= 9; SEM. error bars; n.s., not significant. P= 0.4575, unpaired t-test.

(f) Immunoblots for the pooled gradient polysomes fractions representing the corresponding profile gradient against the presented antibodies for N2a cells transfected with TAOK2αA135P or control plasmid. Note the presence signal of Myc-tag antibody against the Myc-tag polypeptide protein in the TAOK2αA135P in polysomes (lower), while there is no Myc-tag signal detected across the fractions of polysome profile from the control cells (upper). PABP1 and RPl7a were used as house-keeping proteins in the cytoplasmic ribosomal complex and GAPDH as a negative control across polysome profile fractions across the gradient. Input from the total cytoplasmic lysate, either from the TAOK2αA135P transfected cells or the control cells was loaded at the beginning of the blot to verify the specificity of the antibody and the transfection efficiency.

Overexpression of wild type TAOK2β or its A135P mutation (kinase-dead) in N2a cells does not alter only the polysome profiling, but the amount of newly synthesized protein is altered as well. I used the SUnSET assay to quantify the amount of the newly synthesized protein by WB and histochemical analysis. Interestingly, SUnSET analysis of N2a cells either transfected by wild type TAOK2β or with TAOK2β A135P showed decreased or increased levels of newly synthesized proteins identified by puromycin incorporation rate, respectively (Figure 10 a-f). Taken together, these findings suggest that TAOK2 isoforms are present in polysomes - especially the β isoform - and that defects in translational control and global protein synthesis are a direct consequence of the loss of TAOK2β kinase function, but not TAOK2α.

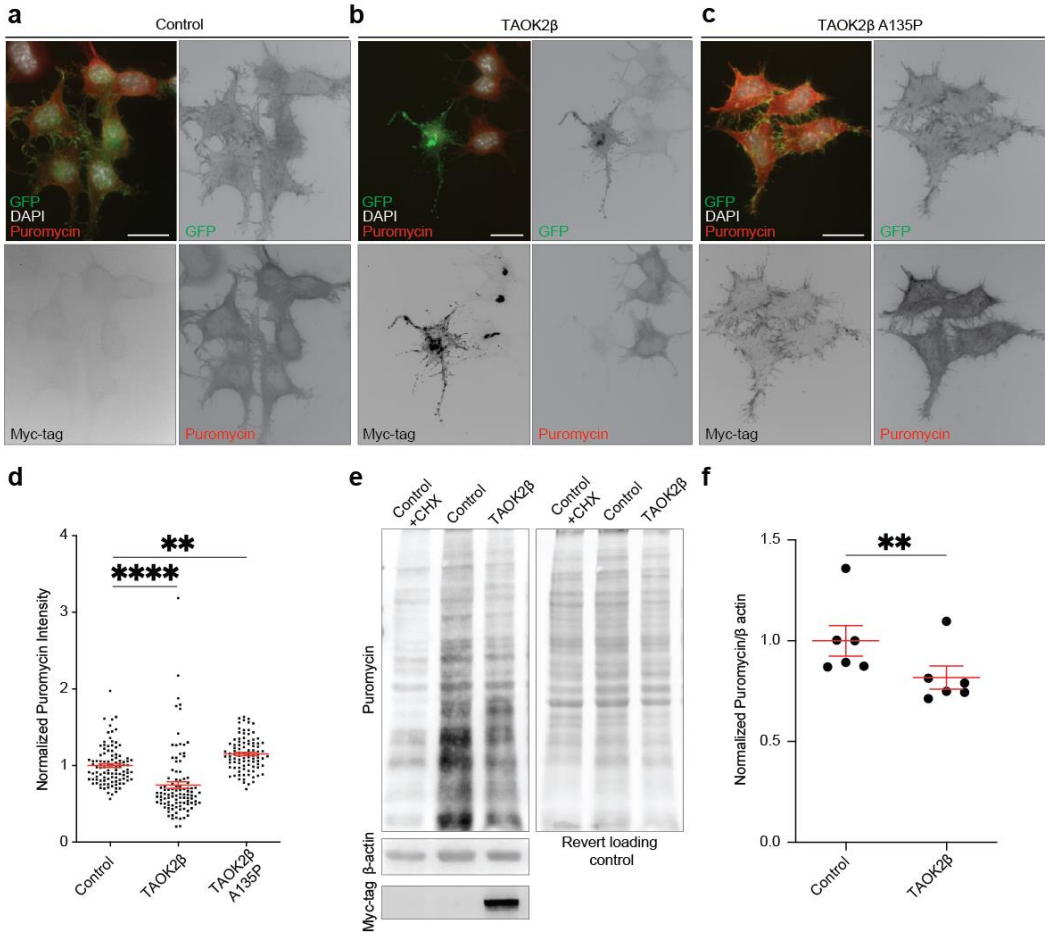

Figure 10: Wild type TAOK2β decreases protein synthesis while its mutation at the kinase domain A135P enhances it in N2a cells.

(a), (b) and (c) Representative Immunostainings N2a untransfected control cells, TAOK2β transfected cells, and TAOK2βA135P cells respectively, treated after 48 hours post-transfection with puromycin (10µg/ml) for 10 minutes to label the newly synthesized protein, fixed and immunostained with anti-puromycin (red) and anti-Myc-tag (grey) antibodies, DAPI (blue) and GFP marker (green).
(d) Quantifications of the normalized puromycin fluorescence intensity in control cells, cells transfected with wild type TAOK2β and TAOK2βA135P show decreased puromycin intensity in control cells and cells transfected with TAOK2β compared to cells transfected with TAOK2βA135P. The number of cells from 3 independent transfection experiments; control transfected cells n=103, wild type TAOK2β transfected cells n=102, TAOK2βA135P transfected cells n=93. SEM error bars; ** $p < 0.01$, **** $p < 0.0001$, ordinary one-way ANOVA followed by Tukey's multiple comparisons test.
(e) Representative WB image for equal amounts of protein from N2a control cells and cells transfected with TAOK2β analyzed by SUnSET assay shows decreased amount of the newly synthesized puromycin-labelled protein in TAOK2β transfected cells. At the first lane, 50 µg/ml of cycloheximide (protein translation inhibitor) was added to the cells for 5 minutes before being treated with puromycin (10 µg/ml) for 10 min to verify the specificity of the puromycin antibody signal and it is protein synthesis dependent. Revert loading control protein stain was used to show the equal loading of the total protein sample in all lanes.
(f) Quantifications for the WB SUnSET assay of N2a untransfected control cells and TAOK2β transfected cells show the decreased normalized puromycin/β actin ratio in TAOK2β transfected cells compared to the control. Number of biological replicates n=6 per condition from 3 different independent transfection experiment, SEM error bars; ** $p < 0.01$, paired t-test.

3.1.3 TAOK2 mutations in LCLs derived from patients enhances global translation

Furthermore, I investigated how TAOK2 mutations can affect the general translation in the disease condition. I used patient-derived LCLs endogenously expressing either TAOK2 with a mutated kinase domain at residue A135P that renders this protein into a kinase-dead form of TAOK2, or with the P1022* mutation at the regulatory region, respectively. Interestingly, polysome profiling and protein synthesis analysis for patient-derived LCLs with A135P mutation at the kinase domain revealed an increased P/M ratio and increased the amount of newly synthesized protein compared to cells derived from the non-affected father (Figure 11 a-d). Consistently, the profiles from patient cells with the C-terminal P1022* mutation have both, increased P/M ratios by polysome profiling analysis and global protein synthesis by SUnSET assay (Figure 11 e-h). These data are consistent with our N2a cells data transfected with TAOK2 mutations. Concurrently, these results suggest that patient-derived de novo mutations in TAOK2 greatly affect its function in translational control and lead to the enhancement of global translation.

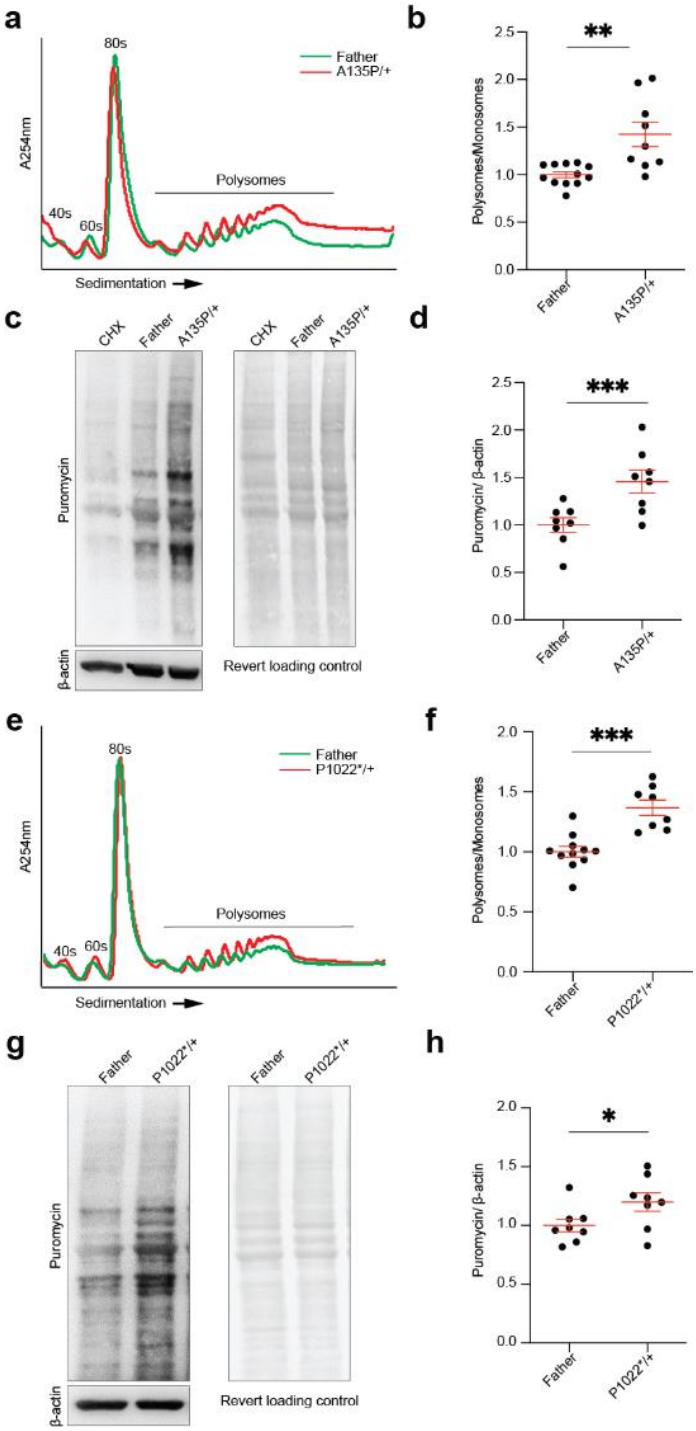

Figure 11: TAOK2 with heterozygous A135P kinase mutation and P1002* mutation increases translation in patient-derived LCLs.

(a) Overlay of representative LCLs polysome profiles from unaffected father and patient with TAOK2 mutated at A135P kinase domain shows increased in P/M ratio of LCLs patient profiles.

(b) Quantifications of the normalized P/M ratio for polysomes profiling in (a) from different experimental replicates reveal a statistically significant increase of P/M ratio in profiles of LCLs from patients with TAOK2 mutated at A135P in the kinase domain compared to the profiles from the unaffected father. Number of biological replicates of LCLs from patients with TAOK2 mutated at A135P in the kinase domain n=9, and n=12 from unaffected father; **P < 0.01, SEM. error bars, unpaired t-test.

(c) Representative WB image for equal amounts of protein from patient-derived LCLs withTAOK2 mutated at A135P kinase domain and LCLs from unaffected father analyzed by SUnSET assay shows increased amount of the newly synthesized puromycin-labelled protein in patient cells. At the first lane, 50 µg/ml of cycloheximide (protein translation inhibitor) was added to the cells for 5 minutes before being treated with puromycin (10 µg/ml) for 10 min to verify the specificity of the puromycin antibody signal and it is protein synthesis dependent. Revert loading control protein stain was used to show the equal loading of the total protein sample in all lanes.

(d) Quantification graph of the WB in (c) from different experimental replicates shows a significant increase of puromycin densiometric signal normalized to β-actin in patient-derived LCLs with A135P mutations in Taok2 kinase domain compared to LCLs from the unaffected father. The number of puromycin-treated LCLs replicates from unaffected father and patient were 8 per condition; ***P < 0.001, SEM. error bars, unpaired t-test.

(e) Overlay of representative LCLs polysome profiles from unaffected father and patient with TAOK2β mutated at P1022* shows increased in (P/M) ratio of LCLs patient profiles.

(f) Quantifications of the normalized P/M ratio for polysomes profiling in (e) from different independent experimental replicates reveal a statistically significant increase of P/M ratio in profiles of LCLs from patients with TAOK2β mutated at P1022* in the regulatory domain compared to the profiles from the unaffected father. Number of biological

replicates of LCLs from patients with TAOK2β mutated at P1022* n=8, and n=11 for cells from the unaffected father; ***P < 0.001, SEM. error bars, unpaired t-test.

(g) Representative WB image for equal amounts of protein from patient-derived LCLs with TAOK2β mutated at P1022* and LCLs from unaffected father analyzed by SUnSET assay shows an increase of the newly synthesized puromycin-labelled protein in patient cells. Puromycin incorporated proteins were detected by immunoblotting using an anti-puromycin antibody. Revert loading control protein stain was used to show the equal loading of the total protein sample in all lanes.

(h) Quantification graph of the WB in (g) from different experimental replicates shows a significant increase in puromycin densiometric signal normalized to β-actin in the puromycin treated LCLs of P1022* proband compared to LCLs from the unaffected father. Number of puromycin treated LCLs replicates from unaffected father and from patients with TAOK2β mutated at P1022* were 8 per condition; *P < 0.05, SEM. error bars, unpaired t-test.

3.1.4 TAOK2 acts as a repressor of translation and protein synthesis in mouse brain tissues

To assess the effect of TAOK2-dependent translation regulation in brain tissues, I performed polysome profiling for different brain regions from *TAOK2* deficient mice. Interestingly, quantifications of polysomes profiling in these brain regions show that the absence of TAOK2 leads to significant changes in the global translation. Cortices (Figure 12 a, b) and cerebella (Supplementary Figure 3 a-c) from *TAOK2* deficient mice showed increased P/M ratios, which indicates the increased amounts of RNA bound to the polyribosomes and strongly suggesting enhanced translation in the *TAOK2* deficient mice

To investigate the effect of TAOK2-dependent translation control on protein biosynthesis, I used an adapted protocol of SUnSET assay (Hoeffer et al., 2011; Schmidt et al., 2009) to measure global protein synthesis in acute brain slices from 4 weeks old mice. Interestingly, the amount of newly synthesized proteins identified by the puromycin incorporation rate in the slices from *TAOK2* $^{d/d}$ and *TAOK2* $^{+/d}$ mice is higher compared to *TAOK2* $^{+/+}$ mice, which suggests the enhanced global protein synthesis in *TAOK2* deficient mice (Figure 12 c-e).

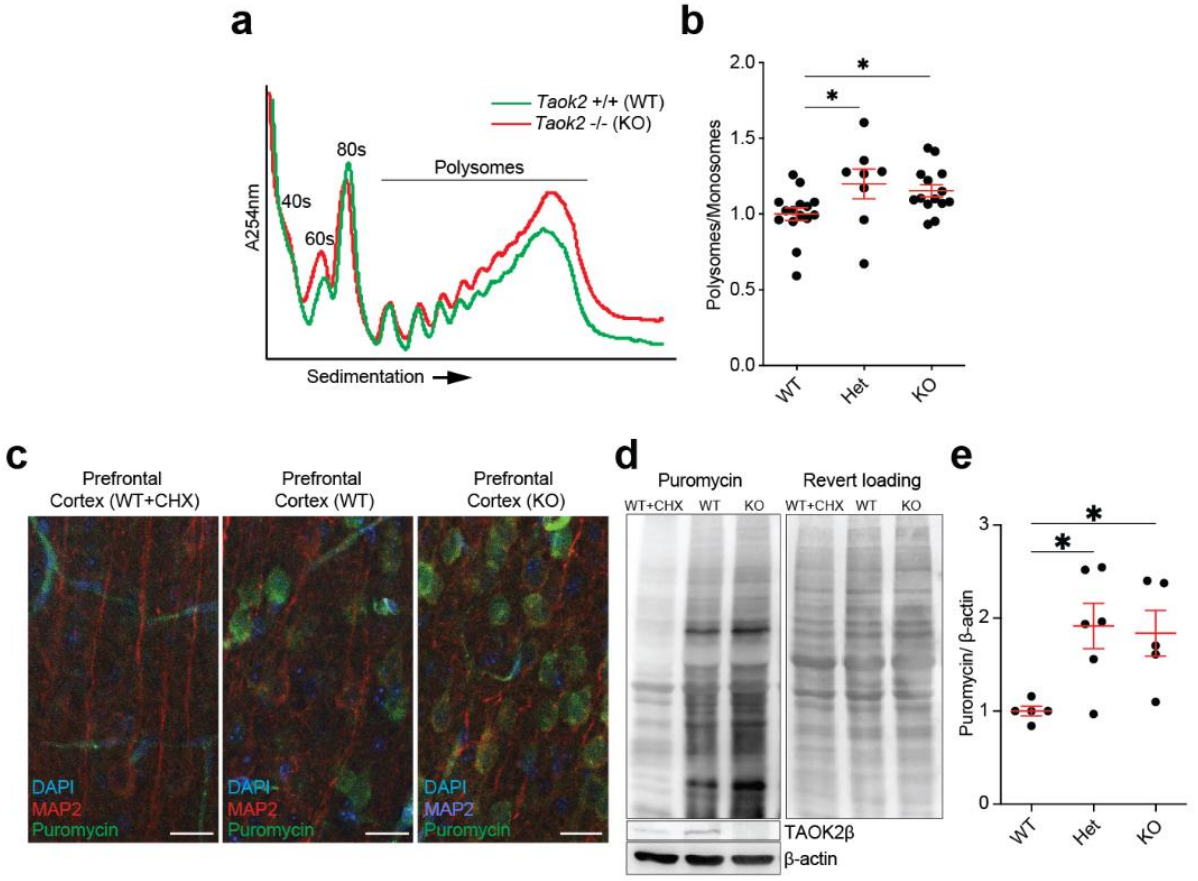

Figure 12: TAOK2 deficiency enhances global translation and protein synthesis.

(a) Representative overlay of polysome profiles from *TAOK2* $^{+/+}$ and *TAOK2* $^{d/d}$ mouse cortices shows an increase in P/M ratio in cortices lacking TAOK2.

(b) Quantification from polysome profiles from cortex showing increased P/M ratios in *TAOK2* $^{d/d}$ and *TAOK2* $^{+/d}$ mice cortices and its decrease in cortices from *TAOK2* $^{+/+}$ mice. Number of animals, *TAOK2* $^{+/+}$ n = 13, *TAOK2* $^{+/d}$ n = 8, *TAOK2* $^{d/d}$ n = 12; SEM error bars, *P < 0.05; ordinary one-way ANOVA followed by Tukey's multiple comparisons test.

(c) Representative images of the prefrontal cortex from cortical acute slices, which were incubated with puromycin (10ug/ml) for 1.5 hr to label newly synthesized proteins and immuno-stained with anti-puromycin (green), anti-MAP2 (red) antibodies, and DAPI (blue) show increased puromycin fluorescence intensity in TAOK2 deficient cortex.

(d) Representative WB image for equal amounts of protein from acute slices analyzed by SUnSET assay and immunoblotted against puromycin antibody shows increased newly synthesized proteins in TAOK2 deficient cortex. WT+CHX, indicates that the wild-type slices were pre-treated with a translation inhibitor cycloheximide (CHX) (10mg/ml) for 30 minutes before puromycin treatment to verify the specificity of puromycin antibody signal and it is protein synthesis-dependent. Revert loading control was used to show equal protein loading for WB.

(e) Quantification for the WB SUnSET assay of cortical acute slices shows the increased normalized puromycin/β actin ratio in *TAOK2* $^{d/d}$ and *TAOK2* $^{+/d}$ mice. Number of animals, *TAOK2* $^{+/+}$ n = 5, *TAOK2* $^{+/d}$ n = 6, *TAOK2* $^{d/d}$ n = 5; SEM error bars, *P < 0.05; ordinary one-way ANOVA followed by Tukey's multiple comparisons test.

To investigate the effect of enhanced translation on the protein expression due TAOK2 loss, we did differential expression protein analysis for *TAOK2* $^{d/d}$ mice PFC in

a cooperation with Prof. Joris de Wit's lab. (Laboratory of synapse biology, Leuven, Belgium). Despite the high number of the total proteomics identified in PFC (3,731), 59 proteins were identified as significantly up-regulated proteins in the PFC of *TAOK2* $^{d/d}$ mice (Figure 13, Supplementary Table 4). Interestingly, functional classification of the upregulated proteins by PANTHER analysis revealed 11 proteins as translational proteins (Figure 14), the strongest upregulated functional group in this comparison. Moreover, the expression of large and small ribosomal proteins (Rpl22l1, Rpl36, Rpl36a, Rps10, Rps21 and Rps6) were among the significantly upregulated proteins, further indicating the enhanced translational machinery and protein synthesis in TAOK2 deficiency.

Figure 13: Deficiency of TAOK2 increases the differentially expressed proteins in the PFC from mouse. Volcano plot of differentially expressed proteins of PFC proteomics from *TAOK2* $^{+/+}$ and *TAOK2* $^{d/d}$ are depicted with the fold change and calculated by a two-sample t-test with a permutation-based FDR of 0.05 and an S0 value of 0.05 for truncation with a total of 250 randomizations. Blue and orange circles show the significantly up-regulated and down-regulated proteins in the PFC of *TAOK2* $^{d/d}$ mice, respectively. Green circle refers to TAOK2 protein.

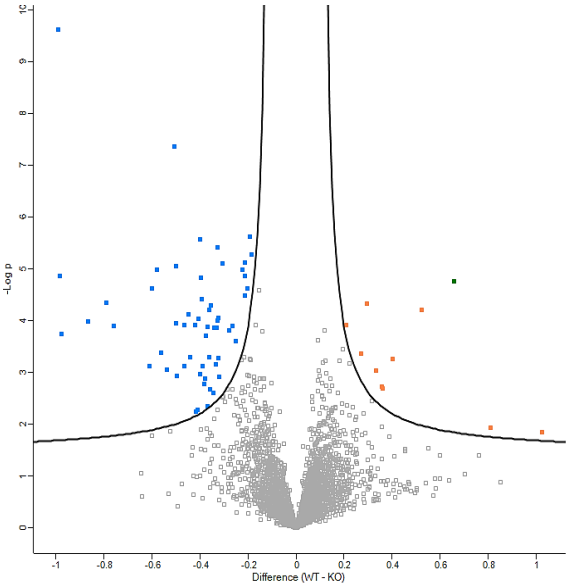

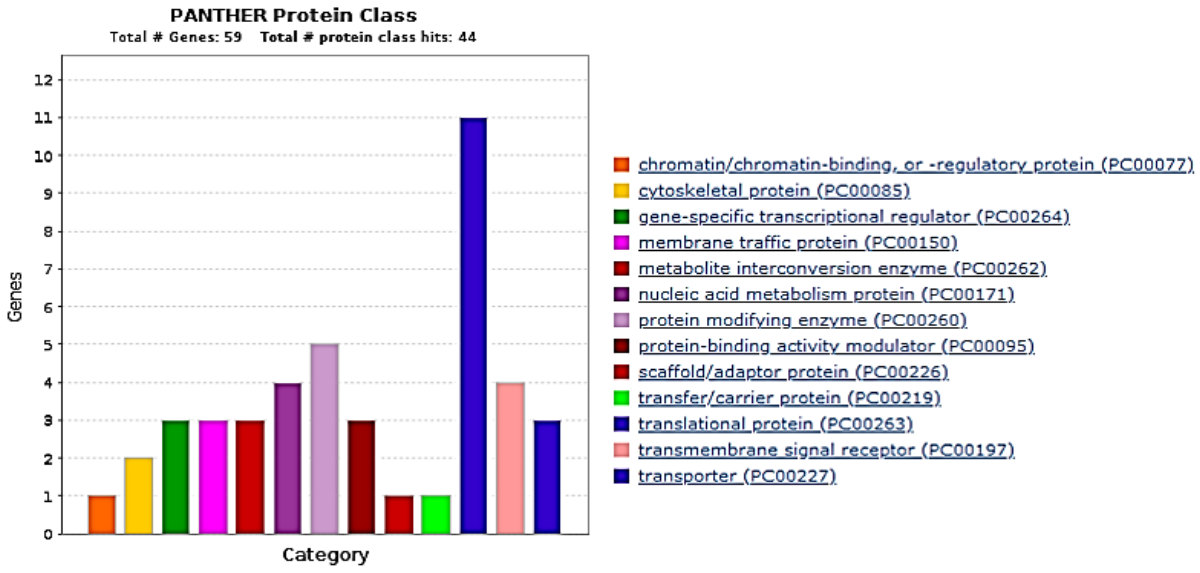

Figure 14: Translational related proteins are highly upregulated in the PFC of *TAOK2* $^{d/d}$ mice.

PANTHER bar graph shows the functional classification of the significantly upregulated proteins the PFC of *TAOK2* $^{d/d}$ mice. Translational protein (blue bar) has the highest coverage of 11 for all gene categories. (See Supplementary Table 4 for details).

To further understand the TAOK2-dependent translation effect in neurons, cortical neuronal cultures at 7DIV or 21DIV were treated with puromycin (10µg/ml) to label the newly synthesized proteins, and quantitative immunofluorescence SUnSET analysis was performed. Interestingly, *TAOK2* $^{d/d}$ and *TAOK2* $^{+/d}$ neurons show a significant increase in the incorporated puromycin signal compared to the control cells reflecting the increased neuronal protein synthesis (Figure 15 a-c).

Altogether, these data obtained from polysome profiling from cortices and cerebella as well as SUnSET assay from cortex and cortical neurons suggest a functional role of TAOK2 as a repressor of translation in the brain.

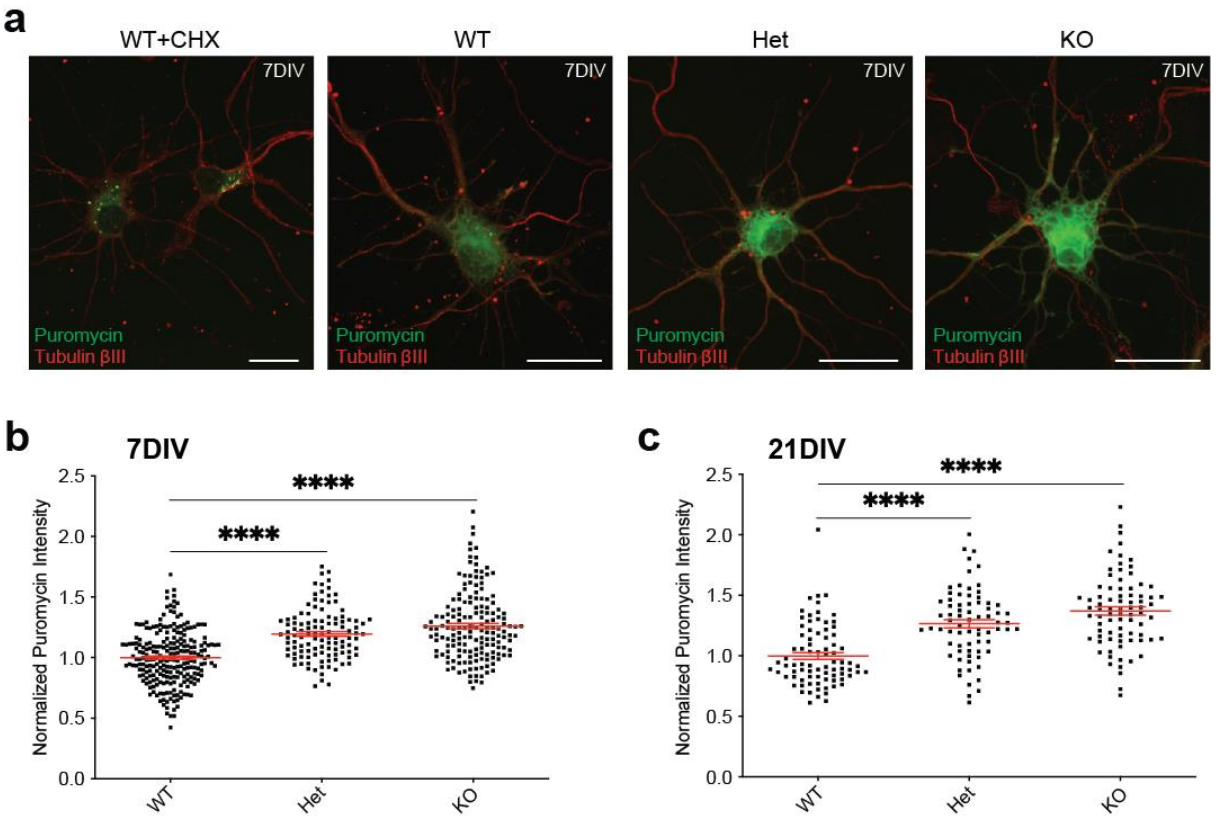

Figure 15: TAOK2 deficiency increases protein synthesis in neurons.

(a) Representative Immunostainings of primary neurons 7DIV were treated with puromycin (10µg/ml) for 10 minutes to label the newly synthesized protein, fixed and immunostained with anti-puromycin (green) and anti-tubulin βIII (red) antibodies show increased puromycin labeling intensity in TAOK2 deficient neurons. WT+CHX, indicates that the cultured neurons were pre-treated with cycloheximide (CHX) (10mg/ml) for 10 minutes before puromycin treatment to verify the specificity of puromycin antibody signal and it is protein synthesis dependent.
(b) and **(c)** Quantifications of normalized puromycin fluorescence intensity at 7DIV neurons or 21DIV, respectively, show increased newly synthesized protein by SUnSET assay in TAOK2 deficient neurons compared to the control

neurons. Number of 7DIV cells, *TAOK2* $^{+/+}$ n= 236, *TAOK2* $^{+/d}$ n= 113, *TAOK2* $^{d/d}$ n= 166, from 5 different individual embryos for *TAOK2* $^{+/+}$ and 4 embryos for each *TAOK2* $^{+/+}$ and *TAOK2* $^{d/d}$. Number of 21DIV cells, *TAOK2* $^{+/+}$ n= 81, *TAOK2* $^{+/d}$ n= 73, *TAOK2* $^{d/d}$ n= 79, from 3 different individual embryos for *TAOK2* $^{+/+}$ and *TAOK2* $^{d/d}$ and from 2 embryos for *TAOK2* $^{+/d}$. SEM error bars, **** $p < 0.0001$, ordinary one-way ANOVA followed by Tukey's multiple comparisons test.

3.2 *16p11.2* microdeletion displays dysregulated global translation that can be corrected with TAOK2β:

3.2.1 Enhanced global translation and protein synthesis in cortex and neurons of *16p11.2del* $^{+/d}$ mice.

Since our data from *TAOK2* deficient mice, patient derived LCLs cells with TAOK2 mutations, and N2a cells transiently transfected with TAOK2 isoforms recapitulate dysregulated global translation, I asked whether hallmark translational defects were also present in the *16p11.2* microdeletion mouse model. Similarly, I found that cortices from a mouse model of *16p11.2* deletion have increased P/M ratios by polysome profiling analysis; thus, reflecting enhanced global translation. Furthermore, *16p11.2del* $^{+/d}$ cortical neurons treated with puromycin show an elevated rate of puromycin labelling of the newly synthesized protein compared to WT cells (Figure 16 a-e).

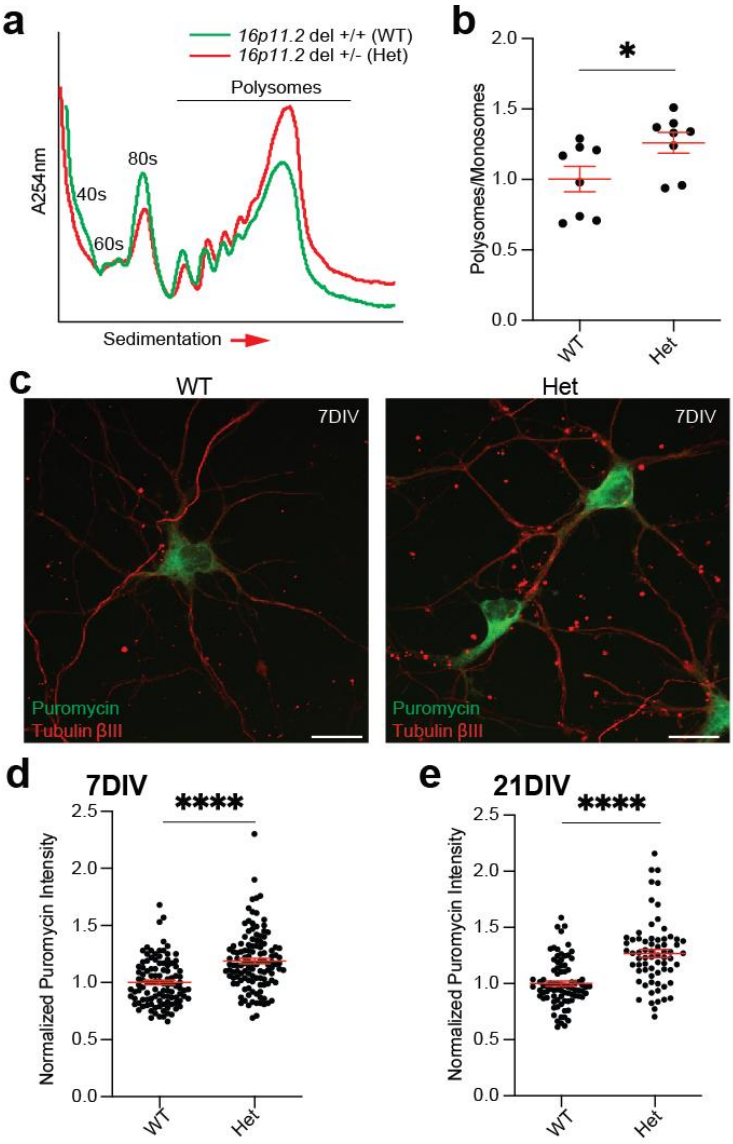

Figure 16: *16p11.2del* $^{+/d}$ mice show increase in the P/M ratio and global protein synthesis.

(a) Representative overlay of polysome profiles from *16p11.2del* $^{+/+}$ and *16p11.2del* $^{+/d}$ mice cortices shows an increase in P/M ratio in cortices of *16p11.2del* $^{+/d}$ mice.

(b) Quantification from (a) showing significantly increased P/M ratios in *16p11.2del* $^{+/d}$ mouse cortex in comparison with the WT cortex. Number of animals, *16p11.2del* $^{+/+}$ n =8, *16p11.2del* $^{+/d}$ n = 8; SEM error bars, *P < 0.05; SEM. error bars, unpaired t test.

(c) Representative Immunostainings of primary neurons 7DIV treated with puromycin (10µg/ml) for 10 minutes to label newly synthesized protein, fixed and immunostained with anti-puromycin (green) and anti-tubulin βIII (red) antibodies show increased puromycin labelling intensity in *16p11.2del* $^{+/d}$ deficient neurons.

(d) and **(e)** Quantifications of puromycin fluorescence intensity at 7DIV neurons or 21DIV, respectively, show increased newly synthesized protein by SUnSET assay in *16p11.2del* $^{+/d}$ deficient neurons compared to the control neurons. Number of 7DIV cells, *16p11.2del* $^{+/+}$ n= 107, *16p11.2del* $^{+/d}$ n= 119, from 3 different individual embryos of *16p11.2del* $^{+/+}$and 4 embryos of *16p11.2del* $^{+/d}$. Number of 21DIV cells, *16p11.2del* $^{+/+}$ n= 85, *16p11.2del* $^{+/d}$ n= 68, from 5 different individual embryos of *16p11.2del* $^{+/+}$ and 4 embryos of *16p11.2del* $^{+/d}$. SEM error bars, **** p < 0.0001, ordinary one-way ANOVA followed by Tukey's multiple comparisons test.

3.2.2 TAOK2β rescues the increased protein synthesis in *16p11.2del* $^{+/d}$ cortical neurons.

My data show the overexpression of TAOK2β in the N2a cells represses translation and decreases protein synthesis, while its kinase mutation enhances translation and increase the amount of newly synthesized protein (Figure 10 a-f), therefore we predicted that the re-introduction of TAOK2β in cultured neurons derived from cortices of *16p11.2del* $^{+/d}$ mice could rescue the observed translational defects (Figure 16 a-e). We first transfected the cortical neurons of *16p11.2del* $^{+/d}$ embryos with TAOK2β via *in utero* electroporation (IUE) followed by primary culture neuron preparation at 72 hours post-transfection to ensure the expression of TAOK2β in the neurons. Afterward, the neurons were treated with puromycin to label the nascent proteins after 7 days culture and immune-stained with puromycin antibody. As expected, the introduction of TAOK2β via IUE decreased the puromycin immunostaining intensity in cultured *16p11.2del* $^{+/d}$ cortical neurons to similar levels detected in WT neurons (Figure 17 a, b).

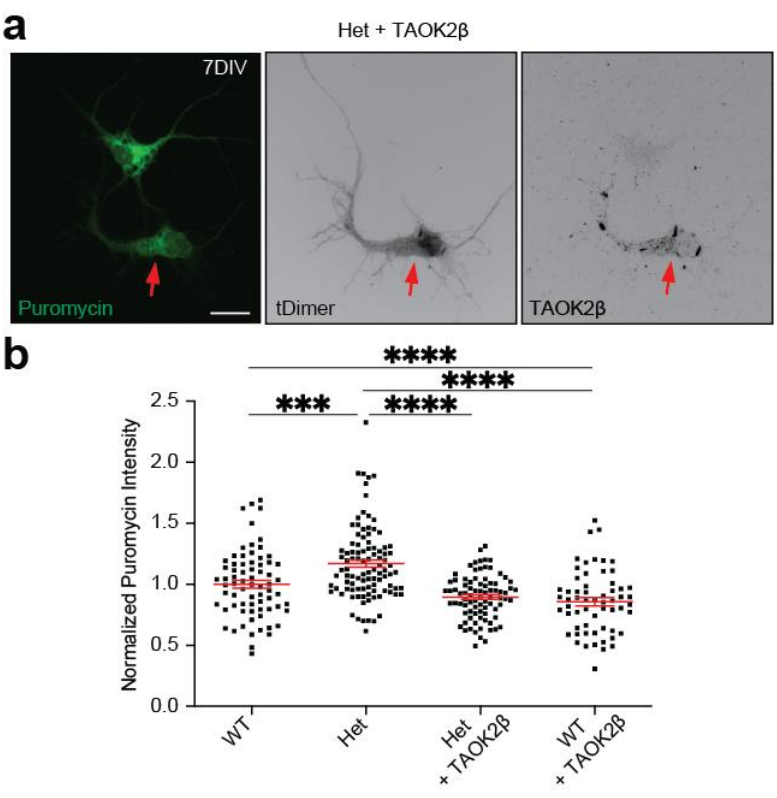

Figure 17: TAOK2β normalizes the increased protein synthesis in the electroporated *16p11.2del* $^{+/d}$ cortical neurons.

(a) Representative Immunostaining of *16p11.2del* $^{+/d}$ cortical neurons after IUE at E15.5 with TAOK2β and t-dimer plasmids treated at 7DIV with puromycin (10µg/ml) for 10 minutes to label newly synthesized protein, fixed and immunostained with anti-puromycin (green) and anti-TAOK2β (grey) antibodies shows a reduction of puromycin fluorescence intensity in the transfected cells.
(b) Quantifications from (a) show a significant decrease in puromycin intensity in *16p11.2del* $^{+/d}$ (to the normal level in *16p11.2del* $^{+/+}$ neurons) and *16p11.2del* $^{+/+}$ cortical neurons transfected with TAOK2β compared to their corresponding controls, non-transfected *16p11.2del* $^{+/d}$ and *16p11.2del* $^{+/+}$ cortical neurons, respectively. Number of cells, non-transfected wild type cells n= 71, wild type cells + TAOK2β n=60 from 4 different embryos; non transfected type *16p11.2del* $^{+/d}$ cells n= 99, *16p11.2del* $^{+/d}$ + TAOK2β n=84 from 4 different embryos. SEM error bars, ***P < 0.001, **** p < 0.0001, ordinary one-way ANOVA followed by Tukey's multiple comparisons test.

This normalization of the upregulated protein synthesis in the *16p11.2* microdeletion neuron supports the role of TAOK2β as a repressor of translation. Altogether, my results suggest that TAOK2 is a major risk gene causally involved in ASDs linked to *16p11.2* microdeletion, due to translation dysregulation.

3.3 TAOK2 involved in regulation of translation initiation and translation elongation.

3.3.1 TAOK2 is involved in phosphorylation of the eukaryotic initiation factor (eIF2α)

Phosphorylation of the eIF2α at its Ser51 by the four eIF2α kinases, PKR-like ER kinase (PERK), dsRNA dependent protein kinase (PKR), general control nonderepressible-2 (GCN2), and heme-regulated inhibitor (HRI) is considered a major regulator of translation initiation (Donnelly et al., 2013). Once eIF2α is phosphorylated at its residue Ser51, it becomes a competitive inhibitor to the guanine nucleotide exchange factor (GEF), eIF2B. This leads to decreased availability of eIF2-GTP for ternary complex formation required to start translation initiation, thus resulting in reduced global protein synthesis (Sonenberg & Hinnebusch, 2009). Therefore, I analyzed how TAOK2 is mechanistically involved in protein synthesis. I examined the phosphorylation level of Ser51 of the eIF2α that is targeted by all four eIF2α kinases by WB analysis. Interestingly, TAOK2 deficient cortices and patient-derived LCLs with a TAOK2 point mutation at A135P in the kinase domain revealed reduced levels of eIF2α phosphorylation (Figure 18 a-d). On the other hand, overexpression of TAOK2β in N2a cells showed increased levels of eIF2α phosphorylation (Figure 18 e and f). These results suggest

that TAOK2 might regulate translation control at the initiation stage through phosphorylation of the eIF2α.

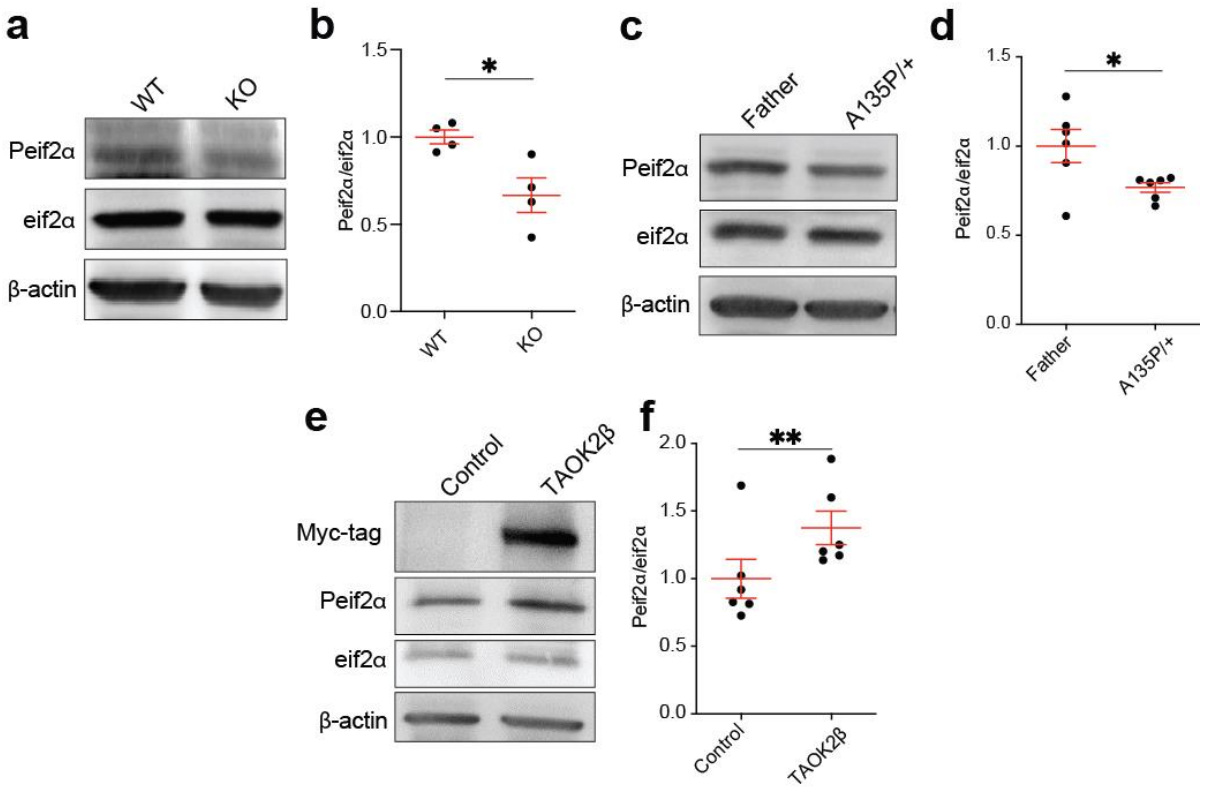

Figure 18: TAOK2 phosphorylates eIF2α.

(a) Representative WB images for the cortex of *TAOK2* $^{+/+}$ and *TAOK2* $^{d/d}$ and **(b)** quantifications for (a) show significantly increased P-eIF2α normalized to the total eIF2α level in cortices of WT animals. Number of animals per genotype n=4; *P < 0.05, SEM. error bars, unpaired t-test.
(c) Representative WB images for LCLs with TAOK2 mutations A135P at its kinase domain and non-affected father and **(d)** quantifications for (c) show significantly decreased level of P-eIF2α to the total eIF2α. Number of biological replicates n=6 per condition; *P < 0.05, SEM. error bars, unpaired t test.
(e) Representative WB images for N2a cells transfected with wild type TAOK2β and its respective control and **(f)** quantifications for (e) show significantly increased level of P-eIF2α to the total eIF2α in the cells transfected with wild type TAOK2β compared to the non-transfected control cells. Number of biological replicates n=6 per condition from different independent transfection experiments; **P < 0.05, SEM. error bars, unpaired t-test.

My data suggest that TAOK2 phosphorylates eIF2α. However, IP-MS analysis of immunoprecipitation complexes using TAOK2β antibody did not identify eIF2α as a direct binding partner to TAOK2β. Additionally, TAOK2 does not interact with any of the eIF2α-phosphorylating kinases, which increases the probability that TAOK2 phos-

phorylates eIF2α indirectly through activation of one or more the eIF2α kinases. Interestingly, our IP-MS analysis revealed that TAOK2β interacts with GCN1 (Supplementary Figure 2 and Supplementary Table 2), an activator of GCN2 that forms a trimeric complex with the translating ribosomes and GCN2 and simultaneously stimulates GCN2 kinase activity (Cambiaghi et al., 2014; Roffé et al., 2013). These data suggest one possible mechanism by which TAOK2 phosphorylates eIF2α through activity modulation of GCN1 and GCN2 leading to a subsequent inhibition of translation initiation and reduction of protein synthesis. Further work will be required to provide mechanistic insights into the molecular pathway by which TAOK2 regulates translation initiation through eIF2α phosphorylation, and its consequences on neuronal development due to altered synaptic protein synthesis, this will be discussed later.

3.3.2 TAOK2 binds and phosphorylates the eukaryotic elongation factor eEF2

Regulation of translation at the elongation step mainly depends on the active less phosphorylated status of the elongation factor eEF2, which help in binding the ribosomes to the mRNA (Schuller & Green, 2018). My western blots data suggest that TAOK2 phosphorylates the Thr56 of the eEF2, which might lead to inactivation of the eEF2 and subsequent slowing down the translation elongation step. Cortices form *TAOK2* $^{d/d}$ mice show decreased phosphorylated eEF2/total eEF2 ratios (Figure 19 a). While LCLs from ASD patient with mutated TAOK2 in its kinase domain and N2a cells overexpressing the kinase dead form of TAOK2 (TAOK2βA135P) show a reduction in the phosphorylated eEF2 (Figure 19 b and c), N2a cells overexpressing wild type TAOK2β show increased phosphorylation of the eEF2 (Figure 19 d). This suggest that TAOK2 is phosphorylating the eEF2 via its kinase functional domain. To further understand how TAOK2 can modulate the activity of the eEF2, I did TAOK2β IPs from cytoplasmic lysate from transfected N2a cells expressing Wild type TAOK2β: Proteins captured by TAOK2β antibodies were immunodetected by WB. Interestingly, the detection of eEF2 by an eEF2 antibody revealed its presence in the protein complex of TAOK2β, which was clearly detectable after overexpression of TAOK2β compared to endogenously expressed TAOK2β in N2a cells (Figure 19 e). This data shows that eEF2 interacts with TAOK2 and suggests that TAOK2 might phosphorylate eEF2 directly. Further studies will be required to investigate whether the TAOK2 directly binds and phosphorylates eEF2 or acts on the upstream molecules of eEF2.

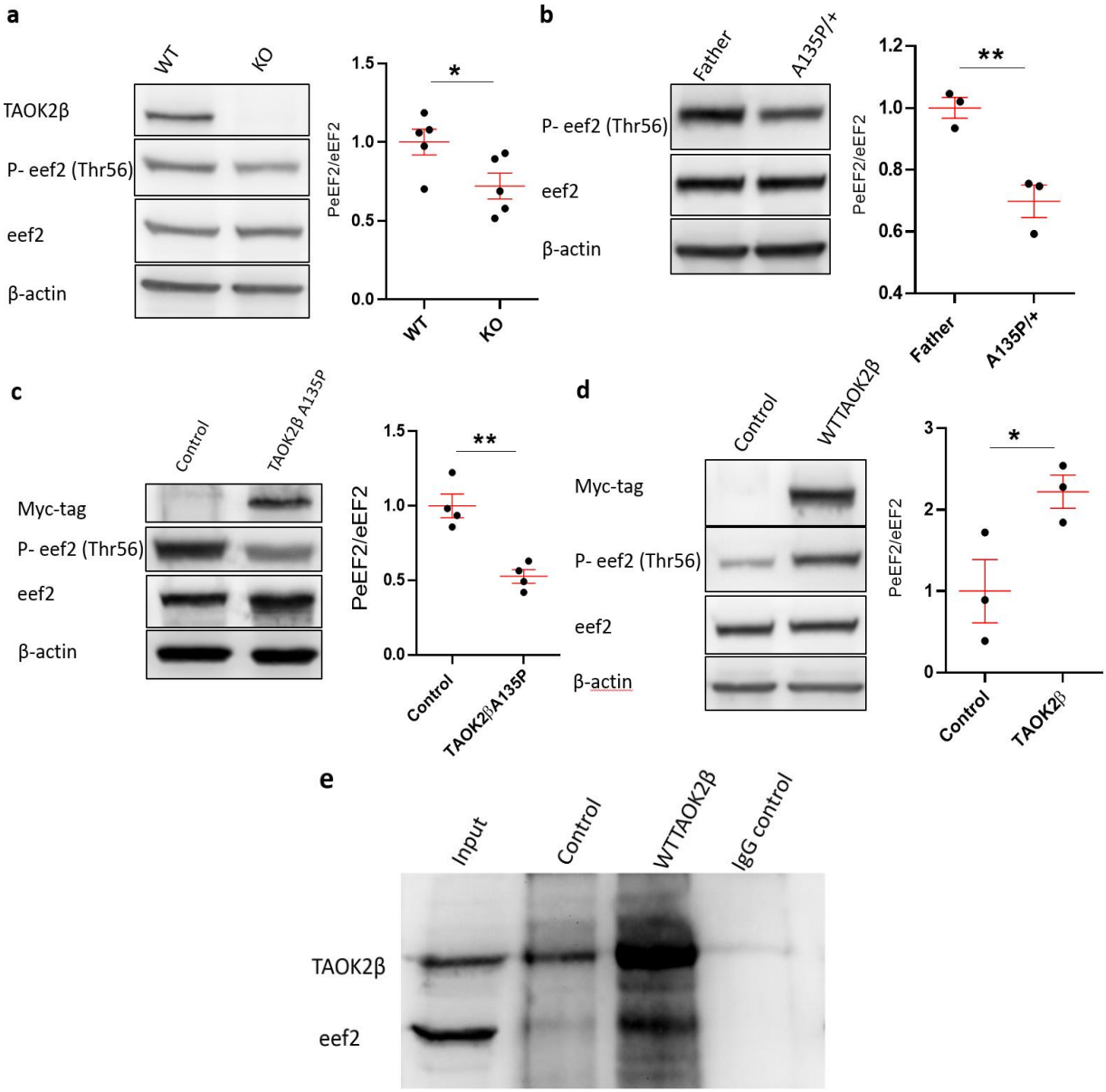

Figure 19: TAOK2 phosphorylates and binds the elongation factor eEF2.

(a) Representative WB image and quantifications for the cortex of *TAOK2* $^{+/+}$ and *TAOK2* $^{d/d}$ show significantly increased P-eef2 normalized to the eef2 levels in cortices of WT animals. Number of animals per genotype n=5; *P < 0.05, SEM. error bars, unpaired t-test.

(b) Representative WB images and quantifications for LCLs with TAOK2 mutations A135P at its kinase domain and non-affected father show significantly decreased level of P-eef2 to the total eef2. Number of biological replicates n=3 per condition; **P < 0.05, SEM. error bars, unpaired t test.

(c) Representative WB image and quantifications for N2a cells transfected with TAOK2βA135P and its respective control show significantly decreased levels of P-eef2 to the eef2 in the cells transfected with TAOK2βA135P compared to the non-transfected control cells. Number of biological replicates n=4 per condition from different independent transfection experiments; **P < 0.01, SEM. error bars, unpaired t-test.

(d) Representative WB image and quantifications for N2a cells transfected with wild type TAOK2β and its respective control significantly increased levels of P-eef2 to the eef2 in the cells transfected with wild type TAOK2β compared to the non-transfected control cells. Number of biological replicates n=3 per condition from different independent transfection experiments; *P < 0.05, SEM. error bars, unpaired t-test.

(e) WB image of the TAOK2β immunoprecipitation (IPs) from non-transfected N2a cells and cells overexpressing wild type TAOK2β shows the interaction of TAOK2β with the eEF2. Membrane was immunoblotted against TAOK2β and eEF2. Unspecific rabbit IgGs and total cytoplasmic lysate (input) were used as IP controls.

Collectively, my data are shedding the light on a new function for TAOK2 as a novel candidate controls translation for the following summarized reasons: The IP-MS analysis of immunoprecipitation complexes using a TAOK2β antibody in cytoplasmic lysates from mouse cortex and N2a cells overexpressed with wild type TAOK2β revealed the interaction of TAOK2 with several proteins associated with translational control machinery. Moreover, I could show for the first time that TAOK2 isoforms, α and β, are present in the polyribosome complex and regulate translation in different biological samples, like brain tissues (cortex, cerebellum), primary neurons, human LCLs from ASD patients and N2a cells. I show that TAOK2 isoforms affect general translation and their mutations – especially in the isoform β - increase the puromycin incorporation rate into the newly synthesized proteins in neuronal and non-neuronal cells, which reflects the increased protein synthesis. Furthermore, I could demonstrate that TAOK2 deficiency increases translation in mice brain tissues, and I showed that TAOK2 contributes to the altered global translation in the mouse model of *16p11.2* deletion. These data suggest the role of TAOK2 as a repressor of translation. Finally, I provided mechanistic insights by which TAOK2 regulates translation at both initiation and elongation steps where it phosphorylates the eIF2α, interacts with, and phosphorylates the eEF2 respectively.

4. Discussion:

ASDs are complex neurodevelopmental disorders characterized by cognitive impairments, behavioral and social abnormalities and have a 1-2% worldwide prevalence (Kim et al., 2011). Moreover, ASD represents a growing financial and emotional overload on the societies because it is a long-lasting condition and the autistic patients require special support in the early life (Lavelle et al., 2014). The main reasons for development of the ASD have not yet been well understood, which are reflected on the limited availability of effective treatment for ASD. Importantly, recent studies suggest that the development of ASD results from the dysregulation of the neuronal translation, which leads to deficits and neurotransmission imbalance at the synaptic level (Kelleher

et al., 2008). Here, I show that *TAOK2* – an ASD susceptibility gene – regulates translation in neuronal and non-neuronal tissues. Wherein, TAOK2 deficiency and the *de novo* mutations in TAOK2, identified in ASD patients, display upregulated global translation and increased protein synthesis. Moreover, I showed that TAOK2 represses translation by phosphorylation of the eIF2α and eEF2 that inhibits translation initiation and translation elongation, respectively. In accordance with that TAOK2 could normalize the dysregulated global translation observed in *16p11.2* $^{+/d}$ deletion models.

In this study, I used polysome profiling, SUnSET assay, and different analytic protein assays to study the role of TAOK2 in translational regulation in brain tissues and primary neurons from the *TAOK2* and *16p11.2* $^{+/d}$ del autistic mice models, non-neuronal cells (LCLs) from ASD patients and N2a cells.

4.1 The ASD relevant gene *TAOK2* is involved in translational regulation

TAOK2 is an autism-associated gene and its loss leads to impaired dendrite and synapse formation, autistic-like behaviors and altered brain anatomy in mice, such as increased midbrain size and reduced cortical volumes (De Anda et al., 2012; M. Richter et al., 2019). Here, we described a new function for TAOK2 due to its association with the translational control machinery. The polysome profiling analysis revealed enhanced global translation in cortices and cerebella of *TAOK2* deficient mice. Furthermore, analysis of the proteins extracted from polysomes of *Taok2* $^{+/+}$ cortices revealed the presence of TAOK2 in the polyribosome complex while the β isoform is more abundant in polysomes than α isoform. Accordingly, the IP/MS analysis of immunocomplexes purified using a TAOK2β antibody showed the association of TAOK2 with many proteins involved in translational regulation, ribonucleoprotein complex formation, peptide biosynthesis, and RNA binding in addition to its association with proteins regulating synapse and cytoskeleton organization. These results suggest the involvement of TAOK2 in the translational control machinery through protein-protein interactions, as TAOK2 has no RNA binding site and it was not identified as an mRNA-binding protein in the global mRNA interactome capture experiments (Castello et al., 2012; Caudron-Herger et al., 2019).

It is noteworthy to mention that many ASD-associated genes, which are classified as SFARI group I genes, encode proteins (eIF4E, eIF3g, eEF1A2, RPL10, eIF4EBP2, and UPF3B) that are present in the translational machinery complex and involved in the different stages of translation (Chen et al., 2019). Additionally, many

RNA-binding proteins (RBPs), that regulate mRNA translation processes, are known ASD risk genes. For example, FMRP, a well-known ASD-associated gene, is one of the best characterized translation repressing RBPs, where its deficiency or mutations participates in the pathogenesis of the fragile X syndrome (FXS) (Zalfa et al., 2003). Cell cycle-associated protein 1 (Caprin1) is another RNA-binding protein present in polyribosomes where it interacts with FMRP and modulates its activity (El Fatimy et al., 2012) and upon deficiency, *CAPRIN1* heterozygous mice exhibit autistic like behaviors (Ohashi et al., 2016). Janus kinase and microtubule-interacting protein 1 (JAKMIP1) is present in the polyribosome complex interacting with several translation-associated proteins and ribosomal subunits, such as FMRP, poly (A) binding protein cytoplasmic 1 (PABPC1), eEF1A, eEF2 to regulate neuronal translation. JAKMIP1 deficiency leads to abnormal translation in neurons and *JAKMIP1* deficient mice exhibit social abnormalities and autistic-like behaviors (Berg et al., 2015). Translin is also another RNA binding protein that regulates neuronal translation by regulating the mRNA transport via its association with microtubules and motor proteins (Wu et al., 2011). *Translin* deficient mice show neurochemical and behavioral abnormalities resembling several neurological disorders, including ASD, due to disturbances in protein synthesis (Stein et al., 2006). My data suggest that TAOK2 shares common features described for the previously mentioned ASD risk genes as it associates with the translation complex and regulates neuronal translation. I thereby hypothesize that this translational dysregulation, due to TAOK2 deficiency in mice or due to functional mutations or loss of TAOK2 (*16p11.2* microdeletion) in humans, contributes to the autistic-like behaviors displayed in *TAOK2* deficient mice (M. Richter et al., 2019) as well as in autistic humans, respectively.

4.2 Deficiency of TAOK2 and its de novo mutations increases the amount of the newly synthesized proteins in neuronal and non-neuronal cells

Several studies suggest that disturbances in translational control machinery and the subsequent dysregulated synaptic proteins are one of the molecular mechanisms underlying the etiology for synaptopathies in ASD (Kelleher et al., 2008; Santini et al., 2013; Suzuki et al., 2015). Therefore, dysregulated protein synthesis is considered a common feature in most of the autistic phenotypes, particularly excessive neuronal protein synthesis are observed in FXS pathogenesis (Santoro et al., 2012), and in different forms of autism (Gkogkas et al., 2013; Santini et al., 2013). Surprisingly, meas-

urement of the amount of the newly synthesized protein by SUnSET assay shows enhanced protein synthesis in cortex and neurons from *TAOK2* deficient mice compared to the wild type controls. This data suggest that TAOK2 is a repressor of the neuronal translation, similar to the most known autism-linked genes, such as *FMRP*, *PTEN*, and *TSC1/2*, wherein mutations in these genes disturb the translation repression, cause aberrant protein synthesis and lead to the autistic phenotypes (Kelleher et al., 2008). Consistently, analysis of the de novo global protein synthesis in animal models of FXS, and in different cells derived from FSX patients, such as lymphoblastoid cells, fibroblasts as well as induced pluripotent stem cell (iPSC)-derived neural progenitor (NPCs), revealed the increased global protein synthesis due to the absence of translation repression by *FMRP* (Gross & Bassell, 2012; Jacquemont et al., 2018; Raj et al., 2021). Similarly, lymphoblastoid cells from autistic patients with TAOK2 mutated at the at residue A135P in the kinase domain, which leads to loss of the TAOK2 kinase function, showed enhanced global translation by polysome profiling analysis and increased amount of newly synthesized proteins compared to cells derived from the non-affected father. These data indicate that the role of TAOK2 in translational repression is mainly achieved through its kinase function and suggest that TAOK2 regulates translation in non-neuronal tissues. Furthermore, N2a cells, a neural crest-derived cell line, transfected with wild type TAOK2β or wild type TAOK2α, revealed reduced translation compared to the control. However, when these cells were transfected with the kinase-dead TAOK2β A135P mutation, the global translation, as analyzed by calculating the P/M ratio and the amount of protein synthesis measured by puromycin incorporation rate, were elevated in comparison with control cells. In contrast, cells expressing the TAOK2α A135P mutated isoform did not reveal any significant change in the global translation, wherein the P/M ratios were similar to the control. Thus, these data suggest that the defects in translational control and global protein synthesis are a direct consequence of the loss of TAOK2β kinase function, but not TAOK2α. One possible explanation for the isoform-specific role of TAOK2 in regulating transaltion is the isoform abundance in the polyribosome complex. Wherein, the β isoform is more abundant in polysomes than the α isoform as identified by LC-MS/MS analysis for extracted proteins from polysomes of *Taok2* $^{+/+}$ cortices and by WB analysis for the polysomes of N2a cells transfected with wild type TAOK2β or wild type TAOK2α. Another possible explanation is the expression levels of the TAOK2α A135P isoform in the N2a cells that might not be expressed proficiently to produce any striking effect on translation.

However, we concluded that the first explanation is more realistic since my data show less abundance of TAOK2α isoform in the polyribosome complex, and the transfection efficiency for the cells used in the experiments were more than 70% with good expression level (Figure 9 F).

4.3 Deficiency of TAOK2 upregulates ribosomal proteins and proteins involved in translation regulation

Loss of TAOK2 or loss-of-function TAOK2 de novo mutations increases protein synthesis in murine cortex or derived neurons. Accordingly, the differential expression protein analysis for the PFC from *TAOK2* knock out mice showed significantly upregulated proteins of the translational machinery components, especially the ribosomal proteins. Recently, Griesi-Oliveira et al. (2021) examined the transcriptome of iPSC-derived neurons from ASD patients and they showed upregulation of the co-expressed genes involved in the translation processes in the NPCs, which leads to abnormalities of the expressed genes related to synaptic functions in neurons. Interestingly, genes encoding ribosomal proteins were also upregulated in post-mortem cortical tissues and iPSC- derived neural progenitor cells, as well as in the non-neuronal cell types such as lymphocytes from ASD patients (Lombardo, 2020; Tylee et al., 2017). Collectively, our data suggest that the upregulation of ribosomal genes and its subsequent effects on cellular translation are important for ASD biology. These insights highlighting questions for future work to understand the mechanisms that lead to the increased ribosomal proteins in the brain and their relevance for the development of ASD. Here, in case of TAOK2 deficiency, the upregulation of ribosomal proteins could be due to two possible reasons. First, the increased translation of the existing mRNAs is due to the absence of the translational repressor role of TAOK2 at the initiation and elongation stages, which subsequently modulates the expression of these genes. Second, TAOK2 - especially TAOK2β - has a cytoplasmic and nuclear localization, as indicated by the myc-tag signal in the N2a cells expressing Wild type TAOK2β (Figure 10 b), where the ribosome biogenesis takes place. Thus, the ribosome biogenesis is possibly activated that might leads to stimulation of protein synthesis in case of lack of TAOK2. Accordingly, further future investigations exploring ribosome biogenesis in TAOK2 deficient samples could be relevant for ASD research, particularly the dysregulated ribosome biogenesis could lead to excitation/inhibition imbalance if it affects specifically certain types of neurons such as the excitatory neurons, inhibitory neurons, or radial glia cells as previously suggested (Lombardo, 2020).

4.4 TAOK2 is a key contributor within *16p11.2* microdeletion and restores the protein homeostasis in the *16p11.2* microdeletion phenotypes

While many genes have been linked to ASDs, the CNVs in *16p11.2* microdeletion account for more than 1% of all individuals diagnosed with ASD suggesting it is a major risk factor (Weiss et al., 2008). Several evidences suggest that *TAOK2* is a major player among the 30 genes, located in the 16p 11.2 locus, for the development of ASD. Recently, we identified ASD-linked mutations in TAOK2. Consistently, *Taok2* knockout mouse models recapitulate key morphological, physiological, and behavioral abnormalities of the *16p11.2* microdeletion syndrome (M. Richter et al., 2019). Furthermore, unpublished data from our group revealed that TAOK2 – especially the isoform α that localizes mainly in microtubules – could rescue migration defects of cortical neurons in the *16p 11.2* $^{+/d}$ microdeletion mouse model. Additionally, in this study, polysome profiling and SUnSET assays analysis for *16p 11.2* $^{+/d}$ microdeletion models recapitulate upregulated global translation in the cortex and increased protein synthesis in the cultured cortical neurons. This exaggerated protein synthesis and enhanced translation in *16p 11.2* $^{+/d}$ microdeletion are probably due to the absence of TAOK2 as a translational repressor, particularly, since none of the other genes located in the *16p 11.2* chromosomal region has been identified yet to be involved translation regulation. Together with the original studies, these data strongly suggest the high relevance of *TAOK2* within the 16p 11.2 locus.

Disturbance in translational control and its implications on neuronal protein synthesis are considered a major mechanism responsible for the synaptopathies in ASD. Thus, several pharmacological and genetic interventions have been successfully corrected the dysregulated protein synthesis and ameliorated its related autistic phenotypes in ASD mouse models (Dölen et al., 2007; Gkogkas et al., 2013). Targeting inhibition of the metabotropic glutamate receptors (mGluR) activity ameliorates the autistic phenotype in *Fmr1* deficient mice (Bear et al., 2004; Dölen et al., 2007), while inhibition of mTOR pathway using rapamycin reverses the cognitive abnormalities in *Tsc2* $^{+/-}$ mice (Ehninger et al., 2008). Moreover, pharmacological downregulation of the exaggerated cap-dependent translation observed in different autistic mouse models (transgenic mice overexpressing eIF4E, *4EBP2* deficient mice, and *FMRP* deficient mice) by 4EGI-1 that inhibits eIF4E–eIF4G complex formation, rescues the autistic behaviors and the dysregulated protein synthesis (Gkogkas et al., 2013; Santini et al., 2013, 2017). Several noteworthy findings suggest that pharmacological inhibition of

MAP kinase-interacting kinases (MNKs), which regulate the mRNA translation in signaling dependent pathways, could rescue the dysregulated translation and the autistic phenotypes in two different studies. It restored the abnormal translational level and the autistic behaviors in the synaptic adhesion protein *Nlgn3* knock out mice via restoring oxytocin signaling activity (Hörnberg et al., 2020), as well as correction of FXS pathophysiologies in *Fmr1* knockout mice (J. D. Richter et al., 2015). Our results show significant upregulation of 59 proteins identified in the PFC of *TAOK2* $^{d/d}$ mice (Supplementary Table 4), including the metabotropic glutamate receptor 2. Several studies highlighted the importance of the mGluR in the synaptic neurotransmission and development of ASD (Edfawy et al., 2019; Salpietro et al., 2019). Therefore, future studies targeting the activity of these differentially expressed proteins will elucidate new avenues for therapeutic strategies overcoming morphological and functional defects of genetic forms of ASD linked to the TAOK2 pathway.

Interestingly, studies based on compensating translation function have been done to restore the translational homeostasis in ASD pathogenesis. Wherein they used genetic and pharmacological manipulations to compensate the loss effect of a positive translational regulator with the loss effect of a negative translational regulator and vice versa. For example, *Fmr1* $^{-/y}$ / *Cpeb1* $^{-/-}$ knockout mice – result from the crossing of *Fmr* $^{-/y}$ mice (lacks the translational repressor FMRP) with *Cpeb1* $^{-/-}$ mice (lack cytoplasmic polyadenylation element–binding protein (CPEB), a translational activator) – display normalized translation and different phenotypes associated with FXS since the ablation of the translational activator CPEB1 compensates for deficiency of the translational repressor FMRP (Udagawa et al., 2013). Consistently, the dysregulated transcriptional activity and the decreased protein synthesis in *MECP2* knockout human embryonic stem cell-derived neurons, a model of Rett syndrome that related to ASD, are restored by stimulation of AKT/mTOR signaling by growth factors or by knocking down PTEN, a negative regulator of AKT/mTOR pathway (Yun Li et al., 2013). Our results are consistent with these previous studies, where re-introduction of TAOK2β – a translational repressor - via *IUE* in cortices of *16p11.2del* $^{+/d}$ mice could rescue the translational defects. Accordingly, the puromycin immunostaining intensities, identified by SUnSET assay in cultured *16p11.2del* $^{+/d}$ cortical neurons transfected with wild type TAOK2β, were normalized to similar levels of wild type neurons. This data highlights the potential role of TAOK2β as a translational repressor and its role as a risk gene for mental dis-

orders, including ASDs linked to *16p11.2* microdeletion, due to translational dysregulation. It will be interesting to explore the role of TAOK2 as a translational repressor in the *16p11.2del* $^{+/d}$ mouse model in a wider view. Our group has produced a *16p11.2del* $^{+/d}$ / *TAOK2* $^{+/+}$ mouse – a mouse model with heterogenous *16p11.2* microdeletion with genomic re-introduction of TAOK2 - to analyze whether TAOK2 rescues morphological, functional, and behavioral abnormalities in the *16p11.2* microdeletion mouse model.

4.5 TAOK2 regulates translation through phosphorylation of the initiation factor eIF2α and the elongation factor eEF2

Translational control is important for gene expression in response to different physiological and pathological conditions, such as development and differentiation, neuronal function, aging, stress and nutrient deprivation, as well as diseases (Hershey et al., 2019). Currently, elucidating the mechanisms regulating translation, particularly at the initiation and the elongation stages, are considered a hot spot in different physiological and pathological conditions. Accordingly, protein kinases phosphorylate different components of the translational machinery complex, especially the initiation and elongation factors. These phosphorylation events regulate the activity and interactions of these factors with other molecules in the translational machinery complex and thereby regulate translation (Proud, 2019).

mTOR pathway with its two multi-subunit complexes (mTORC1 and mTORC2) is considered the main kinase that regulates the translational machinery components as well as the kinases that phosphorylate different elongation and initiation factors (Saxton & Sabatini, 2017). In neurons, the PI3K-mTOR and the RAS-ERK signaling pathways regulate phosphorylation of multiple factors in the translational complex such as eIF4E, 4E-BP, eIF4B, eEF2, and RPS6, that subsequently affects protein synthesis (Chen et al., 2019). Furthermore, both signaling pathway controls protein synthesis and local translation at synapses in response to neuronal activity (Costa-Mattioli et al., 2009; Sutton & Schuman, 2006). Therefore, dysregulation in these signaling pathways exaggerates general protein and synaptic protein synthesis, and this imbalance participates in the development of ASD.

eIF2α is phosphorylated by the four eIF2α kinases in response to different cellular stimuli that activates the adaptive pathway of the integrated stress response (ISR)

(Pakos-Zebrucka et al., 2016). Activation of the ISR leads to phosphorylation of the α subunit of the eIF2 on Ser51 with subsequent inhibition of the translation initiation and protein synthesis (Harding et al., 2003). In this study, my western blot data revealed increased eIF2α phosphorylation in N2a cells overexpressing TAOK2β and reduced phosphorylation in TAOK2 deficient cortices and patient-derived LCLs with a loss-of-function mutation of TAOK2 at A135P in the kinase domain. Consistently, general translation and protein synthesis after overexpressing wild type TAOK2 is decreased in neuronal cells, while increased in cortices of TAOK2 deficiency mice or after over-expression of functional mutations in neuronal cells, respectively. This suggests that TAOK2 regulates translational control through phosphorylation of the eIF2α. In accordance with that, our IP-MS analysis revealed that TAOK2β interacts with GCN1, an activator of GCN2 that forms a trimeric complex with the translating ribosomes and GCN2 and stimulates GCN2 kinase activity (Cambiaghi et al., 2014; Roffé et al., 2013). This suggests, that TAOK2 regulates translation through the activity of the GCN1-GCN2-eIF2α pathway. Further studies are required to investigate how TAOK2 kinase activity modulates the activity of GCN1, like in vitro kinase assay using the commercially available GCN1 recombinant protein. Additionally, the activity level of other kinases upstream of eIF2α (PERK, PKR, and HRI) need to be explored to understand how TAOK2 deficiency affects their activity and leads to reduced eIF2α phosphorylation and enhanced protein synthesis.

Moreover, my results show less phosphorylation of eIF2α in *TAOK2* $^{d/d}$ mice and LCLs cells with functional mutations in the kinase domain of TAOK2, resulting in increased translation compared to controls. Therefore, we are assuming that the increased translation in case of TAOK2 deficiency is due to reduced phosphorylation of eIF2α, and further studies are required to test this hypothesis. Thus, I suggest to directly induce eIF2α phosphorylation pharmacologically to test whether increased phosphorylation of eIF2α in TAOK2 deficient cells can normalize the dysregulated translation. As targeting the upstream kinases of eIF2α is difficult, targeting the activity of phospho-eIF2α phosphatases pharmacologically will be a straightforward approach. In fact, Salubrinal is a specific inhibitor for phospho-eIF2α phosphatases (GADD34/PP1c and CReP/PP1c) and reduces the dephosphorylation of eIF2α (Boyce et al., 2005). Therefore, treatment of primary cortical neurons from *TAOK2* $^{d/d}$ embryos or cells expressing TAOK2 mutations especially the kinase domain with Salubrinal as previously described (Boyce et al., 2005; O'Connor et al., 2008) will be necessary to induce eIF2α

phosphorylation. Thereafter, monitoring the translation level in the treated cells will provide mechanistic evidence that TAOK2 represses translation by eIF2α phosphorylation depending on its kinase function. Providing mechanistic insight into how TAOK2 controls translation through the eIF2α phosphorylation pathway will substantially impact this highly relevant field of ASD research. Additionally, the pharmacological interventions of eIF2α phosphorylation will elucidate new avenues for therapeutic strategies overcoming morphological and functional defects of genetic forms of ASD linked to the TAOK2 pathway.

My study not only suggests that TAOK2 regulates translation at the initiation stage but is also involved in the regulation of translation elongation through its effect on the elongation factor eEF2. Studies showed that the phosphorylation of the eEF2 at Thr56 by eEF2 kinase (eEF2K) inactivates it and subsequently inhibits ribosomes translocation and represses translation elongation (Price et al., 1991; Redpath et al., 1993; Ryazanov, A., Shestakova, E. & Natapov, 1988). Interestingly, the eEF2K is dependent on calcium and calmodulin levels and its activity is regulated by mTOR signaling (Browne & Proud, 2004; Redpath et al., 1996) as well as several regulatory synaptic proteins in neurons such as Arc/Arg3.1, α CamK II and BDNF (Park et al., 2008; Scheetz et al., 2000; Verpelli et al., 2010). Here we show that TAOK2 phosphorylates residue Thr56 of eEF2 in neuronal and non-neuronal tissues. Wherein loss of TAOK2 in mouse cortex and its kinase mutations in the LCLs cells show reduced eEF2 phosphorylation, and overexpression of wild type TAOK2β increases eEF2 phosphorylation. Furthermore, data from a phosphoproteomics analysis for different brain regions identified residue Thr56 of eEF2 as a target phosphorylation site by TAOK2 (data not shown here). Consistently, my IP experiments using Taok2β antibody identified eEF2 is an interacting partner for TAOK2. Altogether, these data strongly suggest that TAOK2 regulates translation through phosphorylation of the eEF2 that inhibits translation elongation. As regulation of translation at the elongation steps is acquiring great interest in maintaining different functions in neuronal and non-neuronal cells (Kenney et al., 2014), it will be necessary to elucidate in detail the underlying mechanism by which TAOK2 is phosphorylating eEF2. Either by investigating the role of TAOK2 in direct phosphorylation of Thr56 by an in vitro kinase assay or indirectly by analyzing eEF2K activity and its upstream effectors in the absence of TAOK2.

Taken together, the consequence of an absence of TAOK2 phosphorylating eIF2α and eEF2 is an increase in protein synthesis observed in cortices and cortical

neurons deficient for TAOK2 as well as in N2a cells and LCLs bearing loss-of-function kinase mutations of TAOK2. These findings support the role of TAOK2 in repressing translation at both initiation, and elongation steps. Interestingly, FMRP represses translation at the initiation step, where it binds with CYFIP1 and inhibits cap dependent translation initiation by blocking eIF4E– eIF4G interaction (Napoli et al., 2008) as well as at the elongation step by stalling ribosomes on its target mRNAs (Darnell et al., 2011). Here, I report that TAOK2 can halt translation initiation as it phosphorylates residue Ser51 of eIF2α. Since phosphorylated eIF2α serves as a competitive inhibitor for the guanine nucleotide exchange factor, eIF2B leading to a decrease in the availability of eIF2-GTP for the ternary complex formation to start translation initiation. Furthermore, TAOK2 phosphorylates Thr56 of the elongation factor eEF2 at the elongation step resulting in reduced translation elongation and global protein synthesis.

In this study, we show that TAOK2 is associated with several translational proteins and present in the polyribosome complex, where its deficiency increases protein synthesis similar to the effect of some ASD-risk genes controlling translation. Moreover, TAOK2 deficiency upregulates several ribosomal proteins, which is considered a common feature in different autistic models as well as autistic patients. Additionally, like different kinases controlling translation by their phosphorylating action of different components of the translational complex, TAOK2 is involved in phosphorylation of the initiation factor eIF2α and the elongation factor eEF2 through its kinase function, which leads to translation inhibition. Accordingly, *TAOK2* acts as a translational repressor within the *16p11.2* chromosomal region.

5. Future Perspectives

In addition to the points previously described in the discussion section as future perspectives, noteworthy points that have important implications in ASD research are interesting to be highlighted. Imbalance in excitatory and inhibitory synaptic transmission is a common feature in ASDs (Nelson & Valakh, 2015). Therefore, a primary goal in ASD research is to identify the dysregulated synaptic proteins, and how up - or down-regulation of these proteins contributes to the phenotypes of ASD. We showed that the TAOK2β isoform - the abundant isoform of TAOK2 in the polyribosome complex – accumulates in synapses and binds RhoA to maintain normal synaptic connectivity. Additionally, the IP-MS data revealed that TAOK2β interacts with synaptic proteins (Supplementary Figure 1, Supplementary Table 1), including Syn1, Syn2 and Shank2,

which are associated with autism (Fassio et al., 2011; Zaslavsky et al., 2019). Based on our data shedding the light on new functions of TAOK2 in controlling translation and general protein synthesis, we predict that TAOK2 affects synthesis of proteins related to synaptic functions. Therefore, it will be essential to identify changes in nascent synaptic proteins due to the loss of the translational repressor TAOK2β. In order to check this, we take advantage of O-propargyl- puromycin (OPP) -mediated identification (OPP-ID) technique (Forester et al., 2018) combined with preparation of synaptoneurosomes (intact presynaptic and postsynaptic structures), a commonly used method to study translation and protein synthesis in synapses (Kuzniewska et al., 2018; Scheetz et al., 2000). This technique will be applied to acute coronal brain slices (where all synaptic networks are established and maintained in *situ*) from 4 weeks old *TAOK2* $^{d/d}$ and *TAOK2* $^{+/+}$ mice as depicted in (Figure 20). This approach will provide precise identification and quantification of the newly synthetized synaptic proteome from synaptic material. Furthermore, it will provide information on the altered landscape of synaptic proteins regulated by TAOK2 leading to a better understanding of the neuronal processes essential for synaptic connectivity. Additionally, it will be ample evidence that TAOK2 can directly affect synaptic transmission through its control of protein synthesis. Identification of the altered potential candidates and targeting of these synaptic proteins will open new fields for investigating therapeutic targets for the treatment of ASDs, also in the context of *16p11.2* deletion.

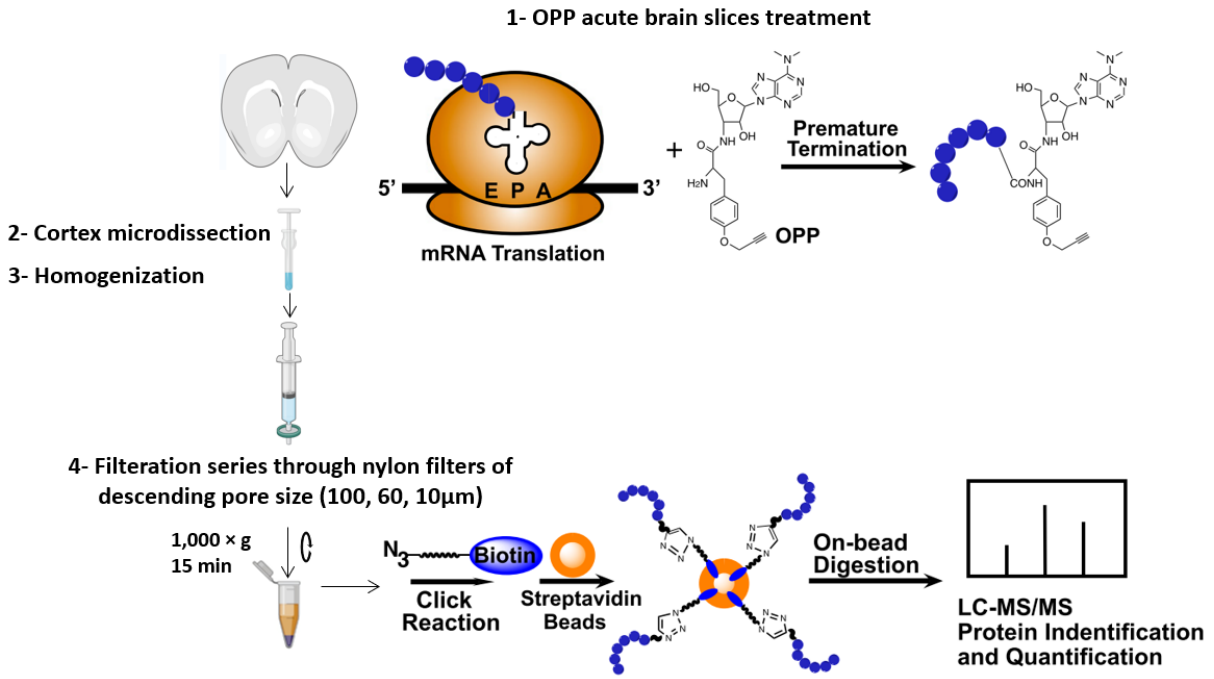

Figure 20: OPP-ID technique combined with synaptoneurosomes (SNs) preparation.

(1) Treatment of acute brain slices with OPP where it is incorporated into the nascent elongating polypeptides and leads to early termination of translation and release of polypeptides bearing OPP. **(2, 3, 4)** Synaptoneurosomes preparation from the micro dissected cortex. **(5)** The nascent polypeptides tagged with OPP in SNs are conjugated to biotin-azide, using click chemistry. The biotinylated proteins are captured with streptavidin beads, followed by on-bead digestion of the immobilized samples and the digests are analyzed LC-MS/MS. Figure modified from (Forester et al., 2018; Kuzniewska et al., 2018).

Dysregulation of protein synthesis in different neuronal compartments at the neuronal pre-and post-synaptic synaptic sites participates in the abnormal neurotransmission and connectivity in different neurological disorders including ASD (reviewed by Holt & Schuman, 2013). A study from Poon et al., (2006) provided a suitable approach to study the translation regulation of the local mRNAs in different compartments of the neurons: Here, they used polycarbonate filters where the neuronal soma grows above the surface while dendrites and axons pass through to grow beneath the filter surface. Another recent study by Biever et al. (2020) used this approach, combined with polysome profiling together with ribosome footprinting, showed the enrichment of monosomes in neurites/neuropil of pyramidal neurons, while polysomes were enriched in the soma. Moreover, monosomes actively translate synaptic mRNAs; thus, monosomes contribute to the local (synaptic) neuronal proteome.

In this study, we show that cortices from *Taok2* KO mice and from cortices lacking the *16p11.2* chromosomal region have increased polysome/monosome ratios which

suggests an altered translational control in both ASD mouse models. Thus, it will be relevant to explore how TAOK2 controls gene expression through regulation of the local mRNAs in different neuronal compartments. Particularly, TAOK2 associates with myosin Va and facilitates its localization in the synapses (Ultanir et al., 2014) and mRNAs transcripts bound to specific RBPs are transported to the dendritic spines by different motor proteins, including myosin Va (Hirokawa & Takemura, 2005; Yoshimura et al., 2006). To address this, it will be interesting to culture the neurons derived from the two ASD models used in this study and from patient iPSCs on the perforated membrane. Afterward, polysome profiling analysis for the neurites versus cell bodies will be necessary to identify the differences in the P/M ratios as well as ribosome profiling and RNAseq to identify altered mRNAs transcripts. These experiments will be crucial to understand how TAOK2 regulates local protein synthesis in different neuronal compartments that might affect dendritic spine maturation, the wiring process in the neuron and, eventually, the development of a functional neuronal network. Additionally, targeting the altered translational candidates at the specific compartments of the neuron will open new avenues for potential therapeutics in ASD research.

6. Summary

6.1 English Summary

The TAOK2 gene encodes a serine/threonine protein kinase that is involved in many different processes, including cell signaling, microtubule organization and stability and neuronal differentiation. Alternatively spliced transcript variants encode different isoforms (e.g. murine TAOK2α and β). The human *TAOK2* gene is localized in the *16p11.2* genomic region (*TAOK2* is one of ~30 genes) and copy number variations (CNVs) of this locus are associated with Autism Spectrum Disorders (ASDs). Previously, we performed whole-genome and exome sequencing of ASD families and identified novel *de novo* and inherited mutations in both isoforms of TAOK2, further providing major relevance for TAOK2 as an important ASD-risk gene.

The etiology of ASDs has recently been linked to altered translational control causing an imbalance in synaptic excitation/inhibition and autistic phenotypes. Here, I have shown for the first time that the ASD susceptibility gene TAOK2 is present in the polyribosome complex and regulates translation in neuronal tissue and cells. By western blot and LC/MS protein analysis extracted from polysomes, I could detect both, α and β isoforms of TAOK2, in polysomes with more abundance of TAOK2β in the polyribosome complex. Accordingly, I could demonstrate that TAOK2 deficiency and functional mutations of both isoforms, especially the isoform β, enhance global translation and protein synthesis with a concomitant upregulation of ribosomal proteins. Additionally, I showed that the functional mutations of TAOK2 in LCLs derived from ASD patients display upregulated global translation and protein synthesis. My data suggest that TAOK2 is a repressor of translation. Importantly, I observed a similar phenotype in the *16p11.2* $^{+/d}$ microdeletion mouse and through re-introduction of TAOK2 in *16p11.2* $^{+/d}$ del neurons via IUE, I rescued the dysregulated global translation. I identified how TAOK2 regulates translation mechanistically: I could show that TAOK2 phosphorylates residue Ser51 of the initiation factor eIF2α, while eIF2α phosphorylation inhibits translation at the initiation step. Furthermore, I demonstrated that TAOK2 binds and phosphorylates the elongation factor eEF2 which slows down the translation elongation.

My data provide mechanistic insights into the role of TAOK2 in translational repression, both in initiation and elongation steps, in *16p11.2* microdeletions (CNVs) which could be causative for the development of 16p11.2-linked ASDs.

6.2 German Summary (Zusammenfassung auf Deutsch)

Das TAOK2-Gen kodiert eine Serin/Threonin-Proteinkinase, die an Prozessen wie Signaltransduktion, Mikrotubuli-Organisation/-Stabilität und neuronale Differenzierung beteiligt ist. Alternativ gespleißte Transkriptvarianten kodieren verschiedene Isoformen (z. B. murines TAOK2α und β). Das humane TAOK2-Gen ist in der genomischen Region *16p11.2* lokalisiert (TAOK2 ist eines von ~30 Genen) und Variationen in der Kopienzahl dieser Region (CNVs) sind mit Autismus-Spektrum-Störungen (ASDs) assoziiert. Wir haben Gesamtgenom- und Exom-Sequenzierungen in ASD-Familien durchgeführt und *de novo* sowie vererbbare Mutationen in beiden Isoformen von TAOK2 identifiziert, was die Rolle von TAOK2 als wichtiges ASD-Risikogen bestärkt.

Die Ätiologie von ASDs wird mit einer gestörten Kontrolle der Translation assoziiert, die ein Ungleichgewicht der synaptischen Erregung/Hemmung und autistische Phänotypen verursacht. Ich konnte zeigen, dass das ASD-Risikogen TAOK2 im Polyribosomenkomplex vorhanden ist und die Translation in neuronalem Gewebe und Zellen reguliert. In Western-Blot- und LC/MS-Proteinanalyse von Polysomen konnte ich die α- und β-Isoform von TAOK2 nachweisen, mit einer höheren Expression von TAOK2β im Polyribosomenkomplex. TAOK2-Defizienz sowie funktionelle Mutationen beider Isoformen, insbesondere der β-Isoform, verstärken die globale Translation und Proteinsynthese bei gleichzeitiger Hochregulation ribosomaler Proteine. Ferner zeige ich, dass funktionelle Mutationen von TAOK2 in LCLs von ASD-Patienten eine hochregulierte globale Translation und Proteinsynthese aufweisen. Meine Daten legen nahe, dass TAOK2 ein Translationsrepressor ist. Einen vergleichbaren Phänotyp konnte ich in der *16p11.2* $^{+/d}$ -Mikrodeletionsmaus beschreiben und durch Wiedereinführung von TAOK2 in *16p11.2* $^{+/d}$ del Neurone mittels *in utero* Elektroporation konnte ich die fehlregulierte globale Translation wiederherstellen. Ich konnte mechanistisch beschreiben, wie TAOK2 die Translation reguliert: TAOK2 phosphoryliert den Initiationsfaktors eIF2α an der Position Ser51, um mittels eIF2α-Phosphorylierung die Translation während der Initiation zu hemmen. Ich konnte ferner zeigen, dass TAOK2 den Elongationsfaktor eEF2 bindet und phosphoryliert, um die Elongation zu verlangsamen. Meine Daten liefern mechanistische Erkenntnisse über die Rolle von TAOK2 bei der Translationsrepression, sowohl bei Initiations- als auch bei Elongationsschritten, in 16p11.2-Mikrodeletionen (CNVs), die ursächlich an der Entstehung von 16p11.2-assoziierten ASDs beteiligt sein könnte.

7. Abbreviations:

ASDs:	Autism spectrum disorders
NDDs:	Neurodevelopmental disorders
CNVs:	Copy number variations
***TAOK2*:**	Thousand And One amino acid Kinase 2
STE20:	Mammalian sterile 20
MAP3K:	Mitogen Activated Protein (MAP) kinase kinase kinase
FMRP:	Fragile X Mental Retardation Protein
Sema3A:	Semaphorin 3A
Nrp1:	Neuropilin 1
JNK:	c-Jun N-Terminal Kinase
MST3:	Mammalian Ste20-like protein kinase 3
PSD95:	Postsynaptic density protein 95
RhoA:	Ras homolog family member A
mRNA:	Messenger RNA
tRNAs:	Transfer RNAs
aa-tRNA:	aminoacyl-transfer RNA
Met-tRNAi:	methionyl-tRNA
GTP*:*	Guanosine-5'-triphosphate
GDP:	Guanosine diphosphate
mRNP:	Messenger ribonucleoprotein
eIFs:	eukaryotic translation initiation factors
eIF2:	eukaryotic translation initiation factor2
eIF1:	eukaryotic translation initiation factor1
eIF1A:	eukaryotic translation initiation factor 1A

eIF5:	eukaryotic translation initiation factor 5
eIF3:	eukaryotic translation initiation factor 3
eIF4F:	eukaryotic initiation factor 4F
eIF2α:	eukaryotic translation initiation factor 2 alpha
eIF2:	eukaryotic translation initiation factor2
eIF4E:	eukaryotic initiation factor 4E
eIF4G:	eukaryotic initiation factor 4G
eIF2B:	eukaryotic initiation factor 2B
PABP:	Poly (A) binding protein
PABPC1:	Poly(A) binding protein cytoplasmic 1
eIF3g:	eukaryotic translation initiation factor 3 subunit g
eIF4EBP2:	eukaryotic translation initiation factor 4E-binding protein 2
4EGI-1:	eIF4E/eIF4G interaction inhibitor
RPL7A:	Ribosomal Protein L7a
RPL10:	Ribosomal Protein L10
Caprin1:	Cell cycle-associated protein 1
JAKMIP1:	Janus kinase and microtubule-interacting protein 1
MNKs:	MAP kinase-interacting kinases
eEFs:	eukaryotic elongation factors
eEF2:	eukaryotic elongation factor 2
eEF2K:	eukaryotic elongation factor 2 kinase
eRF1:	eukaryotic translation release factor 1
eRF3:	eukaryotic translation release factor 3
ABCE1:	ATP binding cassette protein 1
AUG:	Adenine, Uracil, Guanine

UAA:	Uracil, Adenine, Adenine
UGA:	Uracil, Guanine, Adenine
UAG:	Uracil, Adenine, Guanine
A-site:	Ribosomal Acceptor site
P-site:	Ribosomal Peptidyl site
ISR:	Integrated stress response
GEF:	Guanine nucleotide exchange factor
PERK:	Protein Kinase RNA-like Endoplasmic Reticulum Kinase
PKR:	dsRNA dependent protein kinase
GCN1:	General control nonderepressible-1
GCN2:	General control nonderepressible-2
HRI:	Heme-regulated inhibitor
PP1:	Protein phosphatase 1
PP1c:	Catalytic subunit of protein phosphatase 1
CReP:	Constitutive Repressor of eIF2α phosphorylation
GADD34:	Growth arrest and DNA damage-inducible 34
4E-BPs:	Eukaryotic translation initiation factor 4E-binding proteins
mTOR:	mammalian target of rapamycin
mTORC1:	mammalian target of rapamycin complex 1
mTORC2:	mammalian target of rapamycin complex 2
S6Ks:	S6 kinases
Ras- MAPK:	Rat sarcoma - mitogen-activated protein kinase
FXS:	Fragile X syndrome
***FMR1*:**	Fragile X mental retardation 1 gene
CYFIP1:	Cytoplasmic FMR1 Interacting Protein 1

Ras/ERK:	Rat sarcoma / extracellular signal-regulated kinase
PI3K/mTOR:	Phosphatidylinositol-3-kinase / mammalian target of rapamycin
NF1:	Neurofibromatosis type 1
TSC:	Tuberous sclerosis complex
PTEN:	Phosphatase and tensin homolog
PIP3:	Phosphatidylinositol-3, 4, 5-triphosphate
PIP2:	Phosphatidylinositol-4, 5-bisphosphate
RHEB:	Ras homologue enhanced in brain
P70S6K:	70 kDa ribosomal protein S6 kinase
Ser51:	Serine 51
Thr56:	Threonine 56
Arc/Arg3.1:	Activity-regulated cytoskeletal-associated protein/ Activity-regulated gene 3.1
CPEB:	Cytoplasmic polyadenylation element binding protein
MECP2:	Methyl CpG binding protein
2α CamK II:	Calcium/calmodulin dependent protein kinase II alpha
mGluRs:	metabotropic glutamate receptors
Syn1:	Synapsin I
Syn2:	Synapsin II
SFARI:	Simons Foundation Autism Research Initiative
AREB:	Animal Research Ethics Board
OD:	Optical density
UV:	Ultraviolet
***EDTA*:**	Ethylenediaminetetraacetic acid
SUnSET:	Surface Sensing of Translation

FACS:	Fluorescence-activated cell sorting
IHC:	Immunohistochemistry
ICC:	Immunocytochemistry
IP:	Immunoprecipitation
LC-MS/MS:	Liquid chromatography-mass spectrometry
IP-MS:	Immunoprecipitation - mass spectrometry
OPP-ID:	O-propargyl- puromycin-mediated identification technique
TRAP:	Translating ribosome affinity purification
qRT-PCR:	Qunaitative reverse transcription - Polymerase chain reaction
HTS:	High-throughput sequencing
PFC:	Prefrontal Cortex
LCLs:	Lymphoblastoid cell line cells
N2a:	Neuro 2a
iPSC:	induced pluripotent stem cell
NPCs:	Neural progenitor cells
GO:	Gene ontology
STRING:	Search Tool for the Retrieval of Interacting Genes/Proteins
ORA:	Over Representation Analysis
PANTHER:	Protein Analysis Through Evolutionary Relationships

8. References:

Aitken, C. E., & Lorsch, J. R. (2012). A mechanistic overview of translation initiation in eukaryotes. *Nature Structural and Molecular Biology*, *19*(6), 568–576. https://doi.org/10.1038/nsmb.2303

Azzam, M. E., & Algranati, I. D. (1973). Mechanism of puromycin action: Fate of ribosomes after release of nascent protein chains from polysomes. *Proceedings of the National Academy of Sciences of the United States of America*, *70*(12 (II)), 3866–3869. https://doi.org/10.1073/pnas.70.12.3866

Bagni, C., & Greenough, W. T. (2005). From mRNP trafficking to spine dysmorphogenesis: The roots of fragile X syndrome. *Nature Reviews Neuroscience*, *6*(5), 376–387. https://doi.org/10.1038/nrn1667

Bailey, D. B., Mesibov, G. B., Hatton, D. D., Clark, R. D., Roberts, J. E., & Mayhew, L. (1998). Autistic

behavior in young boys with fragile X syndrome. *Journal of Autism and Developmental Disorders*, *28*(6), 499–508. https://doi.org/10.1023/A:1026048027397

Bear, M. F., Huber, K. M., & Warren, S. T. (2004). The mGluR theory of fragile X mental retardation. *Trends in Neurosciences*, *27*(7), 370–377. https://doi.org/10.1016/j.tins.2004.04.009

Belmonte, M. K., Allen, G., Beckel-Mitchener, A., Boulanger, L. M., Carper, R. A., & Webb, S. J. (2004). Autism and abnormal development of brain connectivity. *Journal of Neuroscience*, *24*(42), 9228–9231. https://doi.org/10.1523/JNEUROSCI.3340-04.2004

Berg, J. M., Lee, C., Chen, L., Galvan, L., Cepeda, C., Chen, J. Y., Peñagarikano, O., Stein, J. L., Li, A., Oguro-Ando, A., Miller, J. A., Vashisht, A. A., Starks, M. E., Kite, E. P., Tam, E., Gdalyahu, A., Al-Sharif, N. B., Burkett, Z. D., White, S. A., … Geschwind, D. H. (2015). JAKMIP1, a Novel Regulator of Neuronal Translation, Modulates Synaptic Function and Autistic-like Behaviors in Mouse. *Neuron*, *88*(6), 1173–1191. https://doi.org/10.1016/j.neuron.2015.10.031

Biever, A., Glock, C., Tushev, G., Ciirdaeva, E., Dalmay, T., Langer, J. D., & Schuman, E. M. (2020). Monosomes actively translate synaptic mRNAs in neuronal processes. *Science*, *367*(6477). https://doi.org/10.1126/science.aay4991

Bourgeron, T. (2015). From the genetic architecture to synaptic plasticity in autism spectrum disorder. *Nature Reviews Neuroscience*, *16*(9), 551–563. https://doi.org/10.1038/nrn3992

Boyce, M., Bryant, K. F., Jousse, C., Long, K., Harding, H. P., Scheuner, D., Kaufman, R. J., Ma, D., Coen, D. M., Ron, D., & Yuan, J. (2005). A selective inhibitor of eIF2α dephosphorylation protects cells from ER stress. *Science*, *307*(5711), 935–939. https://doi.org/10.1126/science.1101902

Browne, G. J., & Proud, C. G. (2004). A Novel mTOR-Regulated Phosphorylation Site in Elongation Factor 2 Kinase Modulates the Activity of the Kinase and Its Binding to Calmodulin. *Molecular and Cellular Biology*, *24*(7), 2986–2997. https://doi.org/10.1128/mcb.24.7.2986-2997.2004

Butler, M. G., Dazouki, M. J., Zhou, X. P., Talebizadeh, Z., Brown, M., Takahashi, T. N., Miles, J. H., Wang, C. H., Stratton, R., Pilarski, R., & Eng, C. (2005). Subset of individuals with autism spectrum disorders and extreme macrocephaly associated with germline PTEN tumour suppressor gene mutations. *Journal of Medical Genetics*, *42*(4), 318–321. https://doi.org/10.1136/jmg.2004.024646

Cambiaghi, T. D., Pereira, C. M., Shanmugam, R., Bolech, M., Wek, R. C., Sattlegger, E., & Castilho, B. A. (2014). Evolutionarily conserved IMPACT impairs various stress responses that require GCN1 for activating the eIF2 kinase GCN2. *Biochemical and Biophysical Research Communications*, *443*(2), 592–597. https://doi.org/10.1016/j.bbrc.2013.12.021

CARLBERG, U., NILSSON, A., & NYGÅRD, O. (1990). Functional properties of phosphorylated elongation factor 2. *European Journal of Biochemistry*, *191*(3), 639–645. https://doi.org/10.1111/j.1432-1033.1990.tb19169.x

Castello, A., Fischer, B., Eichelbaum, K., Horos, R., Beckmann, B. M., Strein, C., Davey, N. E., Humphreys, D. T., Preiss, T., Steinmetz, L. M., Krijgsveld, J., & Hentze, M. W. (2012). Insights into RNA Biology from an Atlas of Mammalian mRNA-Binding Proteins. *Cell*, *149*(6), 1393–1406. https://doi.org/10.1016/j.cell.2012.04.031

Caudron-Herger, M., Rusin, S. F., Adamo, M. E., Seiler, J., Schmid, V. K., Barreau, E., Kettenbach, A. N., & Diederichs, S. (2019). R-DeeP: Proteome-wide and Quantitative Identification of RNA-Dependent Proteins by Density Gradient Ultracentrifugation. *Molecular Cell*, *75*(1), 184-199.e10. https://doi.org/10.1016/j.molcel.2019.04.018

Chassé, H., Boulben, S., Costache, V., Cormier, P., & Morales, J. (2017). Analysis of translation using polysome profiling. *Nucleic Acids Research*, *45*(3), e15. https://doi.org/10.1093/nar/gkw907

Chen, Y. C., Chang, Y. W., & Huang, Y. S. (2019). Dysregulated Translation in Neurodevelopmental Disorders: An Overview of Autism-Risk Genes Involved in Translation. *Developmental Neurobiology*, *79*(1), 60–74. https://doi.org/10.1002/dneu.22653

Cline, H. (n.d.). *Synaptogenesis : A Balancing Act*. *2*, 203–205.

Cook, E. H., & Scherer, S. W. (2008). Copy-number variations associated with neuropsychiatric conditions. *Nature*, *455*(7215), 919–923. https://doi.org/10.1038/nature07458

Costa-Mattioli, M., Sossin, W. S., Klann, E., & Sonenberg, N. (2009). Translational Control of Long-Lasting Synaptic Plasticity and Memory. *Neuron*, *61*(1), 10–26. https://doi.org/10.1016/j.neuron.2008.10.055

Darnell, J. C., Van Driesche, S. J., Zhang, C., Hung, K. Y. S., Mele, A., Fraser, C. E., Stone, E. F., Chen, C., Fak, J. J., Chi, S. W., Licatalosi, D. D., Richter, J. D., & Darnell, R. B. (2011). FMRP stalls ribosomal translocation on mRNAs linked to synaptic function and autism. *Cell*, *146*(2), 247–261. https://doi.org/10.1016/j.cell.2011.06.013

Dasgupta, B., & Gutmann, D. H. (2003). Neurofibromatosis 1: Closing the GAP between mice and men. *Current Opinion in Genetics and Development*, *13*(1), 20–27. https://doi.org/10.1016/S0959-437X(02)00015-1

De Anda, F. C., Rosario, A. L., Durak, O., Tran, T., Gräff, J., Meletis, K., Rei, D., Soda, T., Madabhushi, R., Ginty, D. D., Kolodkin, A. L., & Tsai, L. H. (2012). Autism spectrum disorder susceptibility gene TAOK2 affects basal dendrite formation in the neocortex. *Nature Neuroscience*, *15*(7), 1022–1031. https://doi.org/10.1038/nn.3141

Del Prete, M. J., Vernal, R., Dolznig, H., Müllner, E. W., & Garcia-Sanz, J. A. (2007). Isolation of polysome-bound mRNA from solid tissues amenable for RT-PCR and profiling experiments. *Rna*, *13*(3), 414–421. https://doi.org/10.1261/rna.79407

Dever, T. E., & Green, R. (2012). The elongation, termination, and recycling phases of translation in eukaryotes. *Cold Spring Harbor Perspectives in Biology*, *4*(7), 1–16. https://doi.org/10.1101/cshperspect.a013706

Dölen, G., Osterweil, E., Rao, B. S. S., Smith, G. B., Auerbach, B. D., Chattarji, S., & Bear, M. F. (2007). Correction of Fragile X Syndrome in Mice. *Neuron*, *56*(6), 955–962. https://doi.org/10.1016/j.neuron.2007.12.001

Donnelly, N., Gorman, A. M., Gupta, S., & Samali, A. (2013). The eIF2α kinases: Their structures and functions. *Cellular and Molecular Life Sciences*, *70*(19), 3493–3511. https://doi.org/10.1007/s00018-012-1252-6

Edfawy, M., Guedes, J. R., Pereira, M. I., Laranjo, M., Carvalho, M. J., Gao, X., Ferreira, P. A., Caldeira, G., Franco, L. O., Wang, D., Cardoso, A. L., Feng, G., Carvalho, A. L., & Peça, J. (2019). Abnormal mGluR-mediated synaptic plasticity and autism-like behaviours in Gprasp2 mutant mice. *Nature Communications*, *10*(1), 1–15. https://doi.org/10.1038/s41467-019-09382-9

Ehninger, D., Han, S., Shilyansky, C., Zhou, Y., Li, W., Kwiatkowski, D. J., Ramesh, V., & Silva, A. J. (2008). Reversal of learning deficits in a Tsc2+/- mouse model of tuberous sclerosis. *Nature Medicine*, *14*(8), 843–848. https://doi.org/10.1038/nm1788

Ehninger, D., & Silva, A. J. (2011). Rapamycin for treating Tuberous sclerosis and Autism spectrum disorders. *Trends in Molecular Medicine*, *17*(2), 78–87. https://doi.org/10.1016/j.molmed.2010.10.002

El Fatimy, R., Tremblay, S., Dury, A. Y., Solomon, S., de Koninck, P., Schrader, J. W., & Khandjian, E. W. (2012). Fragile mental retardation protein interacts with the RNA-binding protein Caprin1 in neuronal ribonucleoprotein complexes. *PLoS ONE*, *7*(6). https://doi.org/10.1371/journal.pone.0039338

Escamilla, C. O., Filonova, I., Walker, A. K., Xuan, Z. X., Holehonnur, R., Espinosa, F., Liu, S., Thyme, S. B., López-García, I. A., Mendoza, D. B., Usui, N., Ellegood, J., Eisch, A. J., Konopka, G., Lerch, J. P., Schier, A. F., Speed, H. E., & Powell, C. M. (2017). Kctd13 deletion reduces synaptic transmission via increased RhoA. *Nature*, *551*(7679), 227–231. https://doi.org/10.1038/nature24470

Fang, C.-Y., Lai, T.-C., Hsiao, M., & Chang, Y.-C. (2020). The Diverse Roles of TAO Kinases in Health and Diseases. *International Journal of Molecular Sciences*, *21*(20), 7463. https://doi.org/10.3390/ijms21207463

Fassio, A., Patry, L., Congia, S., Onofri, F., Piton, A., Gauthier, J., Pozzi, D., Messa, M., Defranchi, E., Fadda, M., Corradi, A., Baldelli, P., Lapointe, L., St-Onge, J., Meloche, C., Mottron, L., Valtorta, F., Nguyen, D. K., Rouleau, G. A., … Cossette, P. (2011). SYN1 loss-of-function mutations in autism

and partial epilepsy cause impaired synaptic function. *Human Molecular Genetics*, *20*(12), 2297–2307. https://doi.org/10.1093/hmg/ddr122

Fenton, T. R., & Gout, I. T. (2011). Functions and regulation of the 70 kDa ribosomal S6 kinases. *International Journal of Biochemistry and Cell Biology*, *43*(1), 47–59. https://doi.org/10.1016/j.biocel.2010.09.018

Fingar, D. C., Salama, S., Tsou, C., Harlow, E., & Blenis, J. (2002). Mammalian cell size is controlled by mTOR and its downstream targets S6K1 and 4EBP1/eIF4E. *Genes and Development*, *16*(12), 1472–1487. https://doi.org/10.1101/gad.995802

Forester, C. M., Zhao, Q., Phillips, N. J., Urisman, A., Chalkley, R. J., Oses-Prieto, J. A., Zhang, L., Ruggero, D., & Burlingame, A. L. (2018). Revealing nascent proteomics in signaling pathways and cell differentiation. *Proceedings of the National Academy of Sciences of the United States of America*, *115*(10), 2353–2358. https://doi.org/10.1073/pnas.1707514115

Frolova, L., Goff, X. L. E., Zhouravleva, G., Davydova, E., Philippe, M., & Kisselev, L. (1996). Eukaryotic polypeptide chain release factor eRF3 is an eRF1- and ribosome-dependent guanosine triphosphatase. In *Rna* (Vol. 2, Issue 4, pp. 334–341).

Fujiwara, K., Ogawa, A., Asada, H., Saikusa, H., Nakamura, H., Ono, S., & Kitagawa, T. (1982). The preparation of puromycin antibody and its use in enzyme immunoassay for the quantification using β-D-galactosidase as a label. *Journal of Biochemistry*, *92*(5), 1599–1605. https://doi.org/10.1093/oxfordjournals.jbchem.a134085

Gingras, A. C., Raught, B., & Sonenberg, N. (2001). Regulation of translation initiation by FRAP/mTOR. *Genes and Development*, *15*(7), 807–826. https://doi.org/10.1101/gad.887201

Gkogkas, C. G., Khoutorsky, A., Ran, I., Rampakakis, E., Nevarko, T., Weatherill, D. B., Vasuta, C., Yee, S., Truitt, M., Dallaire, P., Major, F., Lasko, P., Ruggero, D., Nader, K., Lacaille, J. C., & Sonenberg, N. (2013). Autism-related deficits via dysregulated eIF4E-dependent translational control. *Nature*, *493*(7432), 371–377. https://doi.org/10.1038/nature11628

Glock, C., Heumüller, M., & Schuman, E. M. (2017). mRNA transport & local translation in neurons. *Current Opinion in Neurobiology*, *45*, 169–177. https://doi.org/10.1016/j.conb.2017.05.005

Goodman, C. A., Pierre, P., & Hornberger, T. A. (2012). Imaging of protein synthesis with puromycin. *Proceedings of the National Academy of Sciences of the United States of America*, *109*(17), 2012. https://doi.org/10.1073/pnas.1202000109

Graber, T. E., Hébert-Seropian, S., Khoutorsky, A., David, A., Yewdell, J. W., Lacaille, J. C., & Sossin, W. S. (2013). Reactivation of stalled polyribosomes in synaptic plasticity. *Proceedings of the National Academy of Sciences of the United States of America*, *110*(40), 16205–16210. https://doi.org/10.1073/pnas.1307747110

Griesi-Oliveira, K., Fogo, M. S., Pinto, B. G. G., Alves, A. Y., Suzuki, A. M., Morales, A. G., Ezquina, S., Sosa, O. J., Sutton, G. J., Sunaga-Franze, D. Y., Bueno, A. P., Seabra, G., Sardinha, L., Costa, S. S., Rosenberg, C., Zachi, E. C., Sertie, A. L., Martins-de-Souza, D., Reis, E. M., … Passos-Bueno, M. R. (2021). Transcriptome of iPSC-derived neuronal cells reveals a module of co-expressed genes consistently associated with autism spectrum disorder. *Molecular Psychiatry*, *26*(5), 1589–1605. https://doi.org/10.1038/s41380-020-0669-9

Gross, C., & Bassell, G. J. (2012). Excess protein synthesis in FXS patient lymphoblastoid cells can be rescued with a p110β-selective inhibitor. *Molecular Medicine*, *18*(3), 336–345. https://doi.org/10.2119/molmed.2011.00363

Harding, H. P., Zhang, Y., Zeng, H., Novoa, I., Lu, P. D., Calfon, M., Sadri, N., Yun, C., Popko, B., Paules, R., Stojdl, D. F., Bell, J. C., Hettmann, T., Leiden, J. M., & Ron, D. (2003). An integrated stress response regulates amino acid metabolism and resistance to oxidative stress. *Molecular Cell*, *11*(3), 619–633. https://doi.org/10.1016/S1097-2765(03)00105-9

Heiman, M., Schaefer, A., Gong, S., Peterson, J. D., Day, M., Ramsey, K. E., Suárez-Fariñas, M., Schwarz, C., Stephan, D. A., Surmeier, D. J., Greengard, P., & Heintz, N. (2008). A Translational Profiling Approach for the Molecular Characterization of CNS Cell Types. *Cell*, *135*(4), 738–748. https://doi.org/10.1016/j.cell.2008.10.028

Hershey, J. W. B., Sonenberg, N., & Mathews, M. B. (2019). Principles of translational control. *Cold Spring Harbor Perspectives in Biology*, *11*(9), 1–10. https://doi.org/10.1101/cshperspect.a032607

Hinnebusch, A. G. (2017). Structural Insights into the Mechanism of Scanning and Start Codon Recognition in Eukaryotic Translation Initiation. *Trends in Biochemical Sciences*, *42*(8), 589–611. https://doi.org/10.1016/j.tibs.2017.03.004

Hinnebusch, A. G., & Lorsch, J. R. (2012). The mechanism of eukaryotic translation initiation: New insights and challenges. *Cold Spring Harbor Perspectives in Biology*, *4*(10), 1–25. https://doi.org/10.1101/cshperspect.a011544

Hirokawa, N., & Takemura, R. (2005). Molecular motors and mechanisms of directional transport in neurons. *Nature Reviews Neuroscience*, *6*(3), 201–214. https://doi.org/10.1038/nrn1624

Hobden, A. N., & Cundliffe, E. (1978). The mode of action of alpha sarcin and a novel assay of the puromycin reaction. *Biochemical Journal*, *170*(1), 57–61. https://doi.org/10.1042/bj1700057

Hoeffer, C. A., Cowansage, K. K., Arnold, E. C., Banko, J. L., Moerke, N. J., Rodriguez, R., Schmidt, E. K., Klosi, E., Chorev, M., Lloyd, R. E., Pierre, P., Wagner, G., LeDoux, J. E., & Klann, E. (2011). Inhibition of the interactions between eukaryotic initiation factors 4E and 4G impairs long-term associative memory consolidation but not reconsolidation. *Proceedings of the National Academy of Sciences of the United States of America*, *108*(8), 3383–3388. https://doi.org/10.1073/pnas.1013063108

Hoeffer, C. A., & Klann, E. (2010). mTOR signaling: At the crossroads of plasticity, memory and disease. *Trends in Neurosciences*, *33*(2), 67–75. https://doi.org/10.1016/j.tins.2009.11.003

Holt, C. E., & Schuman, E. M. (2013). The central dogma decentralized: New perspectives on RNA function and local translation in neurons. *Neuron*, *80*(3), 648–657. https://doi.org/10.1016/j.neuron.2013.10.036

Horev, G., Ellegood, J., Lerch, J. P., Son, Y. E. E., Muthuswamy, L., Vogel, H., Krieger, A. M., Buja, A., Henkelman, R. M., Wigler, M., & Mills, A. A. (2011). Dosage-dependent phenotypes in models of 16p11.2 lesions found in autism. *Proceedings of the National Academy of Sciences of the United States of America*, *108*(41), 17076–17081. https://doi.org/10.1073/pnas.1114042108

Hörnberg, H., Pérez-Garci, E., Schreiner, D., Hatstatt-Burklé, L., Magara, F., Baudouin, S., Matter, A., Nacro, K., Pecho-Vrieseling, E., & Scheiffele, P. (2020). Rescue of oxytocin response and social behaviour in a mouse model of autism. *Nature*, *584*(May 2019). https://doi.org/10.1038/s41586-020-2563-7

Hui-Yuen, J., McAllister, S., Koganti, S., Hill, E., & Bhaduri-Mcintosh, S. (2011). Establishment of Epstein-Barr virus growth-transformed lymphoblastoid cell lines. *Journal of Visualized Experiments*, *57*, 2–7. https://doi.org/10.3791/3321

Ingolia, N. T., Ghaemmaghami, S., Newman, J. R. S., & Weissman, J. S. (2009). Genome-wide analysis in vivo of translation with nucleotide resolution using ribosome profiling. *Science*, *324*(5924), 218–223. https://doi.org/10.1126/science.1168978

Jacquemont, S., Pacini, L., Jønch, A. E., Cencelli, G., Rozenberg, I., He, Y., D'Andrea, L., Pedini, G., Eldeeb, M., Willemsen, R., Gasparini, F., Tassone, F., Hagerman, R., Gomez-Mancilla, B., & Bagni, C. (2018). Protein synthesis levels are increased in a subset of individuals with fragile X syndrome. *Human Molecular Genetics*, *27*(12), 2039–2051. https://doi.org/10.1093/hmg/ddy099

Kang, Q., & Pomerening, J. R. (2012). Punctuated cyclin synthesis drives early embryonic cell cycle oscillations. *Molecular Biology of the Cell*, *23*(2), 284–296. https://doi.org/10.1091/mbc.E11-09-0768

Kapfhamer, D., Taylor, S., Zou, M. E., Lim, J. P., Kharazia, V., & Heberlein, U. (2013). Taok2 controls behavioral response to ethanol in mice. *Genes, Brain and Behavior*, *12*(1), 87–97. https://doi.org/10.1111/j.1601-183X.2012.00834.x

Kapur, M., Monaghan, C. E., & Ackerman, S. L. (2017). Regulation of mRNA Translation in Neurons—A Matter of Life and Death. *Neuron*, *96*(3), 616–637. https://doi.org/10.1016/j.neuron.2017.09.057

Kelleher, R. J., Bear, M. F., Urban, J., Magdalon, J., Sánchez-Sánchez, S. M., Griesi-Oliveira, K., Sertié,

A. L., Crino, P. B., Thermo Scientific, Dufner, A., Thomas, G., Medicine, F., Technology, M., Medicine, S., Building, R., Dempsey, L. A., Alessi, D., Kozlowski, M. T., Weng, Q., … Jacquemont, S. (2008). The Autistic Neuron: Troubled Translation? *Cell*, *135*(3), 401–406. https://doi.org/10.1016/j.cell.2008.10.017

Kenney, J. W., Moore, C. E., Wang, X., & Proud, C. G. (2014). Eukaryotic elongation factor 2 kinase, an unusual enzyme with multiple roles. *Advances in Biological Regulation*, *55*, 15–27. https://doi.org/10.1016/j.jbior.2014.04.003

Kim, Y. S., Leventhal, B. L., Koh, Y. J., Fombonne, E., Laska, E., Lim, E. C., Cheon, K. A., Kim, S. J., Kim, Y. K., Lee, H. K., Song, D. H., & Grinker, R. R. (2011). Prevalence of autism spectrum disorders in a total population sample. *American Journal of Psychiatry*, *168*(9), 904–912. https://doi.org/10.1176/appi.ajp.2011.10101532

Kulkarni, V. A., & Firestein, B. L. (2012). The dendritic tree and brain disorders. *Molecular and Cellular Neuroscience*, *50*(1), 10–20. https://doi.org/10.1016/j.mcn.2012.03.005

Kuzniewska, B., Chojnacka, M., Milek, J., & Dziembowska, M. (2018). Preparation of polysomal fractions from mouse brain synaptoneurosomes and analysis of polysomal-bound mRNAs. *Journal of Neuroscience Methods*, *293*, 226–233. https://doi.org/10.1016/j.jneumeth.2017.10.006

Kwan, V., Meka, D. P., White, S. H., Hung, C. L., Holzapfel, N. T., Walker, S., Murtaza, N., Unda, B. K., Schwanke, B., Yuen, R. K. C., Habing, K., Milsom, C., Hope, K. J., Truant, R., Scherer, S. W., Calderon de Anda, F., & Singh, K. K. (2016). DIXDC1 Phosphorylation and Control of Dendritic Morphology Are Impaired by Rare Genetic Variants. *Cell Reports*, *17*(7), 1892–1904. https://doi.org/10.1016/j.celrep.2016.10.047

Kwiatkowski, D. J., & Manning, B. D. (2005). Tuberous sclerosis: A GAP at the crossroads of multiple signaling pathways. *Human Molecular Genetics*, *14*(SUPPL. 2). https://doi.org/10.1093/hmg/ddi260

Kwon, C. H., Luikart, B. W., Powell, C. M., Zhou, J., Matheny, S. A., Zhang, W., Li, Y., Baker, S. J., & Parada, L. F. (2006). Pten Regulates Neuronal Arborization and Social Interaction in Mice. *Neuron*, *50*(3), 377–388. https://doi.org/10.1016/j.neuron.2006.03.023

Lavelle, T. A., Weinstein, M. C., Newhouse, J. P., Munir, K., Kuhlthau, K. A., & Prosser, L. A. (2014). Economic burden of childhood autism spectrum disorders. *Pediatrics*, *133*(3). https://doi.org/10.1542/peds.2013-0763

Li, Ya, He, C. L., Li, W. X., Zhang, R. X., & Duan, Y. (2020). Transcriptome analysis reveals gender-specific differences in overall metabolic response of male and female patients in lung adenocarcinoma. *PLoS ONE*, *15*(4), 1–21. https://doi.org/10.1371/journal.pone.0230796

Li, Yun, Wang, H., Muffat, J., Cheng, A. W., Orlando, D. A., Lovén, J., Kwok, S. M., Feldman, D. A., Bateup, H. S., Gao, Q., Hockemeyer, D., Mitalipova, M., Lewis, C. A., Vander Heiden, M. G., Sur, M., Young, R. A., & Jaenisch, R. (2013). Global transcriptional and translational repression in human-embryonic- stem-cell-derived rett syndrome neurons. *Cell Stem Cell*, *13*(4), 446–458. https://doi.org/10.1016/j.stem.2013.09.001

Liao, Y., Wang, J., Jaehnig, E. J., Shi, Z., & Zhang, B. (2019). WebGestalt 2019: gene set analysis toolkit with revamped UIs and APIs. *Nucleic Acids Research*, *47*(W1), W199–W205. https://doi.org/10.1093/nar/gkz401

Liu, J., Xu, Y., Stoleru, D., & Salic, A. (2012). Imaging protein synthesis in cells and tissues with an alkyne analog of puromycin. *Proceedings of the National Academy of Sciences of the United States of America*, *109*(2), 413–418. https://doi.org/10.1073/pnas.1111561108

Lombardo, M. V. (2020). Ribosomal protein genes in post-mortem cortical tissue and iPSC- derived neural progenitor cells are commonly upregulated in expression in autism. *Molecular Psychiatry*. https://doi.org/10.1038/s41380-020-0773-x

Luo, R., Sanders, S. J., Tian, Y., Voineagu, I., Huang, N., Chu, S. H., Klei, L., Cai, C., Ou, J., Lowe, J. K., Hurles, M. E., Devlin, B., State, M. W., & Geschwind, D. H. (2012). Genome-wide transcriptome profiling reveals the functional impact of rare de novo and recurrent CNVs in autism spectrum disorders. *American Journal of Human Genetics*, *91*(1), 38–55.

https://doi.org/10.1016/j.ajhg.2012.05.011

Ma, X. M., & Blenis, J. (2009). Molecular mechanisms of mTOR-mediated translational control. *Nature Reviews Molecular Cell Biology*, *10*(5), 307–318. https://doi.org/10.1038/nrm2672

Maenner, M. J., Shaw, K. A., Baio, J., Washington, A., Patrick, M., DiRienzo, M., Christensen, D. L., Wiggins, L. D., Pettygrove, S., Andrews, J. G., Lopez, M., Hudson, A., Baroud, T., Schwenk, Y., White, T., Rosenberg, C. R., Lee, L. C., Harrington, R. A., Huston, M., … Dietz, P. M. (2020). Prevalence of autism spectrum disorder among children aged 8 Years-Autism and developmental disabilities monitoring network, 11 Sites, United States, 2016. *MMWR Surveillance Summaries*, *69*(4), 1–12. https://doi.org/10.15585/MMWR.SS6904A1

McCarthy, S. E., Makarov, V., Kirov, G., Addington, A. M., McClellan, J., Yoon, S., Perkins, D. O., Dickel, D. E., Kusenda, M., Krastoshevsky, O., Krause, V., Kumar, R. A., Grozeva, D., Malhotra, D., Walsh, T., Zackai, E. H., Kaplan, P., Ganesh, J., Krantz, I. D., … Sebat, J. (2009). Microduplications of 16p11.2 are associated with schizophrenia. *Nature Genetics*, *41*(11), 1223–1227. https://doi.org/10.1038/ng.474

Mitsopoulos, C., Zihni, C., Garg, R., Ridley, A. J., & Morris, J. D. H. (2003). The prostate-derived sterile 20-like kinase (PSK) regulates microtubule organization and stability. *Journal of Biological Chemistry*, *278*(20), 18085–18091. https://doi.org/10.1074/jbc.M213064200

Moore, T. M., Garg, R., Johnson, C., Coptcoat, M. J., Ridley, A. J., & Morris, J. D. H. (2000). PSK, a novel STE20-like kinase derived from prostatic carcinoma that activates the c-Jun N-terminal kinase mitogen-activated protein kinase pathway and regulates actin cytoskeletal organization. *Journal of Biological Chemistry*, *275*(6), 4311–4322. https://doi.org/10.1074/jbc.275.6.4311

Napoli, I., Mercaldo, V., Boyl, P. P., Eleuteri, B., Zalfa, F., De Rubeis, S., Di Marino, D., Mohr, E., Massimi, M., Falconi, M., Witke, W., Costa-Mattioli, M., Sonenberg, N., Achsel, T., & Bagni, C. (2008). The Fragile X Syndrome Protein Represses Activity-Dependent Translation through CYFIP1, a New 4E-BP. *Cell*, *134*(6), 1042–1054. https://doi.org/10.1016/j.cell.2008.07.031

Nathans, D. (1964). INCORPORATION OF PUROMYCIN INTO locyte. *Pnas*, *51*(1963), 585–592.

Nelson, S. B., & Valakh, V. (2015). Excitatory/Inhibitory Balance and Circuit Homeostasis in Autism Spectrum Disorders. *Neuron*, *87*(4), 684–698. https://doi.org/10.1016/j.neuron.2015.07.033

O'Connor, T., Sadleir, K. R., Maus, E., Velliquette, R. A., Zhao, J., Cole, S. L., Eimer, W. A., Hitt, B., Bembinster, L. A., Lammich, S., Lichtenthaler, S. F., Hébert, S. S., De Strooper, B., Haass, C., Bennett, D. A., & Vassar, R. (2008). Phosphorylation of the Translation Initiation Factor eIF2α Increases BACE1 Levels and Promotes Amyloidogenesis. *Neuron*, *60*(6), 988–1009. https://doi.org/10.1016/j.neuron.2008.10.047

Ohashi, R., Takao, K., Miyakawa, T., & Shiina, N. (2016). Comprehensive behavioral analysis of RNG105 (Caprin1) heterozygous mice: Reduced social interaction and attenuated response to novelty. *Scientific Reports*, *6*(October 2015), 1–14. https://doi.org/10.1038/srep20775

Pakos-Zebrucka, K., Koryga, I., Mnich, K., Ljujic, M., Samali, A., & Gorman, A. M. (2016). The integrated stress response. *EMBO Reports*, *17*(10), 1374–1395. https://doi.org/10.15252/embr.201642195

Park, S., Park, J. M., Kim, S., Kim, J. A., Shepherd, J. D., Smith-Hicks, C. L., Chowdhury, S., Kaufmann, W., Kuhl, D., Ryazanov, A. G., Huganir, R. L., Linden, D. J., & Worley, P. F. (2008). Elongation Factor 2 and Fragile X Mental Retardation Protein Control the Dynamic Translation of Arc/Arg3.1 Essential for mGluR-LTD. *Neuron*, *59*(1), 70–83. https://doi.org/10.1016/j.neuron.2008.05.023

Pisarev, A. V., Hellen, C. U. T., & Pestova, T. V. (2007). Recycling of Eukaryotic Posttermination Ribosomal Complexes. *Cell*, *131*(2), 286–299. https://doi.org/10.1016/j.cell.2007.08.041

Poon, M. M., Choi, S. H., Jamieson, C. A. M., Geschwind, D. H., & Martin, K. C. (2006). Identification of process-localized mRNAs from cultured rodent hippocampal neurons. *Journal of Neuroscience*, *26*(51), 13390–13399. https://doi.org/10.1523/JNEUROSCI.3432-06.2006

Portmann, T., Yang, M., Mao, R., Panagiotakos, G., Dolen, G., Bader, P. L., Grueter, B. A., Goold, C., Clifford, K., Rengarajan, P., Kalikhman, D., Loureiro, D., Saw, N. L., Zhengqui, Z., Miller, M. A., Lerch, J. P., Henkelman, M., Shamloo, M., Malenka, R. C., … Ricardo, E. (2014). *NIH Public Access*. *7*(4), 1077–1092. https://doi.org/10.1016/j.celrep.2014.03.036.Behavioral

Price, N. T., Redpath, N. T., Severinov, K. V., Campbell, D. G., Russell, J. M., & Proud, C. G. (1991). Identification of the phosphorylation sites in elongation factor-2 from rabbit reticulocytes. *FEBS Letters*, *282*(2), 253–258. https://doi.org/10.1016/0014-5793(91)80489-P

Proud, C. G. (2019). Phosphorylation and signal transduction pathways in translational control. *Cold Spring Harbor Perspectives in Biology*, *11*(7). https://doi.org/10.1101/cshperspect.a033050

Raj, N., McEachin, Z. T., Harousseau, W., Zhou, Y., Zhang, F., Merritt-Garza, M. E., Taliaferro, J. M., Kalinowska, M., Marro, S. G., Hales, C. M., Berry-Kravis, E., Wolf-Ochoa, M. W., Martinez-Cerdeño, V., Wernig, M., Chen, L., Klann, E., Warren, S. T., Jin, P., Wen, Z., & Bassell, G. J. (2021). Cell-type-specific profiling of human cellular models of fragile X syndrome reveal PI3K-dependent defects in translation and neurogenesis. *Cell Reports*, *35*(2). https://doi.org/10.1016/j.celrep.2021.108991

Redpath, N. T., Foulstone, E. J., & Proud, C. G. (1996). Regulation of translation elongation factor-2 by insulin via a rapamycin-sensitive signalling pathway. *EMBO Journal*, *15*(9), 2291–2297. https://doi.org/10.1002/j.1460-2075.1996.tb00582.x

Redpath, N. T., PRICE, N. T., SEVERINOV, K. V., & PROUD, C. G. (1993). Regulation of elongation factor-2 by multisite phosphorylation. *European Journal of Biochemistry*, *213*(2), 689–699. https://doi.org/10.1111/j.1432-1033.1993.tb17809.x

Richter, J. D., Bassell, G. J., & Klann, E. (2015). Dysregulation and restoration of translational homeostasis in fragile X syndrome. *Nature Reviews Neuroscience*, *16*(10), 595–605. https://doi.org/10.1038/nrn4001

Richter, J. D., & Sonenberg, N. (2005). Regulation of cap-dependent translation by eIF4E inhibitory proteins. *Nature*, *433*(7025), 477–480. https://doi.org/10.1038/nature03205

Richter, M., Murtaza, N., Scharrenberg, R., White, S. H., Johanns, O., Walker, S., Yuen, R. K. C., Schwanke, B., Bedürftig, B., Henis, M., Scharf, S., Kraus, V., Dörk, R., Hellmann, J., Lindenmaier, Z., Ellegood, J., Hartung, H., Kwan, V., Sedlacik, J., … Calderon de Anda, F. (2019). Altered TAOK2 activity causes autism-related neurodevelopmental and cognitive abnormalities through RhoA signaling. *Molecular Psychiatry*, *24*(9), 1329–1350. https://doi.org/10.1038/s41380-018-0025-5

Roffé, M., Hajj, G. N. M., Azevedo, H. F., Alves, V. S., & Castilho, B. A. (2013). IMPACT is a developmentally regulated protein in neurons that opposes the eukaryotic initiation factor 2βkinase GCN2 in the modulation of neurite outgrowth. *Journal of Biological Chemistry*, *288*(15), 10860–10869. https://doi.org/10.1074/jbc.M113.461970

Ryazanov, A., Shestakova, E. & Natapov, P. (1988). Phosphorylation of elongation factor 2 by EF-2 kinase affects rate of translation. *Nature*, *334*, 170–173. https://doi.org/https://doi.org/10.1038/334170a0

Salpietro, V., Dixon, C. L., Guo, H., Bello, O. D., Vandrovcova, J., Efthymiou, S., Maroofian, R., Heimer, G., Burglen, L., Valence, S., Torti, E., Hacke, M., Rankin, J., Tariq, H., Colin, E., Procaccio, V., Striano, P., Mankad, K., Lieb, A., … Houlden, H. (2019). AMPA receptor GluA2 subunit defects are a cause of neurodevelopmental disorders. *Nature Communications*, *10*(1). https://doi.org/10.1038/s41467-019-10910-w

Sanchez, L. (2001). TCA protein precipitation protocol. *October*, 2001–2001. https://doi.org/10.1145/2003653.2003657

Santini, E., Huynh, T. N., Longo, F., Koo, S. Y., Mojica, E., D'Andrea, L., Bagni, C., & Klann, E. (2017). Reducing eIF4E-eIF4G interactions restores the balance between protein synthesis and actin dynamics in fragile X syndrome model mice. *Science Signaling*, *10*(504), 41–46. https://doi.org/10.1126/scisignal.aan0665

Santini, E., Huynh, T. N., MacAskill, A. F., Carter, A. G., Pierre, P., Ruggero, D., Kaphzan, H., & Klann, E. (2013). Exaggerated translation causes synaptic and behavioural aberrations associated with autism. *Nature*, *493*(7432), 411–415. https://doi.org/10.1038/nature11782

Santoro, M. R., Bray, S. M., & Warren, S. T. (2012). Molecular mechanisms of fragile X syndrome: A twenty-year perspective. *Annual Review of Pathology: Mechanisms of Disease*, *7*, 219–245.

https://doi.org/10.1146/annurev-pathol-011811-132457

Sarbassov, D. D., Ali, S. M., & Sabatini, D. M. (2005). Growing roles for the mTOR pathway. *Current Opinion in Cell Biology*, *17*(6), 596–603. https://doi.org/10.1016/j.ceb.2005.09.009

Saxton, R. A., & Sabatini, D. M. (2017). mTOR Signaling in Growth, Metabolism, and Disease. *Cell*, *169*(2), 361–371. https://doi.org/10.1016/j.cell.2017.03.035

Scheetz, A. J., Nairn, A. C., & Constantine-paton, M. (2000). *NMDA receptor-mediated control of*. 211–216.

Scheper, G. C., Van Der Knaap, M. S., & Proud, C. G. (2007). Translation matters: Protein synthesis defects in inherited disease. *Nature Reviews Genetics*, *8*(9), 711–723. https://doi.org/10.1038/nrg2142

Schmidt, E. K., Clavarino, G., Ceppi, M., & Pierre, P. (2009). SUnSET, a nonradioactive method to monitor protein synthesis. *Nature Methods*, *6*(4), 275–277. https://doi.org/10.1038/nmeth.1314

Schneider, C. A., Rasband, W. S., & Eliceiri, K. W. (2012). NIH Image to ImageJ: 25 years of image analysis. *Nature Methods*, *9*(7), 671–675. https://doi.org/10.1038/nmeth.2089

Schuller, A. P., & Green, R. (2018). Roadblocks and resolutions in eukaryotic translation. *Nature Reviews Molecular Cell Biology*, *19*(8), 526–541. https://doi.org/10.1038/s41580-018-0011-4

Semenkov, Y. P., Shapkina, T. G., & Kirillov, S. V. (1992). Puromycin reaction of the A-site bound peptidyl-tRNA. *Biochimie*, *74*(5), 411–417. https://doi.org/10.1016/0300-9084(92)90080-X

Shevchenko, A., Tomas, H., Havliš, J., Olsen, J. V., & Mann, M. (2007). In-gel digestion for mass spectrometric characterization of proteins and proteomes. *Nature Protocols*, *1*(6), 2856–2860. https://doi.org/10.1038/nprot.2006.468

Sonenberg, N., & Hinnebusch, A. G. (2007). New Modes of Translational Control in Development, Behavior, and Disease. *Molecular Cell*, *28*(5), 721–729. https://doi.org/10.1016/j.molcel.2007.11.018

Sonenberg, N., & Hinnebusch, A. G. (2009). Regulation of Translation Initiation in Eukaryotes: Mechanisms and Biological Targets. *Cell*, *136*(4), 731–745. https://doi.org/10.1016/j.cell.2009.01.042

Stein, J. M., Bergman, W., Fang, Y., Davison, L. K., Brensinger, C., Robinson, M. B., Hecht, N. B., & Abel, T. (2006). Behavioral and neurochemical alterations in mice lacking the RNA-binding protein translin. *Journal of Neuroscience*, *26*(8), 2184–2196. https://doi.org/10.1523/JNEUROSCI.4437-05.2006

Steinberg, S., Jong, S. De, Mattheisen, M., & Costas, J. (2014). *Europe PMC Funders Group Common Variant at 16p11 . 2 Conferring Risk of Psychosis*. *19*(1), 1–16. https://doi.org/10.1038/mp.2012.157.Common

Südhof, T. C. (2008). Neuroligins and neurexins link synaptic function to cognitive disease. *Nature*, *455*(7215), 903–911. https://doi.org/10.1038/nature07456

Sutton, M. A., & Schuman, E. M. (2006). Dendritic Protein Synthesis, Synaptic Plasticity, and Memory. *Cell*, *127*(1), 49–58. https://doi.org/10.1016/j.cell.2006.09.014

Suzuki, A. M., Griesi-Oliveira, K., De Oliveira Freitas Machado, C., Vadasz, E., Zachi, E. C., Passos-Bueno, M. R., & Sertie, A. L. (2015). Altered mTORC1 signaling in multipotent stem cells from nearly 25% of patients with nonsyndromic autism spectrum disorders. *Molecular Psychiatry*, *20*(5), 550–552. https://doi.org/10.1038/mp.2014.175

Szklarczyk, D., Gable, A. L., Nastou, K. C., Lyon, D., Kirsch, R., Pyysalo, S., Doncheva, N. T., Legeay, M., Fang, T., Bork, P., Jensen, L. J., & von Mering, C. (2021). The STRING database in 2021: Customizable protein-protein networks, and functional characterization of user-uploaded gene/measurement sets. *Nucleic Acids Research*, *49*(D1), D605–D612. https://doi.org/10.1093/nar/gkaa1074

Tylee, D. S., Hess, J. L., Quinn, T. P., Barve, R., Huang, H., Zhang-James, Y., Chang, J., Stamova, B. S., Sharp, F. R., Hertz-Picciotto, I., Faraone, S. V., Kong, S. W., & Glatt, S. J. (2017). Blood

transcriptomic comparison of individuals with and without autism spectrum disorder: A combined-samples mega-analysis. *American Journal of Medical Genetics, Part B: Neuropsychiatric Genetics*, *174*(3), 181–201. https://doi.org/10.1002/ajmg.b.32511

Udagawa, T., Farny, N. G., Jakovcevski, M., Kaphzan, H., Alarcon, J. M., Anilkumar, S., Ivshina, M., Hurt, J. A., Nagaoka, K., Nalavadi, V. C., Lorenz, L. J., Bassell, G. J., Akbarian, S., Chattarji, S., Klann, E., & Richter, J. D. (2013). Genetic and acute CPEB1 depletion ameliorate fragile X pathophysiology. *Nature Medicine*, *19*(11), 1473–1477. https://doi.org/10.1038/nm.3353

Ultanir, S. K., Yadav, S., Hertz, N. T., Oses-Prieto, J. A., Claxton, S., Burlingame, A. L., Shokat, K. M., Jan, L. Y., & Jan, Y. N. (2014). MST3 kinase phosphorylates TAO1/2 to enable myosin va function in promoting spine synapse development. *Neuron*, *84*(5), 968–982. https://doi.org/10.1016/j.neuron.2014.10.025

Verkerk, A. J. M. H., Pieretti, M., Sutcliffe, J. S., Fu, Y. H., Kuhl, D. P. A., Pizzuti, A., Reiner, O., Richards, S., Victoria, M. F., Zhang, F., Eussen, B. E., van Ommen, G. J. B., Blonden, L. A. J., Riggins, G. J., Chastain, J. L., Kunst, C. B., Galjaard, H., Thomas Caskey, C., Nelson, D. L., … Warran, S. T. (1991). Identification of a gene (FMR-1) containing a CGG repeat coincident with a breakpoint cluster region exhibiting length variation in fragile X syndrome. *Cell*, *65*(5), 905–914. https://doi.org/10.1016/0092-8674(91)90397-H

Verpelli, C., Piccoli, G., Zibetti, C., Zanchi, A., Gardoni, F., Huang, K., Brambilla, D., Di Luca, M., Sala, C., & Sala, C. (2010). Synaptic activity controls dendritic spine morphology by modulating eEF2-dependent BDNF synthesis. *Journal of Neuroscience*, *30*(17), 5830–5842. https://doi.org/10.1523/JNEUROSCI.0119-10.2010

Weiss, L. A., Shen, Y., Korn, J. M., Arking, D. E., Miller, D. T., Fossdal, R., Saemundsen, E., Stefansson, H., Ferreira, M. A. R., Green, T., Platt, O. S., Ruderfer, D. M., Walsh, C. A., Altshuler, D., Chakravarti, A., Tanzi, R. E., Stefansson, K., Santangelo, S. L., Gusella, J. F., … Daly, M. J. (2008). *new england journal*.

Wu, Y. C., Williamson, R., Li, Z., Vicario, A., Xu, J., Kasai, M., Chern, Y., Tongiorgi, E., & Baraban, J. M. (2011). Dendritic trafficking of brain-derived neurotrophic factor mRNA: Regulation by translin-dependent and -independent mechanisms. *Journal of Neurochemistry*, *116*(6), 1112–1121. https://doi.org/10.1111/j.1471-4159.2010.07166.x

Yadav, S., Oses-Prieto, J. A., Peters, C. J., Zhou, J., Pleasure, S. J., Burlingame, A. L., Jan, L. Y., & Jan, Y. N. (2017). TAOK2 Kinase Mediates PSD95 Stability and Dendritic Spine Maturation through Septin7 Phosphorylation. *Neuron*, *93*(2), 379–393. https://doi.org/10.1016/j.neuron.2016.12.006

Yasuda, S., Tanaka, H., Sugiura, H., Okamura, K., Sakaguchi, T., Tran, U., Takemiya, T., Mizoguchi, A., Yagita, Y., Sakurai, T., De Robertis, E. M., & Yamagata, K. (2007). Activity-Induced Protocadherin Arcadlin Regulates Dendritic Spine Number by Triggering N-Cadherin Endocytosis via TAO2β and p38 MAP Kinases. *Neuron*, *56*(3), 456–471. https://doi.org/10.1016/j.neuron.2007.08.020

Yoshimura, A., Fujii, R., Watanabe, Y., Okabe, S., Fukui, K., & Takumi, T. (2006). Myosin-Va Facilitates the Accumulation of mRNA/Protein Complex in Dendritic Spines. *Current Biology*, *16*(23), 2345–2351. https://doi.org/10.1016/j.cub.2006.10.024

Zalfa, F., Eleuteri, B., Dickson, K. S., Mercaldo, V., De Rubeis, S., Di Penta, A., Tabolacci, E., Chiurazzi, P., Neri, G., Grant, S. G. N., & Bagni, C. (2007). A new function for the fragile X mental retardation protein in regulation of PSD-95 mRNA stability. *Nature Neuroscience*, *10*(5), 578–587. https://doi.org/10.1038/nn1893

Zalfa, F., Giorgi, M., Primerano, B., Moro, A., Di Penta, A., Reis, S., Oostra, B., & Bagni, C. (2003). The Fragile X syndrome protein FMRP associates with BC1 RNA and regulates the translation of specific mRNAs at synapses. *Cell*, *112*(3), 317–327. https://doi.org/10.1016/S0092-8674(03)00079-5

Zaslavsky, K., Zhang, W. B., McCready, F. P., Rodrigues, D. C., Deneault, E., Loo, C., Zhao, M., Ross, P. J., El Hajjar, J., Romm, A., Thompson, T., Piekna, A., Wei, W., Wang, Z., Khattak, S., Mufteev, M., Pasceri, P., Scherer, S. W., Salter, M. W., & Ellis, J. (2019). SHANK2 mutations associated with autism spectrum disorder cause hyperconnectivity of human neurons. *Nature Neuroscience*,

22(4), 556–564. https://doi.org/10.1038/s41593-019-0365-8

Zhou, T., Raman, M., Gao, Y., Earnest, S., Chen, Z., Machius, M., Cobb, M. H., & Goldsmith, E. J. (2004). Crystal structure of the TAO2 kinase domain: Activation and specificity of a Ste20p MAP3K. *Structure*, *12*(10), 1891–1900. https://doi.org/10.1016/j.str.2004.07.021

Zihni, C., Mitsopoulos, C., Tavares, I. A., Baum, B., Ridley, A. J., & Morris, J. D. H. (2007). Prostate-derived sterile 20-like kinase 1-α induces apoptosis: JNK- and caspase-dependent nuclear localization is a requirement for membrane blebbing. *Journal of Biological Chemistry*, *282*(9), 6484–6493. https://doi.org/10.1074/jbc.M608336200

Zihni, C., Mitsopoulos, C., Tavares, I. A., Ridley, A. J., & Morris, J. D. H. (2006). Prostate-derived sterile 20-like kinase 2 (PSK2) regulates apoptotic morphology via C-Jun N-terminal kinase and Rho kinase-1. *Journal of Biological Chemistry*, *281*(11), 7317–7323. https://doi.org/10.1074/jbc.M513769200

9. Supplementary Information

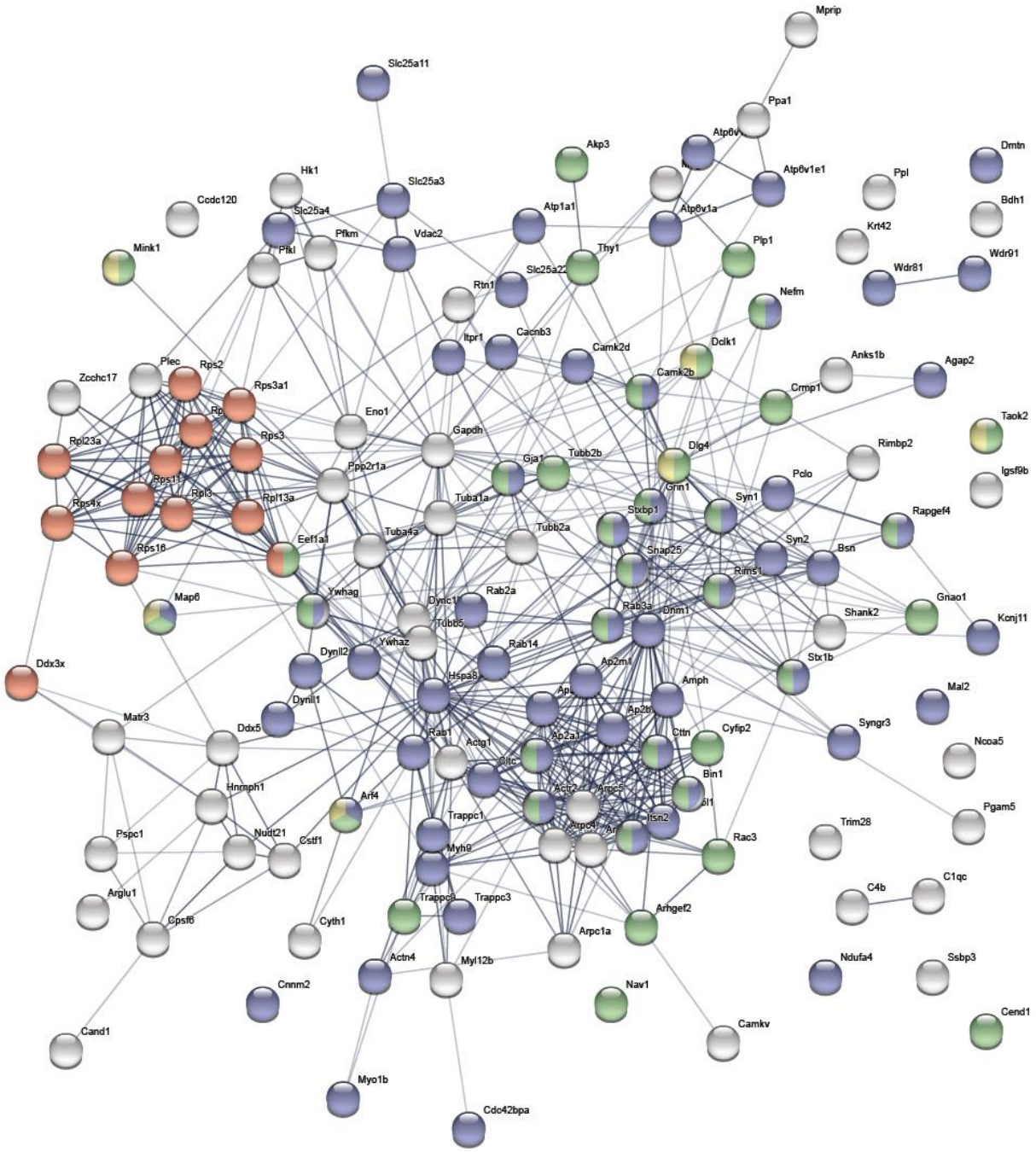

Supplementary Figure 1: Network graph from STRING analysis visualizes of the 153 proteins that were immunoprecipitated by TAOK2-β antibody and identified by IP-MS in the cortex (coefficient of variation (CV) cutoff = 0.1).

The “confidence” link visualization was selected with a medium confidence interaction score (0.400). For details, (Supplementary Table 1)

Supplementary Table 1: list of the 153 enriched protein from wild type cortex identified by IP coupled with LC-MS/MS analysis using TAOK2β antibody. The enriched proteins from the 2 experiments are ordered in a descending order depending on the number of unique peptides identified for each protein. The log2 values of the identified proteins from the 2 experiments separately were showed in their respective columns.

Uniprot Accession #	Gene name	Protein Name	log2 experiment 1	log2 experiment 2	# Peptides
O88737	Bsn	Protein bassoon OS=Mus musculus OX=10090 GN=Bsn PE=1 SV=4	8.586772627	8.655663543	134
Q8VDD5	Myh9	Myosin-9 OS=Mus musculus OX=10090 GN=Myh9 PE=1 SV=4	6.940571035	6.488397513	95
P11881	Itpr1	Inositol 1,4,5-trisphosphate receptor type 1 OS=Mus musculus OX=10090 GN=Itpr1 PE=1 SV=2	7.850189888	6.950732779	64
P39053	Dnm1	Dynamin-1 OS=Mus musculus OX=10090 GN=Dnm1 PE=1 SV=2	8.025646961	7.786364901	59
Q9QYX7	Pclo	Protein piccolo OS=Mus musculus OX=10090 GN=Pclo PE=1 SV=4	7.120384229	7.145817535	49
Q6ZQ29-2	Taok2	Isoform 2 of Serine/threonine-protein kinase TAO2 OS=Mus musculus OX=10090 GN=Taok2	7.227374383	7.18660128	45
Q3UU96	Cdc42bpa	Serine/threonine-protein kinase MRCK alpha OS=Mus musculus OX=10090 GN=Cdc42bpa PE=1 SV=2	5.117427956	5.021320411	32
Q9QXS1	Plec	Plectin OS=Mus musculus OX=10090 GN=Plec PE=1 SV=3	5.99165085	5.397015091	32
P63260	Actg1	Actin, cytoplasmic 2 OS=Mus musculus OX=10090 GN=Actg1 PE=1 SV=1	10.57512499	9.19237003	23
P99024	Tubb5	Tubulin beta-5 chain OS=Mus musculus OX=10090 GN=Tubb5 PE=1 SV=1	6.406424781	5.857780736	21
P68369	Tuba1a	Tubulin alpha-1A chain OS=Mus musculus OX=10090 GN=Tuba1a PE=1 SV=1	5.968914187	5.408384482	19
Q7TMM9	Tubb2a	Tubulin beta-2A chain OS=Mus musculus OX=10090 GN=Tubb2a PE=1 SV=1	6.593270513	6.033454703	19
Q9CWF2	Tubb2b	Tubulin beta-2B chain OS=Mus musculus OX=10090 GN=Tubb2b PE=1 SV=1	11.26279395	10.97008201	19
P28652	Camk2b	Calcium/calmodulin-dependent protein kinase type II subunit beta OS=Mus musculus OX=10090 GN=Camk2b PE=1 SV=2	8.394697058	7.687060814	19
P68368	Tuba4a	Tubulin alpha-4A chain OS=Mus musculus OX=10090 GN=Tuba4a PE=1 SV=1	7.903023581	6.957164471	18
Q62108	Dlg4	Disks large homolog 4 OS=Mus musculus OX=10090 GN=Dlg4 PE=1 SV=1	7.077929782	6.799144892	18
P97434	Mprip	Myosin phosphatase Rho-interacting protein OS=Mus musculus OX=10090 GN=Mprip PE=1 SV=2	13.27884048	11.71171194	18
P63017	Hspa8	Heat shock cognate 71 kDa protein OS=Mus musculus OX=10090 GN=Hspa8 PE=1 SV=1	5.202696098	4.936826968	15

Q03265	Atp5f1a	ATP synthase subunit alpha, mitochondrial OS=Mus musculus OX=10090 GN=Atp5f1a PE=1 SV=1	5.324529879	4.818903192	15
P08553	Nefm	Neurofilament medium polypeptide OS=Mus musculus OX=10090 GN=Nefm PE=1 SV=4	13.28698254	12.39547901	13
E9PZ19	Igsf9b	Protein turtle homolog B OS=Mus musculus OX=10090 GN=Igsf9b PE=1 SV=1	9.490698212	9.494540303	13
P17426	Ap2a1	AP-2 complex subunit alpha-1 OS=Mus musculus OX=10090 GN=Ap2a1 PE=1 SV=1	13.1768101	12.95827409	12
P17427	Ap2a2	AP-2 complex subunit alpha-2 OS=Mus musculus OX=10090 GN=Ap2a2 PE=1 SV=2	11.51433876	11.173153	12
P57780	Actn4	Alpha-actinin-4 OS=Mus musculus OX=10090 GN=Actn4 PE=1 SV=1	9.510409369	8.360603054	12
P48962	Slc25a4	ADP/ATP translocase 1 OS=Mus musculus OX=10090 GN=Slc25a4 PE=1 SV=4	6.387645198	6.579431539	12
P46735	Myo1b	Unconventional myosin-Ib OS=Mus musculus OX=10090 GN=Myo1b PE=1 SV=3	12.64974006	11.29678317	12
Q6IFX2	Krt42	Keratin, type I cytoskeletal 42 OS=Mus musculus OX=10090 GN=Krt42 PE=1 SV=1	1.975438706	2.244379008	11
P17182	Eno1	Alpha-enolase OS=Mus musculus OX=10090 GN=Eno1 PE=1 SV=3	6.441625164	6.316394449	11
Q60902	Eps15l1	Epidermal growth factor receptor substrate 15-like 1 OS=Mus musculus OX=10090 GN=Eps15l1 PE=1 SV=3	6.384853256	7.214178027	11
Q9DBG3	Ap2b1	AP-2 complex subunit beta OS=Mus musculus OX=10090 GN=Ap2b1 PE=1 SV=1	13.01365175	12.62488695	11
Q68FD5	Cltc	Clathrin heavy chain 1 OS=Mus musculus OX=10090 GN=Cltc PE=1 SV=3	10.94620746	10.68158429	10
Q8VDN2	Atp1a1	Sodium/potassium-transporting ATPase subunit alpha-1 OS=Mus musculus OX=10090 GN=Atp1a1 PE=1 SV=1	10.62229834	9.925080539	9
Q6PHZ2	Camk2d	Calcium/calmodulin-dependent protein kinase type II subunit delta OS=Mus musculus OX=10090 GN=Camk2d PE=1 SV=1	11.53597223	10.17749548	9
Q80Z38	Shank2	SH3 and multiple ankyrin repeat domains protein 2 OS=Mus musculus OX=10090 GN=Shank2 PE=1 SV=2	12.0304015	10.53279197	9
Q8BX10	Pgam5	Serine/threonine-protein phosphatase PGAM5, mitochondrial OS=Mus musculus OX=10090 GN=Pgam5 PE=1 SV=1	13.81488017	13.52377776	9
Q9EQZ6	Rapgef4	Rap guanine nucleotide exchange factor 4 OS=Mus musculus OX=10090 GN=Rapgef4 PE=1 SV=1	6.318995393	6.397871092	8
P16858	Gapdh	Glyceraldehyde-3-phosphate dehydrogenase OS=Mus musculus OX=10090 GN=Gapdh PE=1 SV=2	7.287788754	6.48769073	7
Q8BIZ1	Anks1b	Ankyrin repeat and sterile alpha motif domain-containing protein 1B OS=Mus musculus OX=10090 GN=Anks1b PE=1 SV=3	12.61123317	11.16780865	7
P84091	Ap2m1	AP-2 complex subunit mu OS=Mus musculus OX=10090 GN=Ap2m1 PE=1 SV=1	7.76743992	6.924700657	7

P10126	Eef1a1	Elongation factor 1-alpha 1 OS=Mus musculus OX=10090 GN=Eef1a1 PE=1 SV=3	4.833776966	4.674490793	7
Q8CH77	Nav1	Neuron navigator 1 OS=Mus musculus OX=10090 GN=Nav1 PE=1 SV=2	10.401597	9.74591425	7
Q60598	Cttn	Src substrate cortactin OS=Mus musculus OX=10090 GN=Cttn PE=1 SV=2	6.039859626	6.757892727	7
Q99NE5	Rims1	Regulating synaptic membrane exocytosis protein 1 OS=Mus musculus OX=10090 GN=Rims1 PE=1 SV=2	11.07800883	10.74930641	7
P17710	Hk1	Hexokinase-1 OS=Mus musculus OX=10090 GN=Hk1 PE=1 SV=3	11.09925878	10.14140364	7
Q3TLI0	Trappc1	Trafficking protein particle complex subunit 10 OS=Mus musculus OX=10090 GN=Trappc10 PE=1 SV=2	3.956258056	3.943917	7
Q64332	Syn2	Synapsin-2 OS=Mus musculus OX=10090 GN=Syn2 PE=1 SV=2	13.76875274	13.19566938	6
P18872	Gnao1	Guanine nucleotide-binding protein G(o) subunit alpha OS=Mus musculus OX=10090 GN=Gnao1 PE=1 SV=3	6.32539494	5.536818308	6
Q9D6M3	Slc25a22	Mitochondrial glutamate carrier 1 OS=Mus musculus OX=10090 GN=Slc25a22 PE=1 SV=1	11.75722274	11.65577627	6
P63011	Rab3a	Ras-related protein Rab-3A OS=Mus musculus OX=10090 GN=Rab3a PE=1 SV=1	6.197619466	6.132974552	6
O08599	Stxbp1	Syntaxin-binding protein 1 OS=Mus musculus OX=10090 GN=Stxbp1 PE=1 SV=2	11.32998634	11.00200674	6
O88935	Syn1	Synapsin-1 OS=Mus musculus OX=10090 GN=Syn1 PE=1 SV=2	10.25805026	9.759083021	6
Q3TWN3	Cnnm2	Metal transporter CNNM2 OS=Mus musculus OX=10090 GN=Cnnm2 PE=1 SV=3	12.03521084	11.53103786	6
Q3UHD9	Agap2	Arf-GAP with GTPase, ANK repeat and PH domain-containing protein 2 OS=Mus musculus OX=10090 GN=Agap2 PE=1 SV=1	9.428668365	9.555026851	6
P59999	Arpc4	Actin-related protein 2/3 complex subunit 4 OS=Mus musculus OX=10090 GN=Arpc4 PE=1 SV=3	12.83209874	11.86597911	5
Q8BVE3	Atp6v1h	V-type proton ATPase subunit H OS=Mus musculus OX=10090 GN=Atp6v1h PE=1 SV=1	11.55114376	10.51091071	5
Q60930	Vdac2	Voltage-dependent anion-selective channel protein 2 OS=Mus musculus OX=10090 GN=Vdac2 PE=1 SV=2	5.497287796	5.333522559	5
O35737	Hnrnph1	Heterogeneous nuclear ribonucleoprotein H OS=Mus musculus OX=10090 GN=Hnrnph1 PE=1 SV=3	4.60841384	4.663194613	5
Q9D0M5	Dynll2	Dynein light chain 2, cytoplasmic OS=Mus musculus OX=10090 GN=Dynll2 PE=1 SV=1	11.53957012	10.72045155	4
P62242	Rps8	40S ribosomal protein S8 OS=Mus musculus OX=10090 GN=Rps8 PE=1 SV=2	5.629558061	5.980807584	4
P47857	Pfkm	ATP-dependent 6-phosphofructokinase, muscle type OS=Mus musculus OX=10090 GN=Pfkm PE=1 SV=3	10.57312187	10.47491479	4
Q3THE2	Myl12b	Myosin regulatory light chain 12B OS=Mus musculus OX=10090 GN=Myl12b PE=1 SV=2	13.20645927	12.23409499	4

P63168	Dynll1	Dynein light chain 1, cytoplasmic OS=Mus musculus OX=10090 GN=Dynll1 PE=1 SV=1	13.86695722	12.99681623	4
P01867	Igh-3	Ig gamma-3 chain C region OS=Mus musculus OX=10090 PE=1 SV=2	-7.34082083	0.881858273	4
Q91V41	Rab14	Ras-related protein Rab-14 OS=Mus musculus OX=10090 GN=Rab14 PE=1 SV=3	3.307740149	3.06468219	4
Q9Z0R6	Itsn2	Intersectin-2 OS=Mus musculus OX=10090 GN=Itsn2 PE=1 SV=2	9.247454357	9.360680741	4
P35980	Rpl18	60S ribosomal protein L18 OS=Mus musculus OX=10090 GN=Rpl18 PE=1 SV=3	-1.060405424	-0.676743708	4
Q9JM52	Mink1	Misshapen-like kinase 1 OS=Mus musculus OX=10090 GN=Mink1 PE=1 SV=3	10.31534591	9.845998934	4
Q62425	Ndufa4	Cytochrome c oxidase subunit NDUFA4 OS=Mus musculus OX=10090 GN=Ndufa4 PE=1 SV=2	6.299899953	6.863261189	4
Q7TMQ7	Wdr91	WD repeat-containing protein 91 OS=Mus musculus OX=10090 GN=Wdr91 PE=1 SV=1	10.41777014	9.410722608	4
P25444	Rps2	40S ribosomal protein S2 OS=Mus musculus OX=10090 GN=Rps2 PE=1 SV=3	5.104284974	5.621795826	4
P60202	Plp1	Myelin proteolipid protein OS=Mus musculus OX=10090 GN=Plp1 PE=1 SV=2	6.799611806	7.539882052	4
Q99LC2	Cstf1	Cleavage stimulation factor subunit 1 OS=Mus musculus OX=10090 GN=Cstf1 PE=1 SV=1	9.928093082	9.978143575	4
P35438	Grin1	Glutamate receptor ionotropic, NMDA 1 OS=Mus musculus OX=10090 GN=Grin1 PE=1 SV=1	11.38828067	10.28357108	4
Q8VEM8	Slc25a3	Phosphate carrier protein, mitochondrial OS=Mus musculus OX=10090 GN=Slc25a3 PE=1 SV=1	4.232527355	4.253139923	4
P50516	Atp6v1a	V-type proton ATPase catalytic subunit A OS=Mus musculus OX=10090 GN=Atp6v1a PE=1 SV=2	10.65616943	9.381010331	4
Q3UL36	Arglu1	Arginine and glutamate-rich protein 1 OS=Mus musculus OX=10090 GN=Arglu1 PE=1 SV=2	0.605339951	0.643075951	4
Q3U0M1	Trappc9	Trafficking protein particle complex subunit 9 OS=Mus musculus OX=10090 GN=Trappc9 PE=1 SV=2	11.21138967	10.72181846	4
P97351	Rps3a	40S ribosomal protein S3a OS=Mus musculus OX=10090 GN=Rps3a PE=1 SV=3	6.162624524	6.33919236	4
P01867	Igh-3.0	Ig gamma-2B chain C region OS=Mus musculus OX=10090 GN=Igh-3 PE=1 SV=3	0.372671885	-0.978544689	4
P23242	Gja1	Gap junction alpha-1 protein OS=Mus musculus OX=10090 GN=Gja1 PE=1 SV=2	12.75264312	11.88426179	3
Q9ESX4	Zcchc17	Nucleolar protein of 40 kDa OS=Mus musculus OX=10090 GN=Zcchc17 PE=1 SV=1	2.376591188	2.110390947	3
O08539	Bin1	Myc box-dependent-interacting protein 1 OS=Mus musculus OX=10090 GN=Bin1 PE=1 SV=1	9.23975828	9.979449837	3
Q80XN0	Bdh1	D-beta-hydroxybutyrate dehydrogenase, mitochondrial OS=Mus musculus OX=10090 GN=Bdh1 PE=1 SV=2	11.43236715	10.70712062	3
P61161	Actr2	Actin-related protein 2 OS=Mus musculus OX=10090 GN=Actr2 PE=1 SV=1	10.53757147	9.319321925	3

Q8R326	Pspc1	Paraspeckle component 1 OS=Mus musculus OX=10090 GN=Pspc1 PE=1 SV=1	11.33414399	11.03656935	3
P01837	Igkc	Immunoglobulin kappa constant OS=Mus musculus OX=10090 GN=Igkc PE=1 SV=2	-0.822377545	-0.773715114	3
Q7TSJ2	Map6	Microtubule-associated protein 6 OS=Mus musculus OX=10090 GN=Map6 PE=1 SV=2	9.437617746	9.103434673	3
Q9CQF3	Nudt21	Cleavage and polyadenylation specificity factor subunit 5 OS=Mus musculus OX=10090 GN=Nudt21 PE=1 SV=1	11.11988445	10.91962533	3
P97427	Crmp1	Dihydropyrimidinase-related protein 1 OS=Mus musculus OX=10090 GN=Crmp1 PE=1 SV=1	9.443271451	8.972183741	3
Q7TQF7	Amph	Amphiphysin OS=Mus musculus OX=10090 GN=Amph PE=1 SV=1	4.613478203	4.911107707	3
Q6NVF9	Cpsf6	Cleavage and polyadenylation specificity factor subunit 6 OS=Mus musculus OX=10090 GN=Cpsf6 PE=1 SV=1	11.40470447	10.55601518	3
P12382	Pfkl	ATP-dependent 6-phosphofructokinase, liver type OS=Mus musculus OX=10090 GN=Pfkl PE=1 SV=4	8.954441637	8.802497235	3
P54285	Cacnb3	Voltage-dependent L-type calcium channel subunit beta-3 OS=Mus musculus OX=10090 GN=Cacnb3 PE=1 SV=2	9.167559487	9.043085374	3
Q62318	Trim28	Transcription intermediary factor 1-beta OS=Mus musculus OX=10090 GN=Trim28 PE=1 SV=3	10.73374258	10.65061096	3
Q61656	Ddx5	Probable ATP-dependent RNA helicase DDX5 OS=Mus musculus OX=10090 GN=Ddx5 PE=1 SV=2	3.392288985	3.760718087	3
Q5ND34	Wdr81	WD repeat-containing protein 81 OS=Mus musculus OX=10090 GN=Wdr81 PE=1 SV=2	8.658599941	8.374625088	3
P63101	Ywhaz	14-3-3 protein zeta/delta OS=Mus musculus OX=10090 GN=Ywhaz PE=1 SV=1	4.569900118	4.192255986	3
P62821	Rab1A	Ras-related protein Rab-1A OS=Mus musculus OX=10090 GN=Rab1A PE=1 SV=3	7.843336262	7.092971941	3
Q9R0Q6	Arpc1a	Actin-related protein 2/3 complex subunit 1A OS=Mus musculus OX=10090 GN=Arpc1a PE=1 SV=1	10.57201213	9.512971943	2
P50518	Atp6v1e1	V-type proton ATPase subunit E 1 OS=Mus musculus OX=10090 GN=Atp6v1e1 PE=1 SV=2	10.18458516	8.866972588	2
Q8K0T0	Rtn1	Reticulon-1 OS=Mus musculus OX=10090 GN=Rtn1 PE=1 SV=1	10.23891242	9.653519667	2
Q8BI08	Mal2	Protein MAL2 OS=Mus musculus OX=10090 GN=Mal2 PE=1 SV=1	11.37803298	10.27376199	2
Q9DB20	Atp5po	ATP synthase subunit O, mitochondrial OS=Mus musculus OX=10090 GN=Atp5po PE=1 SV=1	10.2698195	10.02463705	2
P60879	Snap25	Synaptosomal-associated protein 25 OS=Mus musculus OX=10090 GN=Snap25 PE=1 SV=1	4.666868891	4.881911781	2
P01831	Thy1	Thy-1 membrane glycoprotein OS=Mus musculus OX=10090 GN=Thy1 PE=1 SV=1	2.613444283	2.290578168	2
Q9JKC6	Cend1	Cell cycle exit and neuronal differentiation protein 1 OS=Mus musculus OX=10090 GN=Cend1 PE=1 SV=1	7.045222567	6.377407813	2

P61264	Stx1b	Syntaxin-1B OS=Mus musculus OX=10090 GN=Stx1b PE=1 SV=1	9.752598803	9.665029427	2
Q62167	Ddx3x	ATP-dependent RNA helicase DDX3X OS=Mus musculus OX=10090 GN=Ddx3x PE=1 SV=3	10.60229625	10.35284173	2
Q8R1Q8	Dync1li1	Cytoplasmic dynein 1 light intermediate chain 1 OS=Mus musculus OX=10090 GN=Dync1li1 PE=1 SV=1	8.817172168	9.169373558	2
Q6ZQ38	Cand1	Cullin-associated NEDD8-dissociated protein 1 OS=Mus musculus OX=10090 GN=Cand1 PE=1 SV=2	8.761306423	8.665841495	2
P61982	Ywhag	14-3-3 protein gamma OS=Mus musculus OX=10090 GN=Ywhag PE=1 SV=2	9.713033622	8.963667649	2
Q5SQX6	Cyfip2	Cytoplasmic FMR1-interacting protein 2 OS=Mus musculus OX=10090 GN=Cyfip2 PE=1 SV=2	9.623789526	9.253146191	2
Q91VR2	Atp5f1c	ATP synthase subunit gamma, mitochondrial OS=Mus musculus OX=10090 GN=Atp5f1c PE=1 SV=1	10.06285093	9.339939074	2
Q76MZ3	Ppp2r1a	Serine/threonine-protein phosphatase 2A 65 kDa regulatory subunit A alpha isoform OS=Mus musculus OX=10090 GN=Ppp2r1a PE=1 SV=3	8.499182889	7.475713643	2
A2AEV7	Ccdc120	Coiled-coil domain-containing protein 120 OS=Mus musculus OX=10090 GN=Ccdc120 PE=1 SV=1	9.537242577	9.285793616	2
Q9JLM8	Dclk1	Serine/threonine-protein kinase DCLK1 OS=Mus musculus OX=10090 GN=Dclk1 PE=1 SV=1	9.625589128	9.418571195	2
Q9DCX2	Atp5pd	ATP synthase subunit d, mitochondrial OS=Mus musculus OX=10090 GN=Atp5pd PE=1 SV=3	10.18766771	9.497687653	2
P27659	Rpl3	60S ribosomal protein L3 OS=Mus musculus OX=10090 GN=Rpl3 PE=1 SV=3	9.855326701	9.629707769	2
P56480	Atp5f1b	ATP synthase subunit beta, mitochondrial OS=Mus musculus OX=10090 GN=Atp5f1b PE=1 SV=2	7.863867618	7.542216903	2
Q9CR62	Slc25a11	Mitochondrial 2-oxoglutarate/malate carrier protein OS=Mus musculus OX=10090 GN=Slc25a11 PE=1 SV=3	8.780698348	8.357531065	2
Q02105	C1qc	Complement C1q subcomponent subunit C OS=Mus musculus OX=10090 GN=C1qc PE=1 SV=2	11.34572603	11.26499531	2
P62281	Rps11	40S ribosomal protein S11 OS=Mus musculus OX=10090 GN=Rps11 PE=1 SV=3	7.631668881	6.984784715	2
P19253	Rpl13a	60S ribosomal protein L13a OS=Mus musculus OX=10090 GN=Rpl13a PE=1 SV=4	8.844790513	8.980213594	2
Q8K310	Matr3	Matrin-3 OS=Mus musculus OX=10090 GN=Matr3 PE=1 SV=1	8.437947723	8.045520385	2
P62702	Rps4x	40S ribosomal protein S4, X isoform OS=Mus musculus OX=10090 GN=Rps4x PE=1 SV=2	7.697210241	7.350342495	2
Q91W39	Ncoa5	Nuclear receptor coactivator 5 OS=Mus musculus OX=10090 GN=Ncoa5 PE=1 SV=1	6.50205093	6.978202373	2
Q80U40	Rimbp2	RIMS-binding protein 2 OS=Mus musculus OX=10090 GN=Rimbp2 PE=1 SV=3	9.797604734	9.191034884	2
Q3UHL1	Camkv	CaM kinase-like vesicle-associated protein OS=Mus musculus OX=10090 GN=Camkv PE=1 SV=2	9.454261997	9.265242463	2

P03977	Ig kappa chain V-III region 50S10.1	Ig kappa chain V-III region 50S10.1 OS=Mus musculus OX=10090 PE=1 SV=1	-0.343287953	-1.002676952	2
P01029	C4b	Complement C4-B OS=Mus musculus OX=10090 GN=C4b PE=1 SV=3	8.710067759	8.247819034	1
Q9CVB6	Arpc2	Actin-related protein 2/3 complex subunit 2 OS=Mus musculus OX=10090 GN=Arpc2 PE=1 SV=3	9.475276387	8.37233278	1
P61750	Arf4	ADP-ribosylation factor 4 OS=Mus musculus OX=10090 GN=Arf4 PE=1 SV=2	3.200780884	3.426142732	1
Q78IK2	Atp5mk	ATP synthase membrane subunit DAPIT, mitochondrial OS=Mus musculus OX=10090 GN=Atp5md PE=1 SV=1	9.42636023	8.564932933	1
P62830	Rpl23	60S ribosomal protein L23 OS=Mus musculus OX=10090 GN=Rpl23 PE=1 SV=1	8.814342385	8.149601852	1
P14131	Rps16	40S ribosomal protein S16 OS=Mus musculus OX=10090 GN=Rps16 PE=1 SV=4	9.366856983	8.264854038	1
P53994	Rab2a	Ras-related protein Rab-2A OS=Mus musculus OX=10090 GN=Rab2a PE=1 SV=1	8.28832807	7.921077288	1
P62908	Rps3	40S ribosomal protein S3 OS=Mus musculus OX=10090 GN=Rps3 PE=1 SV=1	8.883102094	8.39943414	1
P62751	Rpl23a	60S ribosomal protein L23a OS=Mus musculus OX=10090 GN=Rpl23a PE=1 SV=1	2.559650905	2.47476581	1
Q8R191	Syngr3	Synaptogyrin-3 OS=Mus musculus OX=10090 GN=Syngr3 PE=1 SV=1	9.675763148	9.429677203	1
Q61743	Kcnj11	ATP-sensitive inward rectifier potassium channel 11 OS=Mus musculus OX=10090 GN=Kcnj11 PE=1 SV=1	8.551009518	8.692171699	1
Q9WV69	Dmtn	Dematin OS=Mus musculus OX=10090 GN=Dmtn PE=1 SV=1	10.19955733	9.047569612	1
Q9D032	Ssbp3	Single-stranded DNA-binding protein 3 OS=Mus musculus OX=10090 GN=Ssbp3 PE=1 SV=2	9.063874943	8.566752734	1
Q61885	Mog	Myelin-oligodendrocyte glycoprotein OS=Mus musculus OX=10090 GN=Mog PE=1 SV=1	7.74636301	7.481016329	1
Q60875	Arhgef2	Rho guanine nucleotide exchange factor 2 OS=Mus musculus OX=10090 GN=Arhgef2 PE=1 SV=4	8.822360378	8.605882887	1
P03975	Iap	IgE-binding protein OS=Mus musculus OX=10090 GN=Iap PE=2 SV=1	6.298278248	6.077745909	1
Q9QX11	Cyth1	Cytohesin-1 OS=Mus musculus OX=10090 GN=Cyth1 PE=1 SV=2	8.868795714	8.654734022	1
P60764	Rac3	Ras-related C3 botulinum toxin substrate 3 OS=Mus musculus OX=10090 GN=Rac3 PE=1 SV=1	8.779962864	7.993039782	1
Q9D819	Ppa1	Inorganic pyrophosphatase OS=Mus musculus OX=10090 GN=Ppa1 PE=1 SV=1	7.937204256	7.647051581	1
Q9CPW4	Arpc5	Actin-related protein 2/3 complex subunit 5 OS=Mus musculus OX=10090 GN=Arpc5 PE=1 SV=3	10.29516279	9.272721823	1
P10922	H1-0	Histone H1.0 OS=Mus musculus OX=10090 GN=H1-0 PE=2 SV=4	2.28896045	2.575090193	1
P56135	Atp5mf	ATP synthase subunit f, mitochondrial OS=Mus musculus OX=10090 GN=Atp5mf PE=1 SV=3	9.403678201	9.00124582	1
Q9R269	Ppl	Periplakin OS=Mus musculus OX=10090 GN=Ppl PE=1 SV=1	10.27160707	9.936136027	1

O55013	Trappc3	Trafficking protein particle complex subunit 3 OS=Mus musculus OX=10090 GN=Trappc3 PE=1 SV=1	8.702850329	8.821481376	1

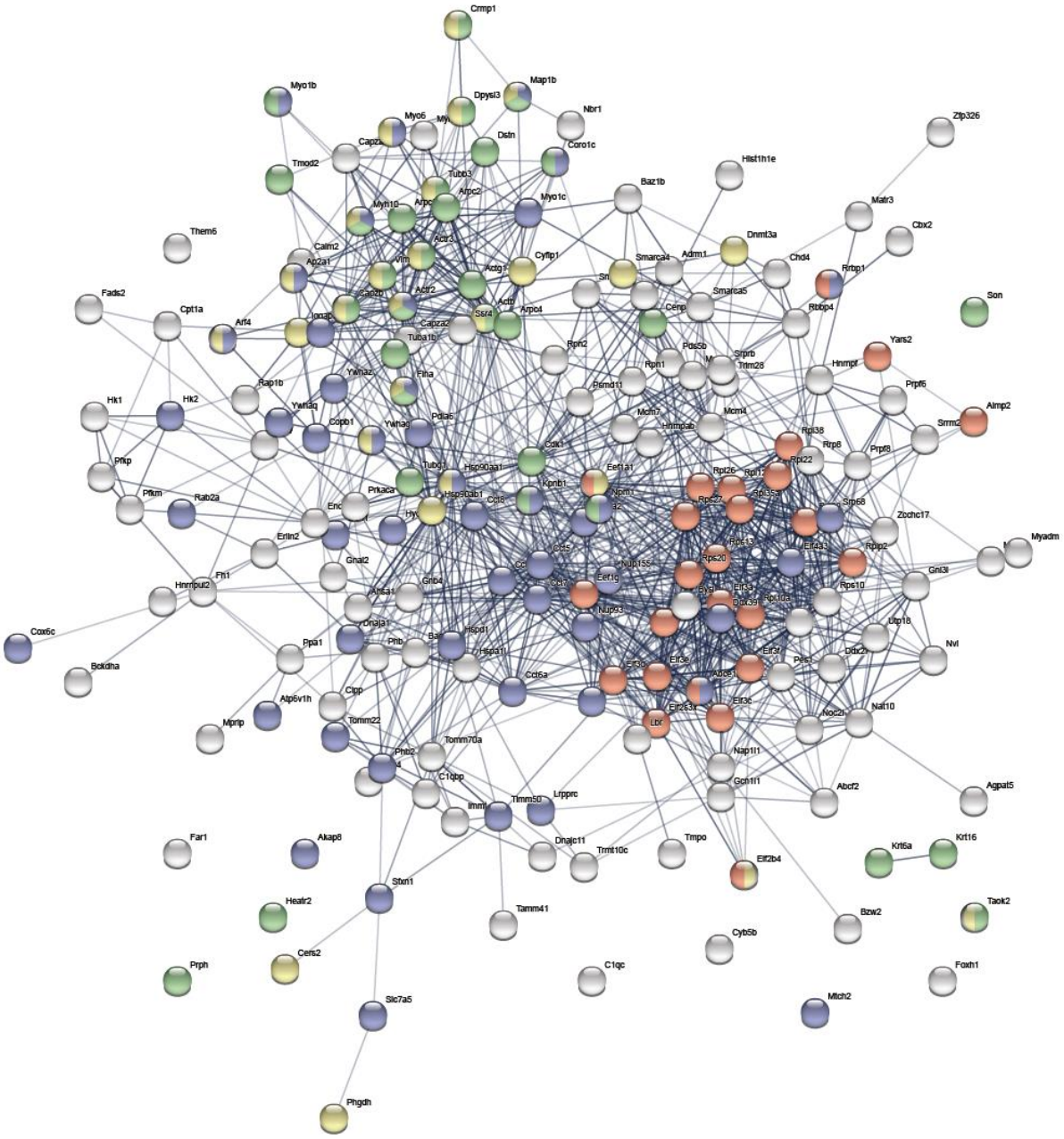

Supplementary Figure 2: Network graph from STRING analysis visualizes the 197 proteins that were immunoprecipitated by TAOK2-β antibody and identified by IP-MS in the N2a cells transfected with wild type TAOK2-β (CV) cutoff = 0.1).

The "confidence" link visualization was selected with a medium confidence interaction score (0.400). For details, (Supplementary Table 2).

Supplementary Table 2: list of the 197 enriched proteins from N2a cells overexpressed with wild type TAOK2β identified by IP coupled with LC-MS/MS analysis

using TAOK2β antibody. The enriched proteins from the 2 experiments are ordered in a descending depending on the number of unique peptides identified for each protein. The log2 values of the identified proteins from the 2 experiments separately were showed in their respective columns.

Uniprot Accession #	Gene name	Protein Name	log2 experiment 1	log2 experiment 2	# Peptides
Q61879	Myh10	Myosin-10 OS=Mus musculus OX=10090 GN=Myh10 PE=1 SV=2	5.151009429	4.886296047	119
Q6ZQ29-2	Taok2	Isoform 2 of Serine/threonine-protein kinase TAO2 OS=Mus musculus OX=10090 GN=Taok2	10.73040582	10.72942309	82
Q9JKF1	Iqgap1	Ras GTPase-activating-like protein IQGAP1 OS=Mus musculus OX=10090 GN=Iqgap1 PE=1 SV=2	3.714355261	3.757263671	42
P20152	Vim	Vimentin OS=Mus musculus OX=10090 GN=Vim PE=1 SV=3	6.24552837	5.493200446	37
P15331	Prph	Peripherin OS=Mus musculus OX=10090 GN=Prph PE=1 SV=2	6.0941751	6.726227403	32
P46735	Myo1b	Unconventional myosin-Ib OS=Mus musculus OX=10090 GN=Myo1b PE=1 SV=3	6.480237633	6.419708392	30
P11499	Hsp90ab1	Heat shock protein HSP 90-beta OS=Mus musculus OX=10090 GN=Hsp90ab1 PE=1 SV=3	5.544637012	6.211940779	28
P63260	Actg1	Actin, cytoplasmic 2 OS=Mus musculus OX=10090 GN=Actg1 PE=1 SV=1	12.14308095	11.12497273	23
P60710	Actb	Actin, cytoplasmic 1 OS=Mus musculus OX=10090 GN=Actb PE=1 SV=1	9.29323274	8.116083723	23
P05213	Tuba1b	Tubulin alpha-1B chain OS=Mus musculus OX=10090 GN=Tuba1b PE=1 SV=2	13.49143147	12.52531565	21
Q9ERD7	Tubb3	Tubulin beta-3 chain OS=Mus musculus OX=10090 GN=Tubb3 PE=1 SV=1	8.61942311	7.709378505	20
P17182	Eno1	Alpha-enolase OS=Mus musculus OX=10090 GN=Eno1 PE=1 SV=3	5.288645675	4.797811098	19
P10126	Eef1a1	Elongation factor 1-alpha 1 OS=Mus musculus OX=10090 GN=Eef1a1 PE=1 SV=3	6.026714595	5.428471161	18
P50446	Krt6a	Keratin, type II cytoskeletal 6A OS=Mus musculus OX=10090 GN=Krt6a PE=1 SV=3	1.248898983	1.156454738	18
P80318	Cct3	T-complex protein 1 subunit gamma OS=Mus musculus OX=10090 GN=Cct3 PE=1 SV=1	9.12692456	7.98340829	17
Q8CAQ8	Immt	MICOS complex subunit Mic60 OS=Mus musculus OX=10090 GN=Immt PE=1 SV=1	7.861208997	6.910107194	16
P17710	Hk1	Hexokinase-1 OS=Mus musculus OX=10090 GN=Hk1 PE=1 SV=3	4.895369015	5.54017374	16
Q62318	Trim28	Transcription intermediary factor 1-beta OS=Mus musculus OX=10090 GN=Trim28 PE=1 SV=3	9.698816228	8.697947072	15
E9PVA8	**Gcn1**	**eIF-2-alpha kinase activator GCN1 OS=Mus musculus OX=10090 GN=Gcn1 PE=1 SV=1**	**5.193400246**	**5.340738078**	**15**
P60843	Eif4a1	Eukaryotic initiation factor 4A-I OS=Mus musculus OX=10090 GN=Eif4a1 PE=1 SV=1	8.053995677	7.710484701	14

Q91ZW3	Smarca5	SWI/SNF-related matrix-associated actin-dependent regulator of chromatin subfamily A member 5 OS=Mus musculus OX=10090 GN=Smarca5 PE=1 SV=1	13.08115505	11.73114095	14
O35129	Phb2	Prohibitin-2 OS=Mus musculus OX=10090 GN=Phb2 PE=1 SV=1	6.282354401	5.70644796	14
Q3TKT4	Smarca4	Transcription activator BRG1 OS=Mus musculus OX=10090 GN=Smarca4 PE=1 SV=1	4.766433398	4.623227184	13
P47753	Capza1	F-actin-capping protein subunit alpha-1 OS=Mus musculus OX=10090 GN=Capza1 PE=1 SV=4	14.58111329	13.88336271	11
P67778	Phb	Prohibitin OS=Mus musculus OX=10090 GN=Phb PE=1 SV=1	5.892575848	5.217582088	11
P07901	Hsp90aa1	Heat shock protein HSP 90-alpha OS=Mus musculus OX=10090 GN=Hsp90aa1 PE=1 SV=4	9.296540279	8.700329751	11
Q8K310	Matr3	Matrin-3 OS=Mus musculus OX=10090 GN=Matr3 PE=1 SV=1	4.434590127	4.247214192	11
O08528	Hk2	Hexokinase-2 OS=Mus musculus OX=10090 GN=Hk2 PE=1 SV=1	5.744594521	5.486600664	11
Q01320	Top2a	DNA topoisomerase 2-alpha OS=Mus musculus OX=10090 GN=Top2a PE=1 SV=2	3.563672007	3.294489425	11
P47757	Capzb	F-actin-capping protein subunit beta OS=Mus musculus OX=10090 GN=Capzb PE=1 SV=3	8.494797702	7.745490183	10
P63038	Hspd1	60 kDa heat shock protein, mitochondrial OS=Mus musculus OX=10090 GN=Hspd1 PE=1 SV=1	4.59911468	4.909785486	10
P47754	Capza2	F-actin-capping protein subunit alpha-2 OS=Mus musculus OX=10090 GN=Capza2 PE=1 SV=3	13.28093809	13.05282176	10
Q91VC3	Eif4a3	Eukaryotic initiation factor 4A-III OS=Mus musculus OX=10090 GN=Eif4a3 PE=1 SV=3	6.189526849	6.658189084	10
Q8BTM8	Flna	Filamin-A OS=Mus musculus OX=10090 GN=Flna PE=1 SV=5	10.65832512	9.909773765	10
Q9Z2K1	Krt16	Keratin, type I cytoskeletal 16 OS=Mus musculus OX=10090 GN=Krt16 PE=1 SV=3	0.767720796	0.872141582	9
P62806	H4c1, H4c4, H4c6, H4c8, H4c9, H4f16, Hist1h4m	Histone H4 OS=Mus musculus OX=10090 GN=H4c1 PE=1 SV=2	2.359781996	2.463368155	8
P62301	Rps13	40S ribosomal protein S13 OS=Mus musculus OX=10090 GN=Rps13 PE=1 SV=2	6.156263881	5.345850897	8
Q61881	Mcm7	DNA replication licensing factor MCM7 OS=Mus musculus OX=10090 GN=Mcm7 PE=1 SV=1	11.49173761	10.75596216	8
P80317	Cct6a	T-complex protein 1 subunit zeta OS=Mus musculus OX=10090 GN=Cct6a PE=1 SV=3	12.84951784	11.91476678	8
Q3U9G9	Lbr	Delta(14)-sterol reductase LBR OS=Mus musculus OX=10090 GN=Lbr PE=1 SV=2	5.719621846	4.968866011	8
Q8K224	Nat10	RNA cytidine acetyltransferase OS=Mus musculus OX=10090 GN=Nat10 PE=1 SV=1	11.91006196	10.44672733	8
P14873	Map1b	Microtubule-associated protein 1B OS=Mus musculus OX=10090 GN=Map1b PE=1 SV=2	12.09134369	11.06289288	7
P97427	Crmp1	Dihydropyrimidinase-related protein 1 OS=Mus musculus OX=10090 GN=Crmp1 PE=1 SV=1	11.83142666	10.41630465	7

Q9ERK4	Cse1l	Exportin-2 OS=Mus musculus OX=10090 GN=Cse1l PE=1 SV=1	2.296697294	2.437509872	7
P43277	H1-3	Histone H1.3 OS=Mus musculus OX=10090 GN=H1-3 PE=1 SV=2	2.714818096	2.546865096	7
Q61753	Phgdh	D-3-phosphoglycerate dehydrogenase OS=Mus musculus OX=10090 GN=Phgdh PE=1 SV=3	10.77900793	10.29771838	7
Q9WTI7	Myo1c	Unconventional myosin-Ic OS=Mus musculus OX=10090 GN=Myo1c PE=1 SV=2	11.18501911	11.16111842	7
P97432	Nbr1	Next to BRCA1 gene 1 protein OS=Mus musculus OX=10090 GN=Nbr1 PE=1 SV=1	10.87172216	10.22239193	7
P43274	H1-4	Histone H1.4 OS=Mus musculus OX=10090 GN=H1-4 PE=1 SV=2	2.060649576	2.06221718	7
Q8VDW0	Ddx39a	ATP-dependent RNA helicase DDX39A OS=Mus musculus OX=10090 GN=Ddx39a PE=1 SV=1	11.85245984	11.08313891	7
P61255	Rpl26	60S ribosomal protein L26 OS=Mus musculus OX=10090 GN=Rpl26 PE=1 SV=1	5.459944504	5.383186815	7
Q9Z2X1	Hnrnpf	Heterogeneous nuclear ribonucleoprotein F OS=Mus musculus OX=10090 GN=Hnrnpf PE=1 SV=3	6.39387217	6.816557999	6
Q64475	H2bc3	Histone H2B type 1-B OS=Mus musculus OX=10090 GN=H2bc3 PE=1 SV=3	3.268044242	3.025534858	6
P56480	Atp5f1b	ATP synthase subunit beta, mitochondrial OS=Mus musculus OX=10090 GN=Atp5f1b PE=1 SV=2	12.36547163	11.48807149	6
Q9DBY8	Nvl	Nuclear valosin-containing protein-like OS=Mus musculus OX=10090 GN=Nvl PE=1 SV=1	11.06965967	9.987720677	6
Q9EQ61	Pes1	Pescadillo homolog OS=Mus musculus OX=10090 GN=Pes1 PE=1 SV=1	3.626805561	3.390752644	6
Q9Z0R9	Fads2	Acyl-CoA 6-desaturase OS=Mus musculus OX=10090 GN=Fads2 PE=1 SV=1	12.09622825	10.63131761	6
O88291	Znf326	DBIRD complex subunit ZNF326 OS=Mus musculus OX=10090 GN=Znf326 PE=1 SV=1	12.28585724	11.39501238	6
P35979	Rpl12	60S ribosomal protein L12 OS=Mus musculus OX=10090 GN=Rpl12 PE=1 SV=2	12.56845909	11.9688519	6
P42932	Cct8	T-complex protein 1 subunit theta OS=Mus musculus OX=10090 GN=Cct8 PE=1 SV=3	5.67164244	5.40430725	6
P0DP27	Calm2	Calmodulin-2 OS=Mus musculus OX=10090 GN=Calm2 PE=1 SV=1	13.60622638	13.53359822	5
Q99LE6	Abcf2	ATP-binding cassette sub-family F member 2 OS=Mus musculus OX=10090 GN=Abcf2 PE=1 SV=1	2.896020052	2.774155795	5
Q4VA53	Pds5b	Sister chromatid cohesion protein PDS5 homolog B OS=Mus musculus OX=10090 GN=Pds5b PE=1 SV=1	9.118045357	8.316161357	5
P63325	Rps10	40S ribosomal protein S10 OS=Mus musculus OX=10090 GN=Rps10 PE=1 SV=1	5.436019908	5.895114246	5
Q3THE2	Myl12b	Myosin regulatory light chain 12B OS=Mus musculus OX=10090 GN=Myl12b PE=1 SV=2	13.46935035	12.62778779	5
P16627	Hspa1l	Heat shock 70 kDa protein 1-like OS=Mus musculus OX=10090 GN=Hspa1l PE=1 SV=4	8.750578807	8.157719926	5

Q62188	Dpysl3	Dihydropyrimidinase-related protein 3 OS=Mus musculus OX=10090 GN=Dpysl3 PE=1 SV=1	10.06430287	8.807844596	5
Q61749	Eif2b4	Translation initiation factor eIF-2B subunit delta OS=Mus musculus OX=10090 GN=Eif2b4 PE=1 SV=2	12.7723324	11.70139182	5
P43276	H1-5	Histone H1.5 OS=Mus musculus OX=10090 GN=H1-5 PE=1 SV=2	3.103932583	2.948808493	5
Q99PL5	Rrbp1	Ribosome-binding protein 1 OS=Mus musculus OX=10090 GN=Rrbp1 PE=1 SV=2	10.15105154	9.326305286	5
P47758	Srprb	Signal recognition particle receptor subunit beta OS=Mus musculus OX=10090 GN=Srprb PE=1 SV=1	10.6524249	9.330155116	5
Q6PB66	Lrpprc	Leucine-rich PPR motif-containing protein, mitochondrial OS=Mus musculus OX=10090 GN=Lrpprc PE=1 SV=2	9.341190047	8.395126357	5
P67984	Rpl22	60S ribosomal protein L22 OS=Mus musculus OX=10090 GN=Rpl22 PE=1 SV=2	8.109193797	7.385480095	5
P11440	Cdk1	Cyclin-dependent kinase 1 OS=Mus musculus OX=10090 GN=Cdk1 PE=1 SV=3	12.05656743	11.3019643	5
P63323	Rps12	40S ribosomal protein S12 OS=Mus musculus OX=10090 GN=Rps12 PE=1 SV=2	7.062590834	6.151819903	5
Q8BYL4	Yars2	Tyrosine--tRNA ligase, mitochondrial OS=Mus musculus OX=10090 GN=Yars2 PE=1 SV=2	12.63970431	11.72184827	5
Q8BFZ9	Erlin2	Erlin-2 OS=Mus musculus OX=10090 GN=Erlin2 PE=1 SV=1	11.30478616	9.865068623	5
P60229	Eif3e	Eukaryotic translation initiation factor 3 subunit E OS=Mus musculus OX=10090 GN=Eif3e PE=1 SV=1	11.38999169	10.22543815	5
Q8BFU2	H2aw	Histone H2A type 3 OS=Mus musculus OX=10090 GN=H2aw PE=1 SV=3	2.417463905	2.300219293	4
Q99JR1	Sfxn1	Sideroflexin-1 OS=Mus musculus OX=10090 GN=Sfxn1 PE=1 SV=3	11.67908428	10.71499013	4
P59999	Arpc4	Actin-related protein 2/3 complex subunit 4 OS=Mus musculus OX=10090 GN=Arpc4 PE=1 SV=3	9.504238604	10.25531537	4
Q9D880	Timm50	Mitochondrial import inner membrane translocase subunit TIM50 OS=Mus musculus OX=10090 GN=Timm50 PE=1 SV=1	13.19736915	11.97406756	4
Q99JY9	Actr3	Actin-related protein 3 OS=Mus musculus OX=10090 GN=Actr3 PE=1 SV=3	11.33895581	10.26334851	4
P60867	Rps20	40S ribosomal protein S20 OS=Mus musculus OX=10090 GN=Rps20 PE=1 SV=1	6.448407842	6.368681625	4
P61222	Abce1	ATP-binding cassette sub-family E member 1 OS=Mus musculus OX=10090 GN=Abce1 PE=1 SV=1	2.843688727	2.997122132	4
Q9WUA3	Pfkp	ATP-dependent 6-phosphofructokinase, platelet type OS=Mus musculus OX=10090 GN=Pfkp PE=1 SV=1	9.51920881	8.390425028	4
O54825	Bysl	Bystin OS=Mus musculus OX=10090 GN=Bysl PE=1 SV=3	9.229909758	9.839889489	4
P80313	Cct7	T-complex protein 1 subunit eta OS=Mus musculus OX=10090 GN=Cct7 PE=1 SV=1	10.23200533	9.131739353	4
O70194	Eif3d	Eukaryotic translation initiation factor 3 subunit D OS=Mus musculus OX=10090 GN=Eif3d PE=1 SV=2	11.08141206	10.20691276	4

Q922J9	Far1	Fatty acyl-CoA reductase 1 OS=Mus musculus OX=10090 GN=Far1 PE=1 SV=1	12.02100977	10.91254219	4
P80316	Cct5	T-complex protein 1 subunit epsilon OS=Mus musculus OX=10090 GN=Cct5 PE=1 SV=1	10.36623282	9.031841933	4
P23116	Eif3a	Eukaryotic translation initiation factor 3 subunit A OS=Mus musculus OX=10090 GN=Eif3a PE=1 SV=5	9.103400515	9.023643688	4
Q9WV70	Noc2l	Nucleolar complex protein 2 homolog OS=Mus musculus OX=10090 GN=Noc2l PE=1 SV=2	10.25466649	9.67984822	4
Q99PV0	Prpf8	Pre-mRNA-processing-splicing factor 8 OS=Mus musculus OX=10090 GN=Prpf8 PE=1 SV=2	9.771712738	8.87831337	4
Q8BK64	Ahsa1	Activator of 90 kDa heat shock protein ATPase homolog 1 OS=Mus musculus OX=10090 GN=Ahsa1 PE=1 SV=2	10.95502905	10.24201478	4
Q9CQX2	Cyb5b	Cytochrome b5 type B OS=Mus musculus OX=10090 GN=Cyb5b PE=1 SV=1	9.642727322	10.17568937	3
P99027	Rplp2	60S acidic ribosomal protein P2 OS=Mus musculus OX=10090 GN=Rplp2 PE=1 SV=3	10.57225647	9.94311003	3
Q9JIF7	Copb1	Coatomer subunit beta OS=Mus musculus OX=10090 GN=Copb1 PE=1 SV=1	8.750527952	8.026778911	3
Q9Z0N1	Eif2s3x	Eukaryotic translation initiation factor 2 subunit 3, X-linked OS=Mus musculus OX=10090 GN=Eif2s3x PE=1 SV=2	9.382928461	8.438828045	3
P63101	Ywhaz	14-3-3 protein zeta/delta OS=Mus musculus OX=10090 GN=Ywhaz PE=1 SV=1	9.666394955	9.721718154	3
Q5SSI6	Utp18	U3 small nucleolar RNA-associated protein 18 homolog OS=Mus musculus OX=10090 GN=Utp18 PE=1 SV=1	9.192925055	8.434936881	3
P61750	Arf4	ADP-ribosylation factor 4 OS=Mus musculus OX=10090 GN=Arf4 PE=1 SV=2	11.86006345	11.23826501	3
Q91YR7	Prpf6	Pre-mRNA-processing factor 6 OS=Mus musculus OX=10090 GN=Prpf6 PE=1 SV=1	10.0693379	9.078695816	3
P97807	Fh	Fumarate hydratase, mitochondrial OS=Mus musculus OX=10090 GN=Fh PE=1 SV=3	9.50444084	8.840172502	3
Q8CI61	Bag4	BAG family molecular chaperone regulator 4 OS=Mus musculus OX=10090 GN=Bag4 PE=1 SV=2	10.71495288	10.18008634	3
Q91YN9	Bag2	BAG family molecular chaperone regulator 2 OS=Mus musculus OX=10090 GN=Bag2 PE=1 SV=1	10.34040754	9.128309837	3
Q922R8	Pdia6	Protein disulfide-isomerase A6 OS=Mus musculus OX=10090 GN=Pdia6 PE=1 SV=3	0.597940123	0.607753326	3
O35658	C1qbp	Complement component 1 Q subcomponent-binding protein, mitochondrial OS=Mus musculus OX=10090 GN=C1qbp PE=1 SV=1	10.35547282	9.517705517	3
Q9ESX4	Zcchc17	Nucleolar protein of 40 kDa OS=Mus musculus OX=10090 GN=Zcchc17 PE=1 SV=1	1.407415366	1.489855012	3
Q9DB20	Atp5po	ATP synthase subunit O, mitochondrial OS=Mus musculus OX=10090 GN=Atp5po PE=1 SV=1	12.35585598	11.02055859	3

Q6ZWU9	Rps27	40S ribosomal protein S27 OS=Mus musculus OX=10090 GN=Rps27 PE=1 SV=3	9.379212428	8.197924261	3
Q8BJ71	Nup93	Nuclear pore complex protein Nup93 OS=Mus musculus OX=10090 GN=Nup93 PE=1 SV=1	8.880661475	9.031165412	3
Q91YQ5	Rpn1	Dolichyl-diphosphooligosaccharide--protein glycosyltransferase subunit 1 OS=Mus musculus OX=10090 GN=Rpn1 PE=1 SV=1	10.12994705	9.19312556	3
Q9WUM4	Coro1c	Coronin-1C OS=Mus musculus OX=10090 GN=Coro1c PE=1 SV=2	9.798743209	9.114744001	3
P97742	Cpt1a	Carnitine O-palmitoyltransferase 1, liver isoform OS=Mus musculus OX=10090 GN=Cpt1a PE=1 SV=4	9.933874542	8.81609323	3
P53994	Rab2a	Ras-related protein Rab-2A OS=Mus musculus OX=10090 GN=Rab2a PE=1 SV=1	9.939226323	8.687131736	3
Q91V92	Acly	ATP-citrate synthase OS=Mus musculus OX=10090 GN=Acly PE=1 SV=1	2.216931794	2.259731788	3
Q99020	Hnrnpab	Heterogeneous nuclear ribonucleoprotein A/B OS=Mus musculus OX=10090 GN=Hnrnpab PE=1 SV=1	3.454175874	3.850331752	3
P63037	Dnaja1	DnaJ homolog subfamily A member 1 OS=Mus musculus OX=10090 GN=Dnaja1 PE=1 SV=1	10.21999797	9.266747694	3
Q61937	Npm1	Nucleophosmin OS=Mus musculus OX=10090 GN=Npm1 PE=1 SV=1	10.94994971	10.13536708	3
Q8CG48	Smc2	Structural maintenance of chromosomes protein 2 OS=Mus musculus OX=10090 GN=Smc2 PE=1 SV=2	7.258276034	7.292785568	3
Q9D819	Ppa1	Inorganic pyrophosphatase OS=Mus musculus OX=10090 GN=Ppa1 PE=1 SV=1	11.55525968	10.70257728	3
Q9JKR6	Hyou1	Hypoxia up-regulated protein 1 OS=Mus musculus OX=10090 GN=Hyou1 PE=1 SV=1	9.380590533	8.612736746	3
P97434	Mprip	Myosin phosphatase Rho-interacting protein OS=Mus musculus OX=10090 GN=Mprip PE=1 SV=2	8.868457009	7.973158163	3
P17426	Ap2a1	AP-2 complex subunit alpha-1 OS=Mus musculus OX=10090 GN=Ap2a1 PE=1 SV=1	9.80621939	8.63934783	3
P97311	Mcm6	DNA replication licensing factor MCM6 OS=Mus musculus OX=10090 GN=Mcm6 PE=1 SV=1	8.874275562	8.557747998	3
Q921N6	Ddx27	Probable ATP-dependent RNA helicase DDX27 OS=Mus musculus OX=10090 GN=Ddx27 PE=1 SV=3	9.045288694	7.887611185	3
Q9JJI8	Rpl38	60S ribosomal protein L38 OS=Mus musculus OX=10090 GN=Rpl38 PE=1 SV=3	12.50178971	11.11227337	2
Q9CPQ3	Tomm22	Mitochondrial import receptor subunit TOM22 homolog OS=Mus musculus OX=10090 GN=Tomm22 PE=1 SV=3	10.3883897	9.614068269	2
Q9DBG6	Rpn2	Dolichyl-diphosphooligosaccharide--protein glycosyltransferase subunit 2 OS=Mus musculus OX=10090 GN=Rpn2 PE=1 SV=1	8.682552205	8.16306457	2
Q8R010	Aimp2	Aminoacyl tRNA synthase complex-interacting multifunctional protein 2 OS=Mus musculus OX=10090 GN=Aimp2 PE=1 SV=2	10.55985685	9.560519721	2

Q05920	Pc	Pyruvate carboxylase, mitochondrial OS=Mus musculus OX=10090 GN=Pc PE=1 SV=1	8.261131224	7.402860228	2
Q8BTI8	Srrm2	Serine/arginine repetitive matrix protein 2 OS=Mus musculus OX=10090 GN=Srrm2 PE=1 SV=3	7.135871925	7.514176956	2
Q60972	Rbbp4	Histone-binding protein RBBP4 OS=Mus musculus OX=10090 GN=Rbbp4 PE=1 SV=5	4.024955328	3.941177603	2
Q61029	Tmpo	Lamina-associated polypeptide 2, isoforms beta/delta/epsilon/gamma OS=Mus musculus OX=10090 GN=Tmpo PE=1 SV=4	8.875132975	8.416743933	2
Q8R1B4	Eif3c	Eukaryotic translation initiation factor 3 subunit C OS=Mus musculus OX=10090 GN=Eif3c PE=1 SV=1	9.296010033	8.804266545	2
B9EJR8	Dnaaf5	Dynein assembly factor 5, axonemal OS=Mus musculus OX=10090 GN=Dnaaf5 PE=1 SV=1	7.292696556	6.619289968	2
P47857	Pfkm	ATP-dependent 6-phosphofructokinase, muscle type OS=Mus musculus OX=10090 GN=Pfkm PE=1 SV=3	9.008041983	8.529748423	2
P08752	Gnai2	Guanine nucleotide-binding protein G(i) subunit alpha-2 OS=Mus musculus OX=10090 GN=Gnai2 PE=1 SV=5	7.532949774	7.1325002	2
Q8BVE3	Atp6v1h	V-type proton ATPase subunit H OS=Mus musculus OX=10090 GN=Atp6v1h PE=1 SV=1	9.777671021	8.591217774	2
Q00PI9	Hnrnpul2	Heterogeneous nuclear ribonucleoprotein U-like protein 2 OS=Mus musculus OX=10090 GN=Hnrnpul2 PE=1 SV=2	9.152122767	8.9274023	2
Q3TUH1	Tamm41	Phosphatidate cytidylyltransferase, mitochondrial OS=Mus musculus OX=10090 GN=Tamm41 PE=1 SV=2	9.712742662	9.324504432	2
Q9DBR0	Akap8	A-kinase anchor protein 8 OS=Mus musculus OX=10090 GN=Akap8 PE=1 SV=1	8.299842295	8.406397066	2
Q5U458	Dnajc11	DnaJ homolog subfamily C member 11 OS=Mus musculus OX=10090 GN=Dnajc11 PE=1 SV=2	9.545402815	8.897735291	2
Q9D8N0	Eef1g	Elongation factor 1-gamma OS=Mus musculus OX=10090 GN=Eef1g PE=1 SV=3	4.904342545	4.499734271	2
Q64331	Myo6	Unconventional myosin-VI OS=Mus musculus OX=10090 GN=Myo6 PE=1 SV=1	8.29900408	8.275000697	2
Q99P88	Nup155	Nuclear pore complex protein Nup155 OS=Mus musculus OX=10090 GN=Nup155 PE=1 SV=1	7.77619676	7.190827496	2
Q91VK1	Bzw2	Basic leucine zipper and W2 domain-containing protein 2 OS=Mus musculus OX=10090 GN=Bzw2 PE=1 SV=1	10.02022496	9.377520014	2
P28656	Nap1l1	Nucleosome assembly protein 1-like 1 OS=Mus musculus OX=10090 GN=Nap1l1 PE=1 SV=2	9.197149488	9.023629497	2
Q9Z277	Baz1b	Tyrosine-protein kinase BAZ1B OS=Mus musculus OX=10090 GN=Baz1b PE=1 SV=2	9.452341517	8.540827934	2
Q9JKK7	Tmod2	Tropomodulin-2 OS=Mus musculus OX=10090 GN=Tmod2 PE=1 SV=2	9.742037792	9.434605959	2

P56135	Atp5mf	ATP synthase subunit f, mitochondrial OS=Mus musculus OX=10090 GN=Atp5mf PE=1 SV=3	6.4230947	5.619781823	2
Q9CPW4	Arpc5	Actin-related protein 2/3 complex subunit 5 OS=Mus musculus OX=10090 GN=Arpc5 PE=1 SV=3	9.476369588	9.467414751	2
P05132	Prkaca	cAMP-dependent protein kinase catalytic subunit alpha OS=Mus musculus OX=10090 GN=Prkaca PE=1 SV=3	9.611939459	8.476227049	2
Q9QX47	Son	Protein SON OS=Mus musculus OX=10090 GN=Son PE=1 SV=2	7.5710412	7.031104315	2
Q8BG32	Psmd11	26S proteasome non-ATPase regulatory subunit 11 OS=Mus musculus OX=10090 GN=Psmd11 PE=1 SV=3	9.562013271	8.958572893	2
Q02105	C1qc	Complement C1q subcomponent subunit C OS=Mus musculus OX=10090 GN=C1qc PE=1 SV=2	10.95621154	11.09377728	2
Q9CVB6	Arpc2	Actin-related protein 2/3 complex subunit 2 OS=Mus musculus OX=10090 GN=Arpc2 PE=1 SV=3	9.990886377	8.942534282	2
Q9CZW5	Tomm70	Mitochondrial import receptor subunit TOM70 OS=Mus musculus OX=10090 GN=Tomm70 PE=1 SV=2	9.325153427	8.647909227	2
Q6PGG6	Gnl3l	Guanine nucleotide-binding protein-like 3-like protein OS=Mus musculus OX=10090 GN=Gnl3l PE=1 SV=1	8.341695805	7.603201173	2
Q924Z4	Cers2	Ceramide synthase 2 OS=Mus musculus OX=10090 GN=Cers2 PE=1 SV=1	9.025137027	8.112740788	2
Q791V5	Mtch2	Mitochondrial carrier homolog 2 OS=Mus musculus OX=10090 GN=Mtch2 PE=1 SV=1	9.680263685	8.779495594	2
Q80ZW2	Them6	Protein THEM6 OS=Mus musculus OX=10090 GN=Them6 PE=1 SV=1	8.28462433	7.658370148	2
P29387	Gnb4	Guanine nucleotide-binding protein subunit beta-4 OS=Mus musculus OX=10090 GN=Gnb4 PE=1 SV=4	4.124312171	4.398376971	2
P49717	Mcm4	DNA replication licensing factor MCM4 OS=Mus musculus OX=10090 GN=Mcm4 PE=1 SV=1	8.519856134	8.25717402	2
O55142	Rpl35a	60S ribosomal protein L35a OS=Mus musculus OX=10090 GN=Rpl35a PE=1 SV=2	3.697111783	3.253919576	2
P53026	Rpl10a	60S ribosomal protein L10a OS=Mus musculus OX=10090 GN=Rpl10a PE=1 SV=3	10.71440584	10.29271446	2
Q8C854	Myef2	Myelin expression factor 2 OS=Mus musculus OX=10090 GN=Myef2 PE=1 SV=1	9.00205197	8.051149725	1
Q6PDQ2	Chd4	Chromodomain-helicase-DNA-binding protein 4 OS=Mus musculus OX=10090 GN=Chd4 PE=1 SV=1	4.404162914	4.043781272	1
Q8BMA6	Srp68	Signal recognition particle subunit SRP68 OS=Mus musculus OX=10090 GN=Srp68 PE=1 SV=2	8.446678217	7.332560275	1
Q3UFY8	Trmt10c	tRNA methyltransferase 10 homolog C OS=Mus musculus OX=10090 GN=Trmt10c PE=1 SV=2	8.711829003	7.810437389	1
O35682	Myadm	Myeloid-associated differentiation marker OS=Mus musculus OX=10090 GN=Myadm PE=1 SV=2	8.070933444	8.017805278	1
P61982	Ywhag	14-3-3 protein gamma OS=Mus musculus OX=10090 GN=Ywhag PE=1 SV=2	7.025895861	7.446516307	1

O88696	Clpp	ATP-dependent Clp protease proteolytic subunit, mitochondrial OS=Mus musculus OX=10090 GN=Clpp PE=1 SV=1	9.732827093	8.643607303	1
P68254	Ywhaq	14-3-3 protein theta OS=Mus musculus OX=10090 GN=Ywhaq PE=1 SV=1	8.977680571	8.222803156	1
Q62186	Ssr4	Translocon-associated protein subunit delta OS=Mus musculus OX=10090 GN=Ssr4 PE=1 SV=1	10.49152738	9.137851856	1
P62892	Rpl39	60S ribosomal protein L39 OS=Mus musculus OX=10090 GN=Rpl39 PE=1 SV=2	1.581386352	1.419670736	1
Q9DCH4	Eif3f	Eukaryotic translation initiation factor 3 subunit F OS=Mus musculus OX=10090 GN=Eif3f PE=1 SV=2	7.91890972	7.930895034	1
E9Q414	Apob	Apolipoprotein B-100 OS=Mus musculus OX=10090 GN=Apob PE=1 SV=1	8.059531122	8.38677912	1
Q9DB85	Rrp8	Ribosomal RNA-processing protein 8 OS=Mus musculus OX=10090 GN=Rrp8 PE=1 SV=1	7.352839946	6.797316289	1
Q9R0P5	Dstn	Destrin OS=Mus musculus OX=10090 GN=Dstn PE=1 SV=3	10.02251885	8.725203453	1
Q06185	Atp5me	ATP synthase subunit e, mitochondrial OS=Mus musculus OX=10090 GN=Atp5me PE=1 SV=2	9.737729476	8.669425654	1
O35216	Cenpa	Histone H3-like centromeric protein A OS=Mus musculus OX=10090 GN=Cenpa PE=2 SV=1	5.774558862	5.870749815	1
Q9Z127	Slc7a5	Large neutral amino acids transporter small subunit 1 OS=Mus musculus OX=10090 GN=Slc7a5 PE=1 SV=2	9.455372031	8.67217486	1
P52293	Kpna2	Importin subunit alpha-1 OS=Mus musculus OX=10090 GN=Kpna2 PE=1 SV=2	8.785734018	8.091747056	1
P61161	Actr2	Actin-related protein 2 OS=Mus musculus OX=10090 GN=Actr2 PE=1 SV=1	8.84707446	8.539087324	1
P50136	Bckdha	2-oxoisovalerate dehydrogenase subunit alpha, mitochondrial OS=Mus musculus OX=10090 GN=Bckdha PE=1 SV=1	5.162983005	5.197038022	1
P01872	Ighm	Immunoglobulin heavy constant mu OS=Mus musculus OX=10090 GN=Ighm PE=1 SV=2	12.28100476	12.21673002	1
P70168	Kpnb1	Importin subunit beta-1 OS=Mus musculus OX=10090 GN=Kpnb1 PE=1 SV=2	8.290886477	7.558121482	1
Q99JI6	Rap1b	Ras-related protein Rap-1b OS=Mus musculus OX=10090 GN=Rap1b PE=1 SV=2	7.995144594	7.845177996	1
P83887	Tubg1	Tubulin gamma-1 chain OS=Mus musculus OX=10090 GN=Tubg1 PE=1 SV=1	9.833010988	8.74834745	1
Q9D1E8	Agpat5	1-acyl-sn-glycerol-3-phosphate acyltransferase epsilon OS=Mus musculus OX=10090 GN=Agpat5 PE=1 SV=2	7.561180946	7.500436368	1
Q9JKV1	Adrm1	Proteasomal ubiquitin receptor ADRM1 OS=Mus musculus OX=10090 GN=Adrm1 PE=1 SV=2	8.093108029	7.717183774	1
Q7TMB8	Cyfip1	Cytoplasmic FMR1-interacting protein 1 OS=Mus musculus OX=10090 GN=Cyfip1 PE=1 SV=1	8.053728552	7.041019399	1

Q99J56	Derl1	Derlin-1 OS=Mus musculus OX=10090 GN=Derl1 PE=1 SV=1	9.16395657	8.558775926	1
Q9CPQ1	Cox6c	Cytochrome c oxidase subunit 6C OS=Mus musculus OX=10090 GN=Cox6c PE=1 SV=3	7.522306744	7.475009268	1
Q9CQQ7	Atp5pb	ATP synthase F(0) complex subunit B1, mitochondrial OS=Mus musculus OX=10090 GN=Atp5pb PE=1 SV=1	10.89938984	9.901975177	1

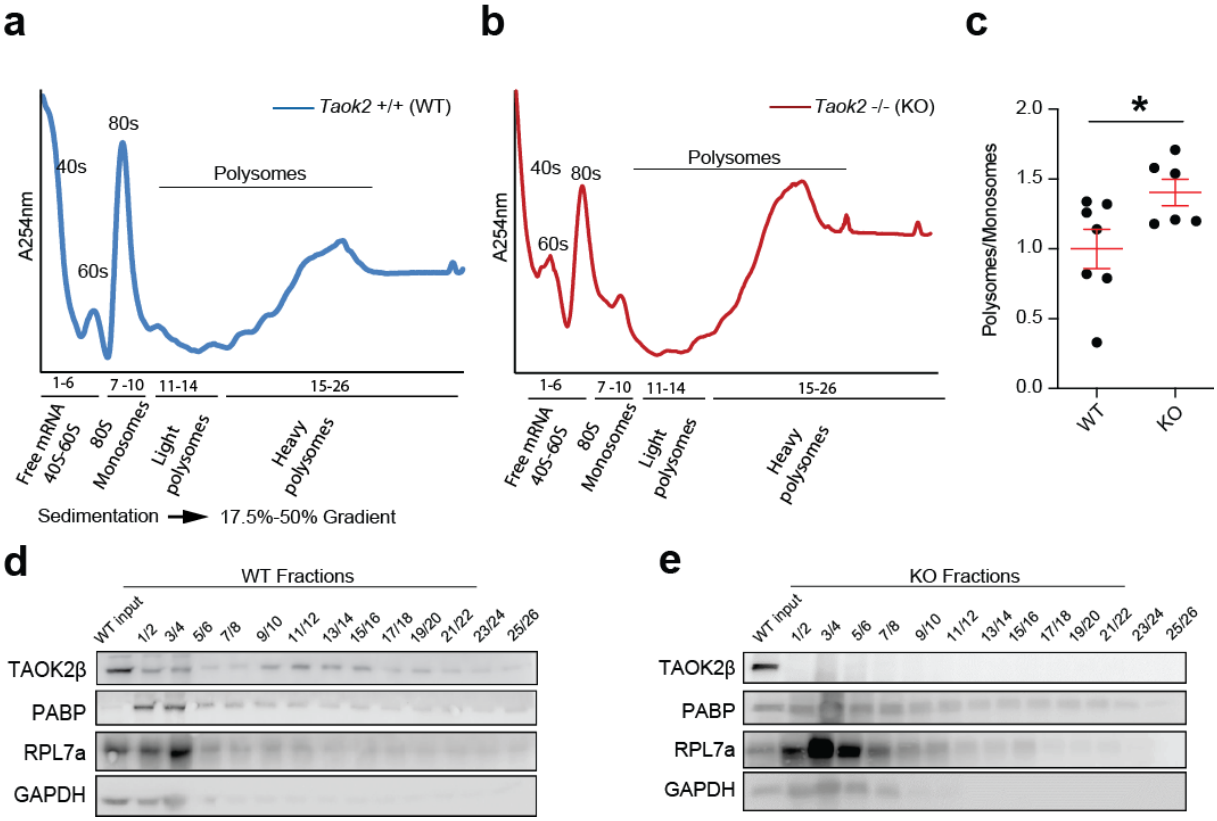

Supplementary Figure 3: TAOK2 associates with the cytoplasmic polyribosome complex in wild type mouse cerebellum and its deficiency enhance general translation.

(a) and **(b)** Representative polysome profiles for cerebella of 4 weeks old *TAOK2* $^{+/+}$ and *TAOK2* $^{d/d}$ mice respectively, fractionated on 17.5% –50% sucrose gradient shows an increase in polysome-to-monosome (p/m) ratio in the profiles of TAOK2 $^{d/d}$ mice.

(c) Quantifications of normalized p/m ratio for polysomes profiles of *TAOK2* $^{+/+}$ and *TAOK2* $^{d/d}$ mice cerebella, shows a statistically significant increase in the P/M ratio in the profiles from *TAOK2* $^{d/d}$ mice. Number of animals, *TAOK2* $^{+/+}$ n=7, *TAOK2* $^{d/d}$ n=6; SEM. error bars, *P < 0.05, unpaired t-test.

(d) and **(e)** Immunoblots of the cerebellar polysomes fractions pooled as in the scheme, showing the presence of TAOK2β across all fractions from polysomes of the *TAOK2* $^{+/+}$ (d) and its absence in the *TAOK2* $^{d/d}$ (e). PABP1 and RPL7a were used as positive controls and GAPDH as a negative control to prove the efficiency of polysomes preparation across the gradient. Input from WT cortex was loaded before the polysomes fractions to verify the specificity of the TAOK2β antibody.

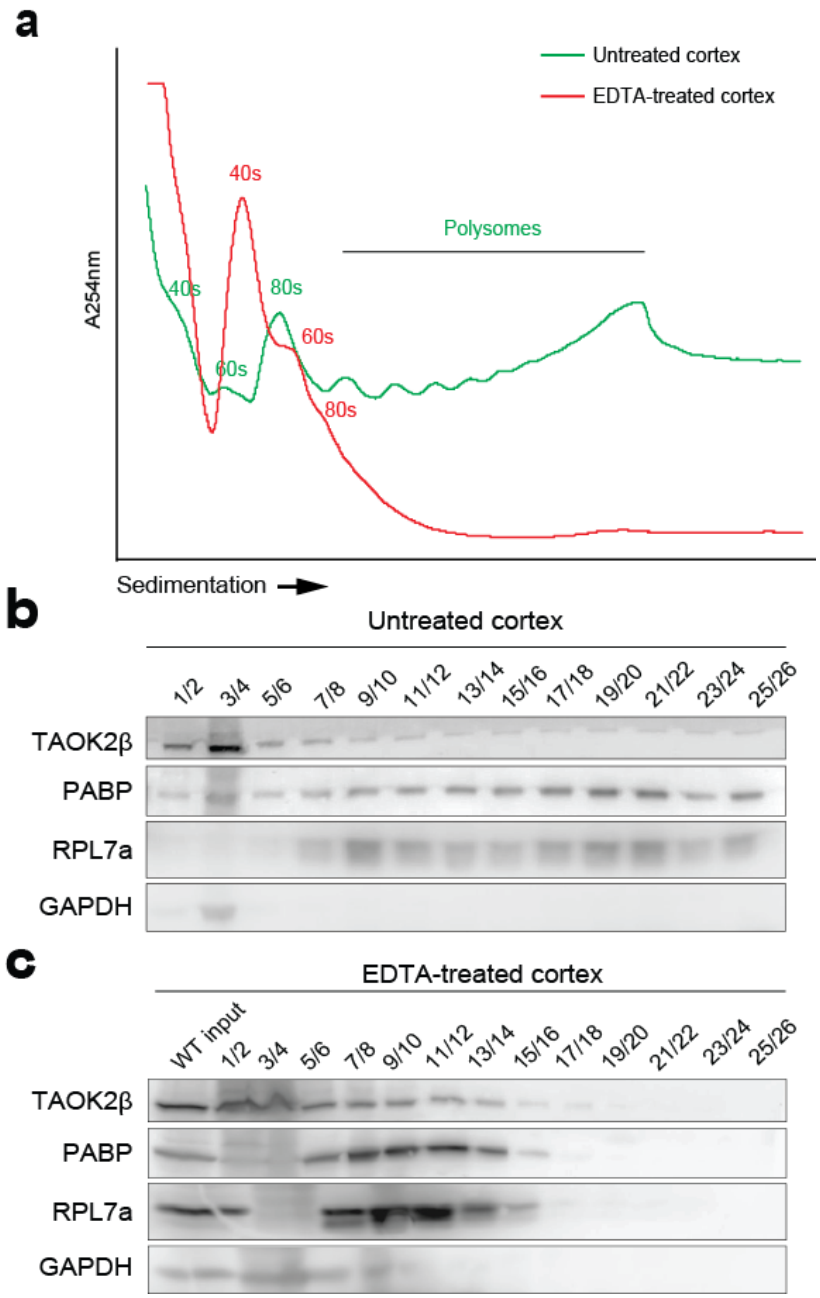

Supplementary Figure 4: TAOK2 associates with the actively translating polyribosome complex.

(a) Representative polysome profiles of cortical *TAOK2* $^{+/+}$ lysate under normal basal conditions or after EDTA treatment to disrupt polysomes, fractionated on 17.5% – 50% sucrose gradients and subjected to polysome profiling. In the EDTA treated profile, the EDTA dissociated the ribosomes leading to the disappearance of polysomes peaks and increase in peaks of monosomes, and the ribosomal subunits 40S and 60S.

(b) and **(c)** Immunoblots against the indicated antibodies from the indicated pooled fractions aligned with the corresponding profile gradient. Note the presence of TAOK2β with PAPB and RPL7a (house-keeping proteins in the cytoplasmic ribosomal complex) across all heavier polysomes fractions from the untreated cortex. In the EDTA-treated fractions, the distribution of PABP1, RPL7a, and TAOK2β signals are not detected in the deeper polysomes fractions and instead accumulate in the unbound and monosome fractions. TAOK2β with PABP1 and RPL7a show the same distribution pattern with an overall shift toward lighter fractions of the gradient, which confirm the presence of TAOK2β in the cytoplasmic ribosomal complex. GAPDH was used as a negative control.

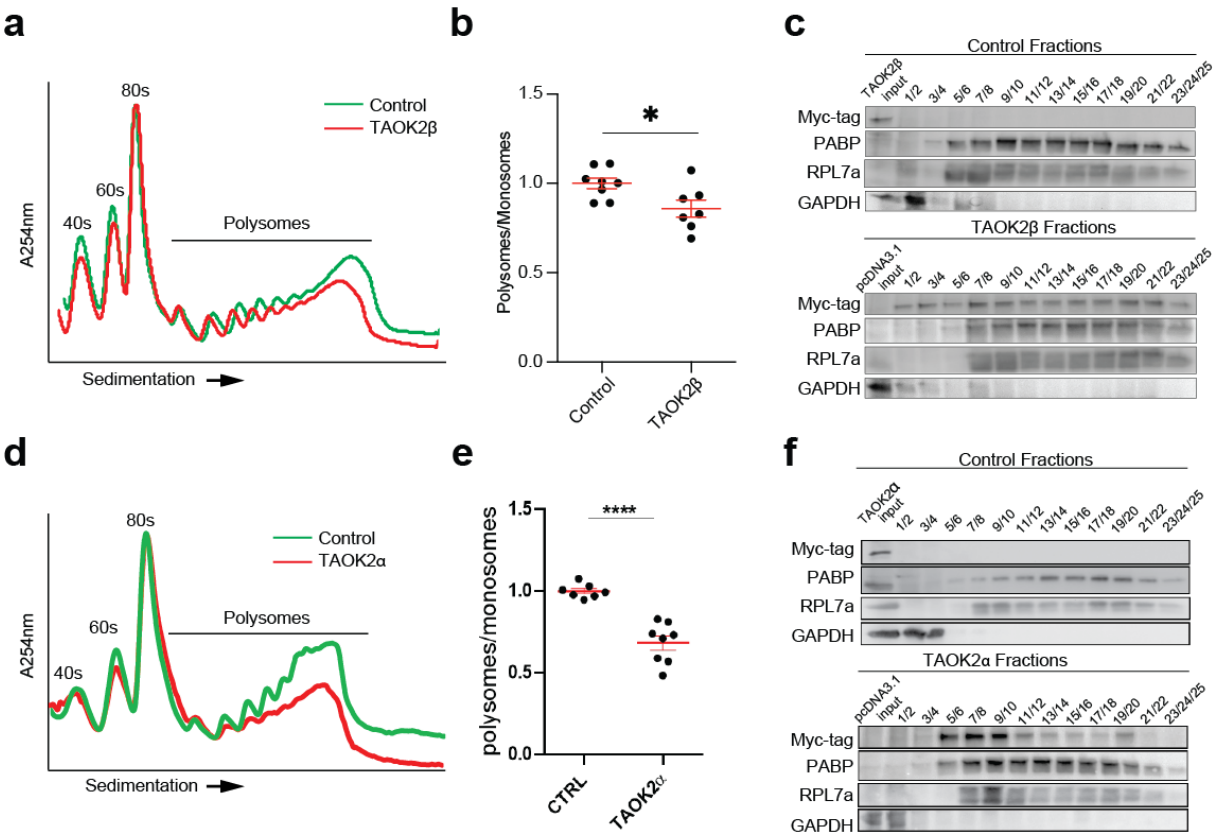

Supplementary Figure 5: Overexpression TAOK2 isoforms β or α in N2a cells suppresses the cellular general translation.

(a) Overlay of representative polysome profiles of transiently transfected (48h post-transfection) with wild type TAOK2β or empty vector control plasmids. pcDNA3.1-myc-tag.

(b) Quantifications of the normalized P/M ratios of polysome profiles from different independent transfection experiments reveal a statistically significant decrease of the P/M ratio in profiles from wild type TAOK2β overexpressed cells compared to the ones from the control cells. The number of biological replicates, wild type TAOK2β transfected cells n= 7, control n= 8, SEM. error bars, *P < 0.05, unpaired t-test.

(c) Immunoblots for the pooled gradient polysomes fractions representing the corresponding profile gradient against the presented antibodies for N2a cells transfected with wild type TAOK2β or control plasmids. Note the clear signal of Myc-tag antibody against the Myc-tag polypeptide protein in the pCMVhuTAOK2β-myc tag isoform in the all fractions of polysomes after wild type TAOK2β isoform overexpression (lower), while there is no Myc-tag signal detected across the fractions of polysome profile from the control cells (upper). PABP1 and RPl7a were used as house-keeping proteins in the cytoplasmic ribosomal complex and GAPDH as a negative control across polysome profile fractions across the gradient. Input from the total cytoplasmic lysate, either from the TAOK2β isoform transfected cells or the control cells was loaded at the beginning of the blot to verify the specificity of the antibody and the transfection efficiency.

(d) Overlay of representative polysome profiles of N2a cells transiently transfected (48h post-transfection) with wild type TAOK2α or control plasmids.

(e) Quantifications of the normalized P/M ratios of polysome profiles from different independent transfection experiments reveal a statistically significant decrease of P/M ratio in profiles from wild type TAOK2α overexpressed cells

compared to the ones from the control cells. The number of biological replicates, wild type TAOK2α transfected cells n= 8, control n= 7, SEM. error bars, **** p < 0.0001, unpaired t-test.

(f) Immunoblots for the pooled gradient polysomes fractions representing the corresponding profile gradient against the presented antibodies for N2a cells transiently transfected with wild type TAOK2α or control plasmids. Note the presence signal of Myc-tag antibody against the Myc-tag polypeptide protein in the pCMVhuTAOK2α-myc tag isoform in most fractions of polysomes after wild type TAOK2α isoform overexpression (lower), while there is no Myc-tag signal detected across the fractions of polysome profile from the control cells (upper). PABP1 and RPl7a were used as house-keeping proteins in the cytoplasmic ribosomal complex and GAPDH as a negative control across polysome profile fractions across the gradient. Input from the total cytoplasmic lysate, either from the TAOK2α isoform transfected cells or the control cells was loaded at the beginning of the blot to verify the specificity of the antibody and the transfection efficiency.

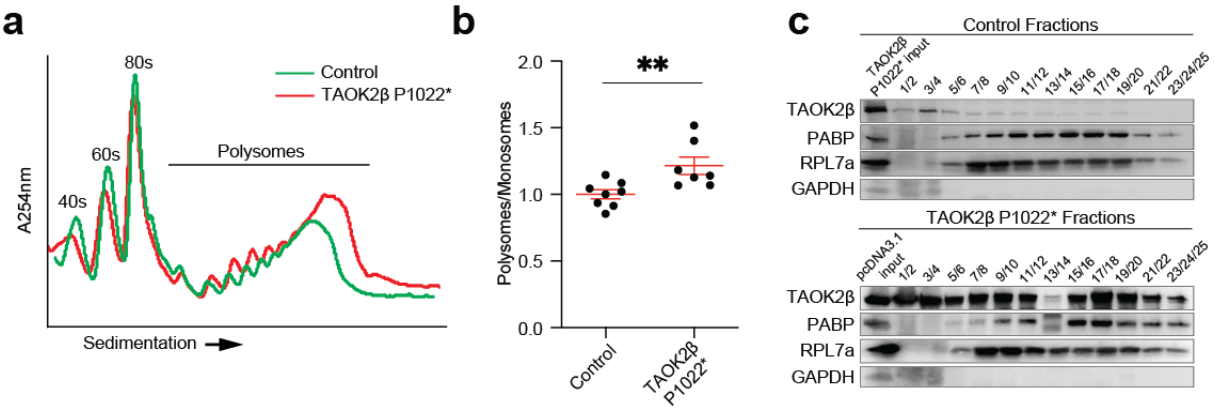

Supplementary Figure 6: TAOK2β mutations P1022* enhances general translation.

(a) Overlay of representative polysome profiles of N2a cells transiently transfected (48h post-transfection) with TAOK2βP1022* or empty vector control plasmids.

(b) Quantifications of the normalized P/M ratios of polysome profiles from different independent transfection experiments reveal a statistically significant increase of P/M ratio in profiles from TAOK2βP1022* transfected cells compared to the ones from the control cells. The number of biological replicates, TAOK2βP1022* transfected cells n= 7, control n= 8; SEM. error bars, **P < 0.01, unpaired t-test.

(c) Immunoblots for the pooled gradient polysomes fractions representing the corresponding profile gradient against the presented antibodies for N2a cells transiently transfected with TAOK2β-P1022* or control plasmids. Note the clear presence of TAOK2β (driven by pCMVhuTAOK2β-P1022* overexpression) in polysomes compared to the less detected endogenous TAOK2β in polysomes of control cells. PABP1 and RPl7a were used as house-keeping proteins in the cytoplasmic ribosomal complex and GAPDH as a negative control across polysome profile fractions. Input from the total cytoplasmic lysate, either from the TAOK2β-P1022* transfected cells or the control cells was loaded at the beginning of the blot to verify the specificity of the antibody and the transfection efficiency.

Supplementary Table 3: TAOK2 isoforms in polysomes from *TAOK2* $^{+/+}$ cortex identified by LC-MS analysis.

Proteins Unique Sequence ID	-7.1E+18	9E+18
Checked	TRUE	TRUE
Accession	Q6ZQ29	Q6ZQ29-2

Protein Name	Serine/threonine - protein kinase TAO2 OS=Mus musculus OX=10090 GN=Taok2 PE=1 SV=3 **(TAOK2 α isoform)**	Isoform 2 of Serine/threonine-protein kinase TAO2 OS=Mus musculus OX=10090 GN=Taok2 **(TAOK2 β isoform)**
# Peptides	6	10
# PSMs	12	21
# Unique Peptides	4	8
MW [kDa]	139.2	119.9
Score Sequest HT: Sequest HT	33.13	62.92
Abundance: Cortex-1	49311054	72746653
Abundance: Cortex-2	11276796	32734750
Abundance: Cortex-3	53828327	79178135
Abundance: Cortex-4	15039645	31026162

Supplementary Table 4: List of the significantly upregulated proteins in the PFC of *TAOK2* $^{d/d}$ mice from the differential expression protein analysis. The values are shown with protein intensity difference and the log2 (P value) as in the columns. The blue color highlights the proteins with translation function.

Protein IDs	**Gene names**	**Protein names**	**Difference**	**- LOG (P-value)**	**Peptides**
A0A0U1RPI0;A0A0U1RPJ7;D6RI64;D3YVR9;Q9R0P4	1110004F10Rik;Smap	Small acidic protein	-0.49801	3.939593	1
A0A338P6L5;Q8K268;A0A338P774	Abcf3	ATP-binding cassette sub-family F member 3	-0.86294	3.976373	2
Q99PT1	Arhgdia	Rho GDP-dissociation inhibitor 1	-0.26566	3.896775	15
P45591;A0A1Y7VJ71	Cfl2	Cofilin-2	-0.50544	7.355158	11
P60824;K4DI65;D3YU80	Cirbp	Cold-inducible RNA-binding protein	-0.5976	4.613841	7
E0CXH4;A0A2I3BPJ4;Q8R1G2;E0CXT6	Cmbl	Carboxymethylenebutenolidase homolog	-0.46519	3.916539	2
Q9WUM3;A0A494B9Y4;A0A494BAI1;D3YUG6	Coro1b	Coronin-1B	-0.19208	5.622938	12

A0A0J9YUM4;A0A0J9YU62;O88712;A0A0J9YTW3;A0A0J9YUR5;A0A0J9YU66;A0A0J9YVI3;E9Q0T4	Ctbp1	C-terminal-binding protein 1	-0.20094	4.622307	10
Q9JLV5;E9Q4T8;F6UY44;F6ZZK0	Cul3	Cullin-3	-0.24951	3.600556	12
Q91YW3	Dnajc3	DnaJ homolog subfamily C member 3	-0.46341	3.125777	3
Q8BZ98;E9QLL2;F2Z460;E0CXZ8	Dnm3	Dynamin-3	-0.32695	5.415404	23
A0A1Y7VLY2;P59764	Dock4	Dedicator of cytokinesis protein 4	-0.36883	2.339841	5
Q8BHA3	Dtd2	Probable D-tyrosyl-tRNA(Tyr) deacylase 2	-0.32432	3.268549	2
Q80UE5;O70318;Q80UE4;Q8C928;A0A1W2P6I5;A0A1W2P7I2;A0A1W2P6H2;A0A1W2P7I4;A0A1W2P896;A0A1W2P7H7;A0A1W2P8C0	Epb4.1l2;Epb41l2	Band 4.1-like protein 2	-0.38184	2.782093	23
A2BDQ4;Q61772;G1K381;Q03145;Q62413	Epha7	Receptor protein-tyrosine kinase;Ephrin type-A receptor 7	-0.98835	9.617365	5
P54763	Ephb2	Ephrin type-B receptor 2	-0.32078	2.918805	5
Q6P5B5;Q9WVR4	Fxr2	Fragile X mental retardation syndrome-related protein 2	-0.49849	5.041863	3
P63213	Gng2	Guanine nucleotide-binding protein G(I)/G(S)/G(O) subunit gamma-2	-0.42095	3.91404	7
Z4YJU8;A0A6I8MWY5;E9PUQ5;A0A6I8MX07;Q	Golga2	Golgin subfamily A member 2	-0.2243	4.97995	7

921M4;A2AN46;A2AN48;A2AN45					
Q60631;B1AT92;B1AT95	Grb2	Growth factor receptor-bound protein 2	-0.18459	5.28051	9
Q14BI2;A0A0J9YVF0;A0A0J9YU95	Grm2	Metabotropic glutamate receptor 2	-0.56213	3.386644	5
Q99N15;A2AFQ2;O08756	Hsd17b10	3-hydroxyacyl-CoA dehydrogenase type-2	-0.32696	3.995538	5
P05532	Kit	Mast/stem cell growth factor receptor Kit	-0.35829	2.67921	1
Q9QYH6	Maged1	Melanoma-associated antigen D1	-0.21393	5.123702	4
A0A0A6YXE3;A0A0A6YWB0;G3X9Q0;A0A0A6YVV8;Q9JKP5;A0A0A6YXP3;A0A0A6YXL7;A0A0A6YWJ5;A0A2I3BRX8;Q3U570;A0A0A6YWG1;Q3U581;A0A0A6YXQ4;S4R267;Q8R003	Mbnl1	Muscleblind-like protein 1	-0.33049	3.853954	4
A2A845;Q9DCS3	Mecr	Trans-2-enoyl-CoA reductase, mitochondrial	-0.49501	2.939272	2
Q8BG81;Q3UDD3	Poldip3	Polymerase delta-interacting protein 3	-0.34108	3.868911	2
A0A0N4SVL9;Q9CQR6;A0A0N4SVE2	Ppp6c	Serine/threonine-protein phosphatase 6 catalytic subunit;Serine/threonine-protein phosphatase 6 catalytic subunit, N-terminally processed	-0.37886	2.887118	4
Q9WTX2	Prkra	Interferon-inducible double-stranded RNA-dependent protein kinase activator A	-0.38855	3.112466	2

Q61136	Prpf4b	Serine/threonine-protein kinase PRP4 homolog	-0.32104	4.052412	2
Q52KR3	Prune2	Protein prune homolog 2	-0.35937	4.200427	2
O09114	Ptgds	Prostaglandin-H2 D-isomerase	-0.41003	2.278132	2
Q8R4E6	Purg	Purine-rich element-binding protein gamma	-0.39094	4.404852	7
O89086;Q8BG13	Rbm3	RNA-binding protein 3	-0.53754	3.047815	5
Q9D8S4;A0A1L1SS58	Rexo2	Oligoribonuclease, mitochondrial	-0.33459	3.154261	3
Q9CQE5	Rgs10	Regulator of G-protein signaling 10	-0.78885	4.338501	2
H3BJB4;Q99MB7	Rnf141	RING finger protein 141	-0.75688	3.903246	1
Q3TDK6;A0A0J9YUG1	Rogdi	Protein rogdi homolog	-0.39869	5.572412	3
Q9D7S7	Rpl22l1	60S ribosomal protein L22-like 1	-0.34397	2.610141	3
Q6ZWZ4;P47964	Rpl36	60S ribosomal protein L36	-0.44578	4.115999	4
A0A2I3BPG9;P83882;A0A0A6YW33	Rpl36a;Gm6525	60S ribosomal protein L36a	-0.4176	2.238067	2
P63325	Rps10	40S ribosomal protein S10	-0.57824	4.987783	6
Q9CQR2	Rps21	40S ribosomal protein S21	-0.30691	5.105988	7
P62754	Rps6	40S ribosomal protein S6	-0.43845	3.292349	9
Q9D1M0	Sec13	Protein SEC13 homolog	-0.36765	3.879319	2
A2BE92;A2BE93;Q9EQU5	Set	Protein SET	-0.39544	4.827507	3
Q8VHL0	Slc14a1	Urea transporter 1	-0.60879	3.114884	2
Q6PGE7	Slc6a7	Sodium-dependent proline transporter	-0.27693	3.806459	2
Q91VZ6;D3YVX4	Smap1	Stromal membrane-associated protein 1	-0.36099	3.285337	3
P62317	Snrpd2	Small nuclear ribonucleoprotein Sm D2	-0.21199	4.481814	3
A0A0R4J124;O54781;A0A3B2	Srpk2	SRSF protein kinase 2;SRSF protein kinase 2 N-	-0.35416	4.299307	3

W7I6;A0A3B2W883		terminal;SRSF protein kinase 2 C-terminal			
H7BX95;Q6PDM2;F7AI47;F6QXN3	Srsf1	Serine/arginine-rich splicing factor 1	-0.37349	3.698437	12
Q9CQA1	Trappc5	Trafficking protein particle complex subunit 5	-0.39995	2.962404	1
Q61187;A0A1B0GS09;A0A1B0GS10;A0A1B0GRX2;D3Z2V5;D3Z0S9	Tsg101	Tumor susceptibility gene 101 protein	-0.213	4.861522	9
Q9WV55;A0A3B2W837	Vapa	Vesicle-associated membrane protein-associated protein A	-0.40543	4.035833	5

Supplementary Table 5: List of the significantly down-regulated proteins in the PFC of *TAOK2* $^{d/d}$ mice from the differential expression protein analysis. The values are shown with protein intensity difference and the log2 (P value) as in the columns.

Protein IDs	Gene names	Protein names	Difference	- LOG (P-value)	Peptides
F2Z4B3;O35207;Q9CPY4	Cdk2ap1;Cdk2ap2	Cyclin-dependent kinase 2-associated protein 1;Cyclin-dependent kinase 2-associated protein 2	0.333499	3.032975	1
Q8BGD5	Cpt1c	Carnitine O-palmitoyltransferase 1, brain isoform	1.022719	1.844631	2
Q62095;P16381	Ddx3y;D1Pas1	ATP-dependent RNA helicase DDX3Y;Putative ATP-dependent RNA helicase Pl10	0.809737	1.927956	14
Q68FM6	Elfn2	Protein phosphatase 1 regulatory subunit 29	0.359496	2.69313	2
P07901;B7ZC50;A2A6A2;B7ZC49	Hsp90aa1	Heat shock protein HSP 90-alpha	0.207462	3.912967	46
D3YXG2;Q9QZ08;Q9D997	Nagk	N-acetyl-D-glucosamine kinase	0.400807	3.251424	2

Q9JIH2	Nup50	Nuclear pore complex protein Nup50	0.271797	3.365532	2
Q8C7K6	Pcyox1l	Prenylcysteine oxidase-like	0.356265	2.727487	1
Q6PB44	Ptpn23	Tyrosine-protein phosphatase non-receptor type 23	0.296004	4.33002	5
Q99N57	Raf1	RAF proto-oncogene serine/threonine-protein kinase	0.523838	4.197362	4
Q6ZQ29	Taok2	Serine/threonine-protein kinase TAO2	0.657589	4.757195	3

10. Acknowledgment

First, I would like to express my sincere gratitude to Prof. Dr. Michael Frotscher (ZMNH, Hamburg University, Hamburg) and Prof. Dr. Ismail Abdel-Aziz Ibrahim (Anatomy & Histology Department, Assiut University, Egypt) for their support at the initial stage of my Ph.D. within the Joint Supervision Program between the two Universities. Their memories will live on forever, and I will be grateful for their support.

My heartfelt thanks and appreciation to my **direct supervisor Dr. Froylan Calderon de Anda** for giving me the opportunity to work in his group **"Neuronal Development, ZMNH, UKE)** and the freedom to develop my project, and for his guidance and friendly supervision during my Ph.D.

I would like to thank my thesis committee members Prof. Dr. Matthias Kneussel, Prof. Dr. Roland Bender, and Prof. Dr. Gabriele M. Rune for their advice during the annual thesis committee meeting for my Ph.D. project.

Many thanks to the Cultural Affairs and Missions Sector, Ministry of Higher Education of the Arab Republic of Egypt for offering me a Joint Supervision Ph.D. Scholarship (ID: 7th plan 2012-2017) for 2 years (June 2016 – June 2018) and supporting me financially. It was a great honor.

Next, I would like to thank the collaborators: Dr. Kent Duncan for his efforts in this project. Thanks to other members of Kent's lab, especially Dr. Nagammal Neelagandan for her help in establishing the polysome profiling and for her advice and discussions. Thanks to the Mass spectrum facility's members in the UKE, Sönke Harder and Dr. Christoph Krisp for their efforts in the proteome analysis. Thanks to Dr. Joris de Wit's lab members in Belgium for the proteome analysis.

I would like to express my heartfelt thanks to Robin Scharrenberg for helping me out especially during the first period when I joined the group, for his advice in imaging and data analysis. For his fruitful contribution in the project by his help in preparation of the brain acute slices and staining. Many thanks for all the private talks that we had about our results in the lab and in our breaks.

I would like to extend my gratitude and thanks to all members who help in this project, especially Dr. Melanie Richter for taking care of the mouse lines, sample preparation to our collaborator in Belgium and for her helpful reading and comments in writing this thesis and the German summary. Many thanks to Birgit Schwanke for her help with the primary neuron cultures and in the utero electroporation. Special thanks to Tabitha Rücker for her help in the bioinformatic analysis of the proteome data. Thanks to Dr. Praveen Meka for his feedback on my thesis. Thanks to Ole Johanns, Shuai Hong, Dr. Peter Soba and his team for the feedback and discussions we had in our meetings. Thanks to all members of the ZMNH and the members of the non-medical Ph.D. Program in the UKE.

Thank you so much to all my friends in Hamburg and elsewhere who made this experience so enjoyable and supportive. A special thanks to my family in Egypt: **My parents, my brother, and my sisters to whom I dedicate this thesis**. Their love, encouragement, and support were crucial in making this work possible.

11. Eidesstattliche Versicherung

Ich versichere ausdrücklich, dass ich die Arbeit selbständig und ohne fremde Hilfe verfasst, andere als die von mir angegebenen Quellen und Hilfsmittel nicht benutzt und die aus den benutzten Werken wörtlich oder inhaltlich entnommenen Stellen einzeln nach Ausgabe (2021), Band und Seite des benutzten Werkes kenntlich gemacht habe.
Ferner versichere ich, dass ich die Dissertation bisher nicht einem Fachvertreter an einer anderen Hochschule zur Überprüfung vorgelegt oder mich anderweitig um Zulassung zur Promotion beworben habe.
Ich erkläre mich einverstanden, dass meine Dissertation vom Dekanat der Medizinischen Fakultät mit einer gängigen Software zur Erkennung von Plagiaten überprüft werden kann.

Unterschrift: